NTNU
Norwegian University of
Science and Technology

Analysis of an Offshore Jacket subjected to Supply Vessel Impacts

Erlend Flatøy

Marine Technology
Submission date: June 2018
Supervisor: Jørgen Amdahl, IMT
Co-supervisor: Zhaolong Yu, IMT

Norwegian University of Science and Technology
Department of Marine Technology

NTNU
Norges teknisk-naturvitenskapelige universitet
Institutt for marin teknikk

MASTER THESIS 2018

for

Stud. Techn. Erlend Flatøy

Analysis of an Offshore Jacket subjected to Supply Vessel Impacts

Analyse av en offshore fagverksplattform utsatt for støt fra forsyningsskip

Supply vessels, passing merchant vessels and shuttle tankers are regarded a major threat for offshore structures and platforms are often designed intentionally to resist collisions. In Norwegian sector of the North Sea the standard design event has been a supply vessel of 5,000 tons displacement sailing into a platform with a speed of 2m/s. With the recent update of NORSOK N-003 the standard size for a supply vessel is 10,000 tons. For bow collisions the speed has increased to 3 m/s. For design purposes standard force-deformation curves for bow, side and stern impacts are defined in NORSOK N-004 Appendix A for bow, sideways and stern impact. Appendix A is essentially identical to the recommended practice DNV-GL RP-C204 from 2010. A revision of RP-C204 is expected in the fall of 2017, with a significant update on design force-deformation curves for supply vessels. However, there are still aspects of supply vessel collisions that deserve attention.

The increase in supply vessel size and geometry may initiate re-evaluation of the collision resistance of existing structures. The objective of this thesis is to investigate the collision resistance of a North Sea integrated production platform by using the most updated analysis tools that are available today: LS-DYNA for local damage analysis and USFOS for global analysis. with a hybrid shell-space frame modeling.

The following topics should be addressed:

1. Identify potential collision scenarios for the jacket. Basis for this evaluation shall be the technical note: “Scenariobeskrivelse for boat impact”. The size, orientation and likely collision speed shall be discussed. It is recommended that the scenarios be described with horizontal and vertical illustrations of ship position relative to the platform in correct scale. It is suggested that impacts that could involve gas and oil risers as well as the conductors be focused, as indicated in the technical note. Discuss also to what extent global (rigid body) ship motions should be included in the analysis.

2. Any deformation of risers and conductors shall be included in the structural analyses. These structures shall be described with special attention to the support configuration and action, deck penetration and pipe flanges, so as to allow best possible modeling for structural analysis. The structural model for USFOS analysis shall be modified to the extent needed.

3. On the basis of the work in pt. 1. and 2. prepare a plan for local (LS-DYNA) and global analysis (USFOS) to be conducted. For the local analysis it is necessary to determine the size of the structural model and relevant boundary conditions. Establish the finite element models of the local platform structure and riser/conductors, mainly by use of shell elements.

4. Perform the local analyses with LS-DYNA using existing models of the stern, side and bow structure of two supply vessels. Determine characteristic force-deformation relationships for the impact to be used for the global analysis with USFOS. Discuss the distribution of energy and damage in the ship and platform. To the extent possible compare with simplified methods. Special focus shall be placed on the deformation and damage to riser and conductors. The risk of riser pipe rupture or flange “opening” shall be considered.

5. Perform global analysis with USFOS with the revised finite element model. Ship (platform) deformation may be modeled with nonlinear springs. The analysis may be carried out statically and dynamically; evaluate which of the two methods that are most suitable in each individual case. To the extent possible, compare FE analysis with the results of simplified methods.

6. Summarize the investigation by preparing a table of collision energy limits for critical events. Discuss the table in view of the new collision requirements.

7. To the extent needed perform residual strength checks of the damaged structure subjected to extreme storms.

8. Conclusions and recommendations for further work

Literature studies of specific topics relevant to the thesis work may be included.

The work scope may prove to be larger than initially anticipated. Subject to approval from the supervisor, topics may be deleted from the list above or reduced in extent.

In the thesis the candidate shall present his personal contribution to the resolution of problems within the scope of the thesis work.

Theories and conclusions should be based on mathematical derivations and/or logic reasoning identifying the various steps in the deduction.

The candidate should utilize the existing possibilities for obtaining relevant literature.

The thesis should be organized in a rational manner to give a clear exposition of results, assessments, and conclusions. The text should be brief and to the point, with a clear language. Telegraphic language should be avoided.

The thesis shall contain the following elements: A text defining the scope, preface, list of contents, summary, main body of thesis, conclusions with recommendations for further work, list of symbols and acronyms, references and (optional) appendices. All figures, tables and equations shall be numerated.

The supervisor may require that the candidate, in an early stage of the work, presents a written plan for the completion of the work. The plan should include a budget for the use of computer and laboratory resources which will be charged to the department. Overruns shall be reported to the supervisor.

The original contribution of the candidate and material taken from other sources shall be clearly defined. Work from other sources shall be properly referenced using an acknowledged referencing system.

The report shall be submitted in two copies:
- Signed by the candidate
- The text defining the scope included
- In bound volume(s)
- Drawings and/or computer prints which cannot be bound should be organised in a separate folder.

Supervisor:
Prof. Jørgen Amdahl

Co-supervisor
PhD Zhaolong Yu

Deadline: June 10 2018

Trondheim, January 15, 2018

Jørgen Amdahl

Abstract

In this master's thesis an offshore jacket platform subjected to supply vessel impacts is analysed. Since the supply vessels have increased in size and have been reinforced through modern ship design it has been of significance to study ship impacts with larger ships.

The collision scenarios are chosen based upon damage potential to critical members such as risers and conductors and the damage potential to structural integrity. Two stern collisions against risers, a side collision against the platform leg and a bow impact against a conductor area have been analyzed. The supply vessel used in this master's thesis had a displacement of 7500 tonnes and according to new ALS-requirements the speed at impact should be 3m/s for bow impacts and 2m/s for side – and stern impacts. Hence, in view of new collision requirements it is desirable to study whether the jacket platform is capable to withstand a bow-, side – and stern impact of 37.12MJ, 21MJ and 16.5MJ, respectively.

Local analyses have been performed with NLFEA in LS-DYNA while the global analyses have been carried out in USFOS. All LS-DYNA analyses are decoupled, which means that rigid body motions of the ship (e.g.: change in speed, direction due to impact) are not considered. Furthermore, the LS-DYNA analyses were performed quasi-statically which means that the ship was pushed towards the jacket platform at constant speed until the internal energy (strain energy) reached the collision energy level.

Structural sub-models of the jacket platform were modelled and meshed in SESAM GeniE. The structural ship models used in the LS-DYNA analyses are the same which are included in DNVGL-RPC208. The bow-, side – and stern model are all designed to be representative for an OSV with a displacement in the range of 6500-10000 tonnes. The USFOS-model was provided and only minor modifications were done. During the LS-DYNA analyses the energy absorption in both ship and jacket was analysed. In USFOS, the ship was presented as a nonlinear spring based upon the ship deformation behaviour observed in LS-DYNA.

The stern collision showed that there were a severe damage potential to the risers. Due to inaccurate modelling of the riser clamps and riser flanges it was not possible to judge the risk of rupture. Inaccurate modelling of one of the clamps between one of the braces and one of the risers caused rupture of the brace, a result which is questionable. Internal pressure and temperature in the risers were not considered in the LS-DYNA analyses. Another uncertainty was that a stern corner was used, and it is therefore questionable if the boundary conditions along the geometrical symmetry plane are accurate. In the side collision analysis deformation of both ship side and platform leg were achieved. Out of a collision energy of 21MJ, 15.5MJ and 5.5MJ were dissipated by jacket and ship, respectively. The bow impact against the conductor area showed that the conductors were strong enough to crush the forecastle and deform the bow. Internal pressure in the conductors was not implemented due to the design of the conductor. Of 37MJ the ship absorbed 30MJ while approximately 7MJ were dissipated by a diagonal which deformed in a three-hinge-mechanism. Due to time limitations a mesh convergence study was not carried out on neither of the sub-models. Furthermore, strain rates were not included. The rupture and tensile fracture criteria are also mesh dependent in NLFEA and must be chosen according to calibration procedures in DNVGL-RPC208. These are the main uncertainties in the LS-DYNA analyses.

In USFOS, the commands BIMPACT, MULT_IMP and SURFIMP were used. Despite challenges of capture the dissipating energy, the energy dissipation results were close to the results obtained with LS-DYNA. The stern collisions in USFOS gave reasonable results regarding fracture of braces. Risers and clamps were also affected by the deformation of the braces. In the side impact against the platform leg there were good coincidence with the results obtained with LS-DYNA. Since the conductors are non-structural in USFOS, the bow impact turned into a capacity check of the diagonal. The diagonal absorbed 9.5MJ before fracture, while the diagonal absorbed 7MJ in LS-DYNA. For all collision scenarios the damaged jacket survived the residual strength check without structural collapse. In the residual strength check, the jacket platform was subjected to a 5^{th} order Stoke wave with a return period of 100 years.

The master's thesis has concluded that the stern corner of the ship managed to do severe damage to the risers before it hit the platform, while the conductors seemed strong enough to crush the ship. Recommendations for the SURFIMP-command are given in Appendix. Based upon observations in LS-DYNA it was concluded that it is too optimistic to set the dent width equal to the height of the contact area between the ship and the platform. The dent widths in LS-DYNA were observed to be in the range of 0.1m-0.3m, instead of 2.5m-3m which was based upon ship geometry from earlier analyses. Smaller dent widths cause a more concentrated collision which reduces the capacity of the platform leg. For ship impacts against platform legs which do not stand perpendicular to the sea surface it is recommended to choose a dent width based upon NLFEA-results rather than ship geometry.

Sammendrag

Denne masteroppgaven omhandler analyser av skipsstøt mot en jacket-plattform. Siden offshore forsyningsskip har blitt større og forsterket gjennom moderne skipsdesign er det av vesentlig betydning å analysere skipsstøt med større skip.

Kollisjonsscenarioene er valgt på bakgrunn av skadepotensial på kritiske elementer som stigerør og lederør, samt skadepotensial på strukturell integritet. To hekkstøt mot stigerør, et sidestøt mot plattformbein og et baugstøt mot lederørsområde har blitt analysert. Forsyningsskipet i denne masteroppgaven har et deplasement på 7500 tonn og i henhold til nye ALS krav skal hastigheten ved sammenstøt være 3m/s for baug samt 2m/s for hekk – og side. I lys av nye kollisjonskrav er det derfor interessant å undersøke om jacket-plattformen evner å stå imot et baug-, side – og hekkstøt på henholdsvis 37.12MJ, 21MJ og 16.5MJ.

Lokale ikke-lineære elementanalyser er blitt utført i LS-DYNA, mens globale analyser er gjennomført i USFOS. Alle analysene i LS-DYNA er ukoplede, som innebærer at globaldeformasjoner (f.eks. endring i skipsbevegelse som følge av støt) ikke er hensyntatt. Analysene i LS-DYNA er gjennomført kvasi-statisk ved at skipet føres mot jacket-plattformen i konstant hastighet helt til indre energi (deformasjonsenergi) når kollisjonsenerginivået.

Strukturelle delmodeller av jacket-plattformen ble modellert og meshet i SESAM GeniE. De strukturelle skipsmodellene som ble benyttet i LS-DYNA analysene er de samme som er inkludert i DNVGL-RPC208. Baug-, side- og hekkmodellen er alle designet for å være representative for et offshore forsyningsskip med deplasement i området 6500 – 10 000 tonn. USFOS-modellen var gitt, og kun mindre endringer ble gjort. I LS-DYNA ble energiabsorberingen i både skip og plattform analysert. I USFOS ble skipet modellert som en ikke-lineær fjær med fjæregenskaper basert på resultater fra LS-DYNA.

Hekkstøtene i LS-DYNA viste at det var et stort skadepotensial mot stigerør. På grunn av unøyaktig modellering av stigerørsklemmer og innfestning var det ikke mulig å si noe om faren for brudd. Unøyaktig modellering av en stigerørsklemme mellom et av avstivningsrørene og en av stigerørene førte til brudd i stigerør, et resultat det kan stilles spørsmål ved. Indre trykk og temperatur i stigerør ble ikke hensyntatt i LS-DYNA-analysene. En annen usikkerhet er at kun en hekkhjørnemodell ble brukt, og det er usikkert om grensebetingelsene langs det geometriske symmetriplanet er fullstendige. I sidestøtet ble det deformasjon i både skip og plattform; i alt absorberte plattform og skip henholdsvis 15.5MJ og 5.5MJ av en total kollisjonsenergi på 21MJ. Baugstøtet mot lederørsområdet viste at lederørene var sterke nok til å knuse baugen. Indre trykk i lederør er ikke hensyntatt, på grunn av lederørenes strukturelle utforming. Av 37MJ absorberte baugen 30MJ. I jacket-plattformen var det kun et skråstilt avstivningsrør foran lederørsområdet som ble deformert

i en 3-leddsmekanisme. På grunn av tidsbegrensinger ble det ikke utført konvergenstest på noen av delmodellene. Tøyningsrate er heller ikke inkludert. Bruddkriterier i elementanalyse avhenger dessuten av elementstørrelse og skal velges ut fra kalibreringstester, som er beskrevet i DNVG-RPC208. Dette er de største usikkerhetene i LS-DYNA-analysene.

I USFOS ble kommandoene BIMPACT, MULT_IMP og SURFIMP brukt. Til tross for utfordringer ved å følge kollisjonsenergien var det samsvar med energiabsorberingsresultatet i LS-DYNA. Hekkstøtene gav fornuftige resultater med tanke på brudd for avstivningsrør. Stigerør og stigerørsklemmer ble også påvirket av deformasjon av avstivningsrør. Sidestøtet i USFOS samsvarte også bra med LS-DYNA. Siden lederørene er ikke-strukturelle i USFOS ble baugstøtet en kapasitetssjekk av det diagonale avstivningsrøret. Avstivningsrøret absorberte 9.5MJ av kollisjonsenergien før brudd. For alle kollisjonsscenarioene overlevde den skadde jacket-plattformen en reststyrkeanalyse. Reststyrkeanalysen innebar at jacket-plattformen skulle overleve en 5.ordens Stokes bølge med returperiode 100 år.

Masteroppgaven har konkludert med at hekkhjørnet er i stand til å påføre stor skade mot stigerør før den treffer et plattformbein, mens lederørene virker sterke nok til å knuse baugen. Anbefalinger for bruk av SURFIMP er gitt i Appendix. Basert på observasjoner i LS-DYNA ble det konkludert med at det var for optimistisk å angi bulkhøyden til å være lik høyden av kontaktflaten mellom skip og plattform. Bulkhøyden i LS-DYNA ble observert til å være i størrelsesområde 0.1m-0.3m, fremfor 2.5m og 3m som var basert på skipsgeometri brukt i tidligere analyser. Lavere bulkbredde fører til mer konsentrert last som igjen fører til redusert kapasitet av plattformbein. For skipsstøt mot plattformbein som ikke står normalt på vannflaten er det derfor anbefalt å velge en bulkbredde basert på ikke-lineær elementanalyse fremfor skipsgeometri.

Preface

This master's thesis is assigned by the Institute of marine technology at the Norwegian University of Science and Technology and carried out under the supervision of Professor Jørgen Amdahl. The report is a continuation of a project work which was carried out during the autumn semester of 2017.

During the semester some aspects of the scope of work turned out to be more time demanding than initially anticipated. Hence, some items have been omitted from the scope with approval from the supervisor. Only the stern-, side - and bow models of one supply vessel were studied in LS-DYNA and the focus on deck penetrations and pipe flanges of risers have not been considered in detail due to limitations in the structural sub-models.

It is expected that the reader should have a fundamental understanding of hydrodynamics and structural mechanics but the master's thesis is written in order to make it possible for a fellow student to understand. However, necessary theory is presented and referred to during the explanation of results. Other basic formulas for cross section analysis are given in the Appendix.

Acknowledgements

I want to express my gratitude to Professor Jørgen Amdahl for good guidance during the past year. His enthusiasm and deep knowledge within the field have been inspiring and valuable discussions with him are highly appreciated. Furthermore, I want to thank my co-supervisor PhD Zhaolong Yu for good guidance related to LS-DYNA and to Yanyan Sha for valuable input regarding modelling. I am also thankful for all help received from competent professionals who despite their tight schedules have answered my questions in detail. Special thanks are also given to the IT Operations Section at NTNU for allowing me to use the supercomputer *VILJE* for simulations in LS-DYNA.

Even though the work with the master's thesis has been both challenging and required hard work, it has been both educational and interesting to study a phenomena in detail. I am grateful for having the opportunity to study marine technology in Trondheim and being a part of an active student society.

I would also like to thank all those who have made the past five years memorable. Among my fellow students, I would like to thank Lars Gellein Halvorsen for reading through my master's thesis and for giving me valuable feedback regarding formulations and layout. I would also like to thank Stian Hagen and Terje Skogan Bøe for good discussions and help related to LS-DYNA. Ida Fagerli Osvoll also deserves a thank for her help and tips related to USFOS. Finally, to my office buddies at office A2.025 - Andreas Bro Kolstø, Eirik B. Vika, Olav Midtgarden and Terje Skogan Bøe: Thank you for making the life in office fun and better than I could ever imagine.

Erlend Flatøy

Tyholt, June 11th 2018
Erlend Flatøy

Table of Contents

Abstract **i**

Sammendrag **iii**

Preface **v**

Acknowledgements **vii**

Table of Contents **xii**

List of Tables **xiii**

List of Figures **xviii**

Abbreviations **xix**

List of symbols **xx**

1 Introduction **1**
- 1.1 Background 1
- 1.2 Objective 4
- 1.3 Thesis organization 4

2 Collision mechanics **5**
- 2.1 Energy dissipation 5
- 2.2 Design principles and design loads 9
- 2.3 Risk analysis for collision scenarios 10

3 Tubular members and joint capacity **11**
- 3.1 Deformation of tubular members 11
- 3.2 Joint capacity 14
  - 3.2.1 Joint geometry 14

3.2.2 Joint resistance 16
3.2.3 Strength - and failure criteria 18

4 Review of solution algorithms 19
4.1 Equation of motion 19
4.2 LS-DYNA: Central difference time integration 20
4.3 USFOS: Solution technique 22
4.3.1 Step-by-step method 22
4.3.2 Arc-length method 25
4.4 Explicit versus implicit solvers 26
4.5 Strain and stress definitions 27

5 Review of previous work 29

6 Material theory 33
6.1 DNVGL-RPC208: Proposed material model 33
6.2 Elastic-plastic material behaviour 34
6.3 Tensile fracture 36

7 Collision scenarios 37
7.1 Scenario 1: Stern collision against leg C2 and C3 39
7.2 Scenario 2: Side collision against leg A4 40
7.3 Scenario 3: Stern collision against leg A1 and A2 41
7.4 Scenario 4: Bow collision against conductor area 42
7.5 Discussion of global ship motions 43

8 Method 45

9 Structural analysis models 47
9.1 Global platform model for USFOS analysis 47
9.2 Ship models for LS-DYNA analysis 52
9.2.1 Material model 53
9.2.2 Boundary conditions 53
9.2.3 Structural failure 57
9.2.4 Element type 57
9.2.5 Dimensions and mesh size 57
9.3 Jacket submodels for LS-DYNA analysis 59
9.3.1 Inaccuracies 63
9.3.2 Boundary conditions 64
9.3.3 Element type and mesh size 64
9.3.4 Material 64
9.3.5 Description and modelling of critical elements 66
9.3.6 Structural failure 68

10 Local collision analysis (LS-DYNA) 69
10.1 Summary of LS-DYNA results 69
10.2 Scenario 1: Stern collision against leg C2 and C3 71
10.3 Scenario 2: Side collision against leg A4 75
10.4 Scenario 3: Stern collision against leg A1 and A2 79
10.5 Scenario 4: Bow collision against conductor area 82

11 Global collision analysis (USFOS) 85
11.1 Summary 85
11.2 Scenario 1: Stern collision against leg C2 and C3 87
11.2.1 Dynamic analysis 87
11.2.2 Static analysis 88
11.3 Scenario 2: Side collision against leg A4 90
11.3.1 Dynamic analysis 90
11.3.2 Static analysis 91
11.3.3 BIMPACT analysis 93
11.3.4 Discussion between static and dynamic analysis 95
11.4 Scenario 3: Stern collision against leg A1 and A2 98
11.5 Scenario 4: Bow collision against conductor area 100
11.5.1 Static analysis 100
11.5.2 Dynamic analysis 101

12 Comparison with hand calculations 103

13 Discussion 107
13.1 Discussions regarding LS-DYNA 107
13.2 Discussion regarding USFOS 109
13.2.1 Dent width B 109
13.2.2 Fracture criteria applied to elements 111
13.2.3 Incremental steps and time steps 111

14 Conclusion and recommendation for further work 113

Bibliography 115

Appendix I

A Structural mechanics III
A.1 Tubular cross section analysis III
A.2 Temperature dependency IV
A.3 Non-linear structural analysis V
A.4 Collapse load and hinge mechanism V

B LS-DYNA: Dimensions of structural ship models IX

C LS-DYNA: Keywords **XIII**
C.1 LS-DYNA: Control XIII
C.2 LS-DYNA: Material XV

D USFOS: Commands **XVII**
D.1 BIMPACT XVII
D.2 SURFIMP XVIII
D.3 WAVEDATA XIX
D.4 CHJOINT XIX
D.5 JntOption XIX

E Recommendations for SURFIMP **XXI**

List of Tables

2.1 Action factors for the ultimate limit state from NORSOK N-001 (2004) . 9

3.1 Values for Q_u according to NORSOK N-004 (rev.3) (2013) 17

6.1 Low resistance values for S235 and S355 (DNVGL RPC208, 2016) . . . 34

7.1 Dimensions of representative vessel 37

10.1 Summary of LS-DYNA results 70

11.1 Summary of USFOS analyses 86

List of Figures

1.1 Big Orange XVIII after impact (PTIL) 2
1.2 Local deformations in ship and platform visualized in LS-DYNA 3
1.3 Ship spring representation in USFOS (Søreide, 1981) 3

2.1 Design principles NORSOK N-004 (2004) 6
2.2 Dissipation of strain energy NORSOK N-004 (2004)) 7
2.3 Collision curves from NORSOK N-004 (2004) 8
2.4 New recommended collision curves (DNVGL RP-C204 (proposed version) (2017)) 8

3.1 Width of contact area of dent (Søreide, 1981) 12
3.2 Resistance curves for $0 < B/D < 2$ according to NORSOK 13
3.3 Resistance curve for $B/D = 0.5$ with axial effects according to USFOS . 13
3.4 Joint definitions (Berge, 2016) 14
3.5 Classification of joints (Amdahl et al., 2010) 15
3.6 50% K, 50% X joint (Amdahl et al., 2010) 16

4.1 Shifted time integration 20
4.2 Newton-Raphson method (Bergan & Syvertsen, 1977) 23
4.3 Modified Newton-Raphson method 24
4.4 Examples of a limit point (A) and a bifurcation point (B) (Søreide et al., 1988) 25
4.5 Arc-length method (Moan 2003) 25
4.6 Bar subjected to a load F 27

5.1 Model for low energy collision scenarios (Hysing, 1978) 30

6.1 Stress-strain curve (DNVGL RPC208, 2016) 33
6.2 Idealized stress-strain plot (Cook et al., 2002) 35

7.1 Comparison between representative vessel and jacket platform 38

7.2 Side collision against leg C2 and C3 39
7.3 Scenario 1 shown in LS-PrePost 39
7.4 Side collision against leg A4 40
7.5 Scenario 2 shown in LS-PrePost 40
7.6 Stern collision against leg A1 and A2 41
7.7 Scenario 3 shown in LS-PrePost 41
7.8 Bow collision against conductor area 42
7.9 Scenario 4 shown in LS-PrePost 42

8.1 Flow chart of method 46

9.1 Jacket platform with soil layers 48
9.2 Example of discretization 50
9.3 Example of small elements in USFOS-model 51
9.4 True - and engineering stress-strain for NV36 and NVNS 53
9.5 Boundary conditions for bow structural model 54
9.6 Boundary conditions for side structural model 55
9.7 Boundary conditions for stern structural model 56
9.8 Belytschko-Lin-Tsay element Haufe et al. (2013) 57
9.9 Mesh for structural side model 58
9.10 Dimensions of structural jacket sub-model for collision scenario 1 60
9.11 Dimensions of structural jacket sub-model for collision scenario 2 61
9.12 Dimensions of structural jacket sub-model for collision scenario 3 62
9.13 Dimensions of structural jacket sub-model for collision scenario 4 63
9.14 True stress-strain curves for materials used in LS-DYNA structural model 65
9.15 Engineering stress-strain curves for materials used in LS-DYNA structural model 65
9.16 Critical elements 66
9.17 Critical elements 67

10.1 Force-deformation curve for stern (Collision against leg C2) 71
10.2 Energy absorption for collision against leg C2 71
10.3 Force-time curve for stern against leg C3 72
10.4 Energy absorption for collision against leg C3 73
10.5 von-Mises plot of the collision against leg C2 when the entire collision energy is absorbed 74
10.6 von-Mises plot of the collision against leg C3 74
10.7 Force-deformation curve for side collision against leg A4 75
10.8 Energy absorption for collision against leg A4 76
10.9 Local damage of plate in structural side model (0.1s<T<0.15s) 77
10.10 Local damage of plate in structural side model (0.2s<T<0.3s) 77
10.11 Jacket after collision seen from right 78
10.12 Jacket after collision seen from left 78
10.13 Force - and energy for stern collision against leg A1 and A2 79
10.14 Dents in stern caused by diagonal (left) and riser (right) 79
10.15 Fracture in brace close to clamp and close to leg A1 80

10.16 Fracture diagonal 81
10.17 Comparison for force-time curves for forecastle at 5m/s and 3m/s 82
10.18 Comparison between force-deformation curves for forecastle in bow at 5m/s and 3m/s 83
10.19 Energy absorption for bow collision against conductor area 83
10.20 Bow model after collision 84
10.21 Jacket model after collision 84

11.1 Force deformation plot for dynamic side collision against leg C2 87
11.2 Energy absorption for dynamic side collision against leg C2 88
11.3 Impact energy for collision against leg C3 89
11.4 Plastic utilization of jacket after impact 89
11.5 Force deformation plot for dynamic side collision against leg A4 90
11.6 Energy absorption for dynamic side collision against leg A4 91
11.7 Comparison of force-deformation curves for scenario 2 91
11.8 Energy absorption for jacket 92
11.9 Impact energy for side collision against leg A4 93
11.10 Plastic utilization after collision 94
11.11 Element numbers close to impact site for scenario 2 94
11.12 Comparison of jacket - and ship displacement 95
11.13 Plastic utilization at maximum energy (Dynamic analysis) 96
11.14 Plastic utilization after collision (Dynamic analysis) 96
11.15 Axial stress at maximum energy 97
11.16 Energy absorption for static stern collision against leg A1 and A2 98
11.17 Jacket in damaged condition after static ship collision (plastic utilization) 99
11.18 Impact energy for static collision against diagonal between leg C1 and C2 100
11.19 Plastic utilization at fracture 101

12.1 Plastic utilization of leg A4 104
12.2 Plastic utilization of diagonal between leg C1 and C2 105

13.1 Comparison of dent width B 109
13.2 Impact sites 110
13.3 Comparison of dent width and height of contact area 111

A.1 Tubular thin-walled cross section III
A.2 Ultimate strength of steel versus temperature (Berge, 2016) IV
A.3 Definitions of stiffness contributions (Bergan & Syvertsen, 1977) V
A.4 Development of plastic hinge VI
A.5 Clamped beam subjected to concentrated force VI
A.6 Collapse mode VII

B.1 Dimensions of structural bulbous bow model IX
B.2 Dimensions of structural side model X
B.3 Dimensions of structural stern corner model XI

D.1 Extent defined in USFOS (USFOS-manual) XVII
D.2 SURFIMP explained XVIII

Abbreviations

ALS = accidential limit state
DNV = Det norske veritas
DNVGL = Det norske veritas - Germanischer Lloyd
FEA = finite element analysis
FEM = finite element method
FLS = fatigue limit state
JIP = joint industry project
NLFEA = nonlinear finite element analysis
NORSOK = Norsk Sokkels Konkurranseposisjon
NCS = Norwegian continental shelf
OSV = offshore supply vessel
PTIL = Petroleumstilsynet
PLS = progressive limit state
RP = recommended practice
ULS = ultimate limit state

List of symbols

$(')\ .ft$ = feet (=30.48 cm)
γ_f = partial safety factor
γ_m = material factor
Δt = time step
ϵ = true strain
ϵ^e = elastic strain
ϵ^p = plastic strain
$\epsilon_{p,y1}$ = strain corresponding to σ_{yield} (see Equation 6.1)
$\epsilon_{p,y2}$ = strain corresponding to $\sigma_{yield,2}$ (see Equation 6.1)
ϵ_{UTS} = strain corresponding to σ_{UTS}
$\boldsymbol{\epsilon}$ = strain vector
ρ = density
σ_θ = hoop stress or circumferential stress
σ_{eng} = engineering stress
σ_{eq} = equivalent stress
σ_{prop} = proportional stress
σ_{true} = true stress
σ_{UTS} = ultimate tensile stress
σ_X = axial stress
σ_{yield} = yield stress
$\sigma_{yield,2}$ = yield stress at end of yield plateu (see Equation 6.1)
a_s = ship added mass
a_x = wave acceleration in x-direction (see Equation 9.1)
B = dent width (see Figure 3.1)
$\boldsymbol{C}$ = damping matrix
C_D = drag coefficient (see Equation 9.1)
C_M = mass coefficient (see Equation 9.1)
D = diameter (for joints: chord diameter)
d = brace diameter
dw_i = indentation installation (see Figure 2.2 and 2.4)
dw_s = indentation in ship (see Figure 2.2 and 2.4)
E = Young's modulus
E = Green strain (see Equation 4.24)
$E_{C,bow}$ = collision energy for bow impacts
$E_{C,side}$ = collision energy for side impacts
$E_{C,stern}$ = collision energy for stern impacts
$E_{k,0}$ = initial kinetic energy
E_k = kinetic energy
E_0 = initial energy
E_S = strain energy or deformation energy
e = engineering strain

$\boldsymbol{F}^n$ = stress divergence vector (see Equation 4.11)
f_y = yield strength
$\boldsymbol{H}^n$ = hourglass resistance vector (see Equation 4.11)
I = second moment of inertia
$\boldsymbol{K}$ = stiffness matrix
K = stiffness
K = material parameter (see Equation 6.1)
K_G = geometric stiffness
K_I = incremental stiffness
K_O = initial stiffness
L_C = effective length of joint can
m_s = ship displacement
$\boldsymbol{M}$ = mass matrix
M = moment
M_p = plastic moment capacity
M_{rd} = joint bending moment resistance
N = axial force
N_P = plastic axial capacity
N_{rd} = joint axial resistance
$N_{rd,can}$ = joint can axial resistance
n = material parameter (see Equation 6.1)
$P_{cr.}$ = critical buckling load
$\boldsymbol{P}^n$ = external force vector (see Equation 4.11)
Q_u = strength factor for joints
r = brace radius
$\boldsymbol{r}$ = degrees of freedom vector
r = joint can parameter (see Equation 3.14)
R = chord radius
R_C = characteristic strength
R_d = design strength
R_0 = collapse load
R_i = reaction force in installation
R_S = reaction force in ship
S_d = design load
t = brace thickness
T = chord thickness
u_x = wave velocity in x-direction (see Equation 9.1)
v_s = ship velocity
W = elastic section modulus
WT = wall thickness
w_d = dent depth
Z = plastic section modulus
Ø = diamater

Chapter 1

Introduction

1.1 Background

The first requirements regarding design checks for ship impacts on the Norwegian Continental Shelf (NCS) were introduced in the early 1980s. Based upon ship statistics from DNV, a striking ship with a displacement of 5000 tonnes traveling at 2m/s was chosen as a representative scenario. Hence, for bow - and stern collisions 11MJ was used as design energy level. For side collisions, the design energy level was set to 14MJ (Moan et al., 2017).

During the last decades the supply vessels who operates on the NCS have increased in size, from approximately 3000 tonnes in 1980 to 10 000 tonnes in recent years. Modern ship geometry with bulbous bows and ice reinforcements have also increased the relative strength of the vessels. Furthermore, human errors in combination with new technology has also lead to high powered collisions where ships have collided with platforms while at service speed.

On 8th of June 2009 the supply vessel *Big Orange XVIII* collided with the water injection platform *Ekofisk 2/4W*. *Big Orange XVIII* had a displacement of 4600 tonnes and due to human errors in combination with autopilot, the ship hit the platform while at service speed (9.3 knots). The collision energy was in the range of 60MJ, significantly higher the original 11MJ requirement for bow impacts (Paulsen, 2011). Figure 1.1 shows the ship in damaged condition and the energy level is indicated by the severe deformations in the bow.

On the background of the *Big Orange XVIII*-incident and similar supply vessel impacts, it was recommended to increase the design energy level for supply vessel impacts to 50MJ (Moan et al., 2017). This was later implemented in NORSOK N-003 (NORSOK N-003, 2017) while both NORSOK-N004 and DNVGL-RPC204 have remained unchanged to this day. However, an upcoming revision of DNVGL-RPC204 with new requirements is under review and expected in the near future.

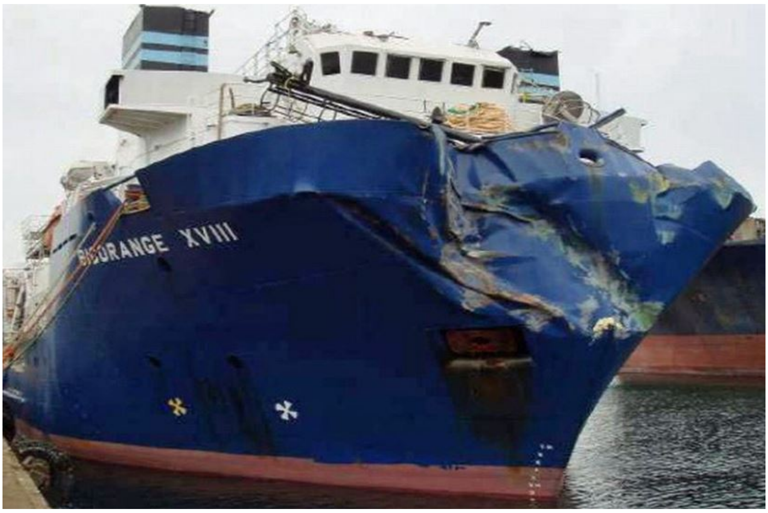

Figure 1.1: Big Orange XVIII after impact (PTIL)

Ship collisions are a major threat to offshore structures and are characterized by the impact energy level. For ship collisions, the impact energy is equal to the kinetic energy of the ship prior to impact, which is to be dissipated during a short period of time. It is hard to design an offshore platform to resist a collision, but the risk could be controlled by keeping the probability of occurrence on a low level (Amdahl and Johansen, 2001). One way of reducing the risk of ship impacts is to establish a safety zone around the platform, while another option is radar surveillance (Moan et al., 2017). However, this will not protect the platforms from *powered collisions*, where the ship is striking a platform in full speed due to the crew's unawareness of the situation. To ensure the structural integrity of the jacket platform an option might be to increase the strength of the platform locally, e.g. the platform legs is capable of crushing a striking ship. Another possibility is redundant design: The structure is designed in such a way that overall structural integrity is maintained even though the structure undergoes local deformations.

Both analysis methods and requirements related to ship impacts have made huge progress over the last couple of years. For analysis of framed offshore structures, USFOS has been frequently used. The software is suitable for global analysis in the post-buckling range, but yet information regarding local ship deformations is needed to obtain a proper presentation of the impact. With nonlinear finite element software such as Abaqus and LS-DYNA it has been possible to investigate the internal mechanics and energy dissipation between the striking ship and struck object. This has provided useful information to requirements regarding ship collisions compared to conservative assumptions and simplified analyses. Figure 1.2 shows a simulation of a side impact against a jacket leg performed in LS-DYNA, and it can be seen that both ship and jacket are deformed.

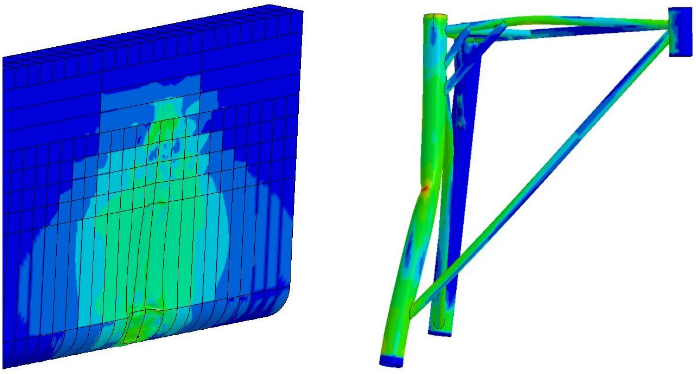

(a) Ship deformation **(b)** Platform deformation

Figure 1.2: Local deformations in ship and platform visualized in LS-DYNA

In USFOS, the deformation behaviour of the ship can be represented in terms of a nonlinear spring, as presented in Figure 1.3.

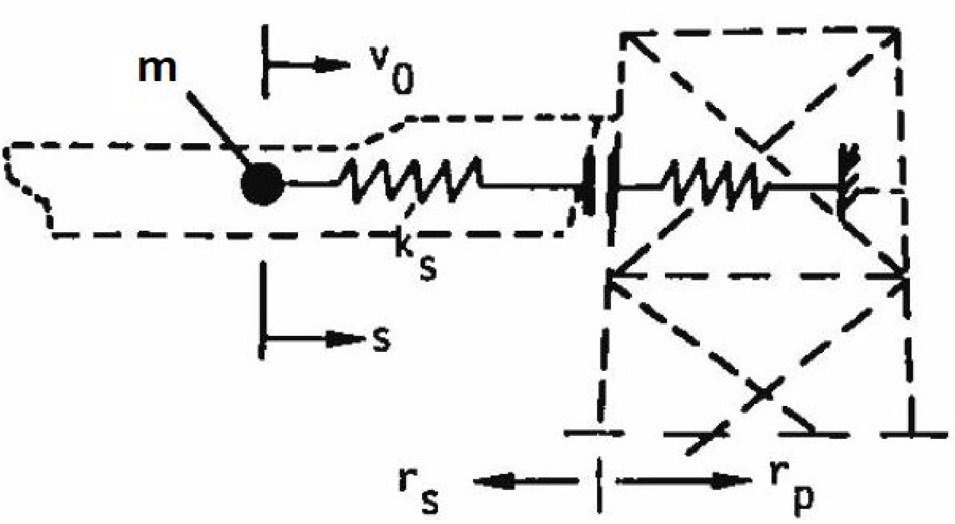

Figure 1.3: Ship spring representation in USFOS (Søreide, 1981)

A few years ago, a joint industry project (JIP) was carried out in order to update DNV-RPC208 and to develop structural ship models to be used for collision analyses. ((DNVGL RPC208, 2016), (DNVGL 2015-0984, 2016)). *DNVGL RPC208: Determination of structural capacity by non-linear finite element analysis methods* was released in 2016 and the structural FE-models were made open to the public. The FE-model library contains six structural FE-models: a side-, stern- and bow model for LS-DYNA - and Abaqus analyses, respectively. Even though the structural models do not represent a specific ship they are designed in such a way to be representative for the offshore supply vessels (OSV) operating on the NSC today.

In addition to overall structural integrity of an offshore structure in damaged condition it is also important to judge potential damage to critical elements such as risers and conductor (Moan et al., 2017). In NORSOK S001 design criteria for critical elements on offshore structures are specified. To reduce risk with respect to accidental actions such as ship collisions, it is desirable to locate risers along the inside of the structure (NORSOK S-001, 2000).

1.2 Objective

The objective of this master's thesis is to study an offshore jacket platform subjected to supply vessel impacts. It is desirable to study the jacket platform in view of the new collision requirements. Furthermore, a comparison study between LS-DYNA and USFOS will be performed. The structural ship models from the FE-model library of DNVGL-RPC208 shall be used in the local analyses. In addition to structural integrity a focus should also be put on potential damages to risers and conductors due to the ship impacts.

1.3 Thesis organization

The thesis is organized into chapters. Basic theory is presented through Chapter 2-4 and will be referred to throughout the explanation of the results. Chapter 5 presents a review of previous work done within ship collision analyses, and is mainly based upon the literature study done during the project thesis. The material model which is used in the LS-DYNA analyses is presented in Chapter 6. The collision scenarios which are to be studied are presented in Chapter 7 with horizontal and vertical illustrations. A discussion regarding global (rigid body) ship motions will also be presented. The method is described in Chapter 8 in terms of a flow chart. To make the thesis easy to follow, the flow chart will be presented in the start of each remaining chapter and highlight the item which is to be presented. Structural models for both LS-DYNA - and USFOS analyses are presented in Chapter 9. Only the structural sub-models of the jacket platform are made by the author. The global USFOS model and the structural ship models from DNVGL-RPC208 are provided and will only be briefly described. The results from the LS-DYNA and USFOS analyses will be presented in Chapter 10 and 11, respectively. The results will be discussed consecutively, and the most important items will be summarized in Chapter 13. Furthermore, Chapter 14 will describe the most important findings and recommendations for further work.

Chapter 2

Collision mechanics

2.1 Energy dissipation

Collisions between ships and offshore structures are characterised by the collision energy, which is equal to the total amount of kinetic energy at the instant of impact. Furthermore, three design principles describe how the energy is dissipated between the striking ship and struck object: *strength design*, *ductility design* and *shared-energy design* (see Figure 2.1).

- *Strength design* implies that the entire collision energy is dissipated by the ship. The installation is strong enough to resist the collision force.
- *Ductility design* implies that the collision energy is dissipated by the installation. Hence, the installation undergoes large plastic deformations.
- *Shared-energy design* implies that both the ship and installation contribute to the energy dissipation.

Both strength design and ductility design assume that one object is almost rigid while the other object contributes to the energy dissipation. Hence, from a calculation point of view strength design and ductility design are desirable (NORSOK N-004, 2004) since coupled deformation behavior can be disregarded. However, both design methods are conservative even though strength design might be typical for ship impacts against concrete structures. Normally both the ship and the installation will contribute to the energy dissipation even though it is the softest structure that will undergo the largest plastic deformations. New techniques such as non-linear finite element analysis (NLFEA) has made it possible to study the shared-energy design where both objects contribute to the energy dissipation. The kinetic energy $E_{k,ship}$ of a ship with a displacement m_s and velocity v_s is given in Equation 2.1

$$E_{k,ship} = \frac{1}{2}\left(m_s + a_s\right){v_s}^2 \tag{2.1}$$

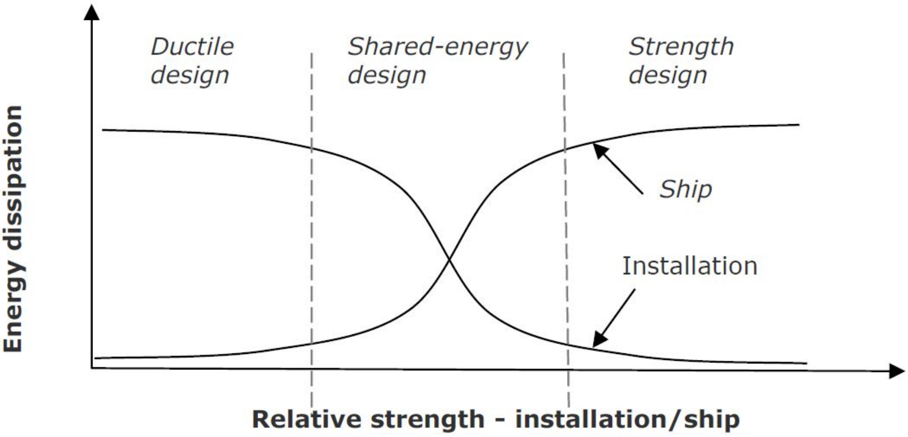

Figure 2.1: Design principles NORSOK N-004 (2004)

where a_s is the added mass. The added mass depends on direction; for side impacts the added mass equals 40% of the displacement, while the added mass equals 10% of the displacement for stern - and bow impacts (NORSOK N-003, 2017). Based upon energy conservation, the collision energy must be preserved throughout the collision. During the collision, the kinetic energy might be converted into strain energy E_S (deformation energy) or remain as kinetic energy E_k

$$E_0 = E$$

$$\frac{1}{2}(m_s + a_s)v_s^2 + \frac{1}{2}(m_i + a_i)v_i^2 = E_S + E_k \tag{2.2}$$

where E_0 is the energy prior to the collision and E is the energy after the collision. In Equation 2.2 v_i is the speed of the installation at impact, m_i is the mass of the installation and a_i is the added mass of the installation. For jacket structures the velocity of the installation is zero.

The amount of kinetic energy which is converted to strain energy E_S during a collision depends both on structure and if the collision is centric - or non-centric. By centric, it is referred to collision scenarios where the collision force goes through the centre of gravity while for non-centric collisions the collision force will cause a torsion moment on the installation. Hence, for non-centric collisions a part of the kinetic energy will remain as kinetic energy after impact, while for centric collisions most of the energy will be converted into strain energy (Amdahl and Johansen, 2001)

From a structural point of view, a jacket platform is *stiffness dominated* which means that the intertia - and dynamic effects are low in comparison with the restoring term and the natural period is low (normally less than 3 seconds) (Larsen, 2014). With respect to a collision scenario the jacket is *fixed* (Faltinsen, 1993) and the jacket and the striking ship can be regarded as *one* body after impact. This implies that the kinetic energy prior to impact is converted into strain energy (NORSOK N-004, 2004). Hence,

$$E_S = \frac{1}{2}(m_s + a_s)v^2$$

Figure 2.2 shows a force-deformation curve where both the striking ship and the installation contribute to energy dissipation. The collision force in the ship R_s and in the installation R_i is plotted against the indentation in the ship δw_s and in the installation δw_i, respectively. The area under each curve represents the strain energy absorbed in both objects.

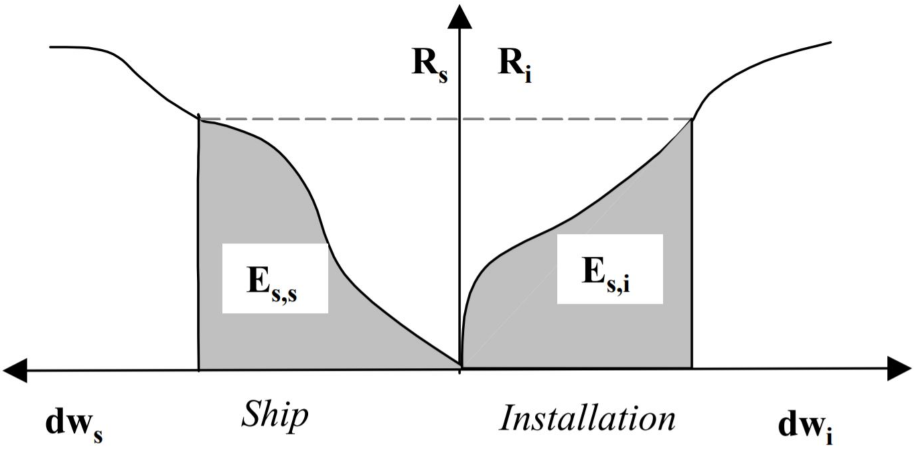

Figure 2.2: Dissipation of strain energy NORSOK N-004 (2004))

Mathematically, the total strain energy E_S equals the sum of strain energy in the ship $E_{S,s}$ and in the installation $E_{S,i}$

$$E_S = E_{S,s} + E_{S,i} = \int_0^{w_{s,max}} R_s dw_s + \int_0^{w_{i,max}} R_i dw_i \tag{2.3}$$

Figure 2.3 shows the current recommended force-deformation curves for ship impacts, which is implemented in NORSOK N-004 (2004). The figure shows the force-deformation curves for side - and stern impacts against rigid cylinders with a diameter of 1.5m and 10m, as well as bow impacts against a rigid wall. The bow curve is based upon raked bow impacts. Furthermore, the collision curves might be relevant for large diameter column collisions, but the bow curve is not valid for collisions against tubular braces.

As mentioned in the Introduction the force-deformation curves in Figure 2.3 were developed during the 1980s and based upon ships with a displacement of 5000 tonnes and impact speed of 2m/s. With an update of the DNVGL-RPC204 new collision curves are proposed, see Figure 2.4. The curves are updated to be valid for modern OSV with a displacement of 6500-10000 tonnes.

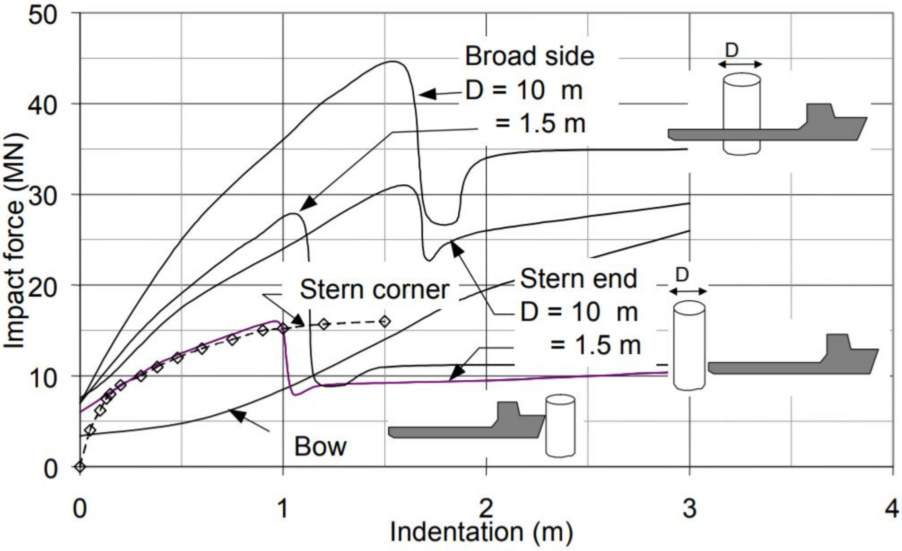

Figure 2.3: Collision curves from NORSOK N-004 (2004)

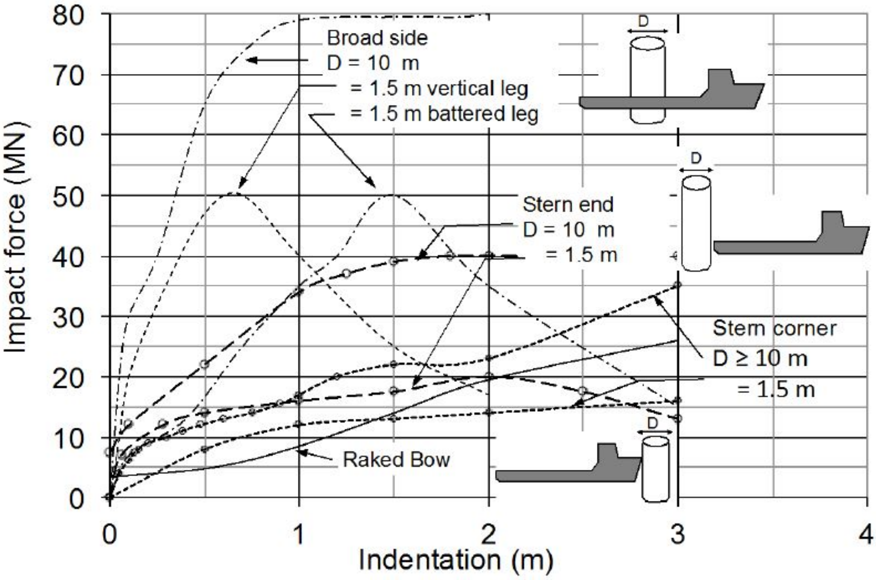

Figure 2.4: New recommended collision curves (DNVGL RP-C204 (proposed version) (2017))

2.2 Design principles and design loads

Offshore platforms are continuously affected by environmental loads from waves, wind and current and functional loads. With human presence, the structures are also subjected to live loads and pay loads in addition to the risk of accidental actions such as ship impacts, fire, technical failures and dropped objects. From a structural design point of view, it is important to clarify - and design a structure with respect to the loads it most probable will face during its lifetime.

The structure must be designed in such a way that a potential failure mode is not reached. A failure mode is often termed a *limit state* and it is common to differ between different *limit states*, e.g. the *ultimate limit state* (ULS) and *accidential limit state* (ALS).

ULS deals with the ultimate strength of the structure and covers resistance towards load carrying capacity and resistance against environmental actions (e.g. waves, wind and current). The *accidental limit state* ALS deals with accidental actions which are loads caused by human failure or technical faults (Moan, 2000). For offshore structures characteristic loads or design loads depends on the design criteria. Normally, characteristic environmental loads for ULS and ALS have annual probability of exceedance 10^{-2} (100-year event) and 10^{-4} (10 000 year event), respectively (NORSOK N-003, 2017).

With respect to magnitude there will always be uncertainties related to loads. Hence, saftety factors (also called action factors) are used to calculate the design load. In a ULS check the determination of design load is done in the following steps:

1. The present loads (also denoted actions) are divided into the sub-groups *permanent actions*, *variable actions* and *environmental actions*
2. The present loads are then multiplied with an action factor, depending on their respective action sub-group (see Table 2.1).
3. The total design load is the sum of the pre-multiplied loads. The combination which yields the highest design load shall be used.

Table 2.1: Action factors for the ultimate limit state from NORSOK N-001 (2004)

Combination	Permanent action	Variable action	Environmental action
A	1.3	1.3	0.7
B	1.0	1.0	1.3

In addition, there might be uncertainties related to structural models which are taken into account by introducing partial safety factors (NORSOK N-003, 2017). As shown in Equation 2.4 the design strength R_d of the structure must be greater than or at least equal to the sum of all design loads S_d

$$R_d = \frac{R_C}{\gamma_m} \geq \sum_i S(\gamma_{f,i}, Q_i) = S_d \tag{2.4}$$

where γ_f and γ_m are partial safety factors for loads and material, respectively. For ALS cheks, however all safety factors are set to unity.

In NORSOK N-003, the ship speed for ULS - and ALS design for bow impacts are 0.5 m/s and 3 m/s, respectively. For side - and stern impacts, the ship speed for ULS - and ALS-design are 0.5 m/s and 2m/s, respectively (NORSOK N-003, 2017). With respect to ship collisions it is desirable to study (1) the structural capacity against accidential actions and (2) the structural capacity (residual strength) in damaged condition. In step (2) the structure is subjected to a load with an annual exceedance probability of 10^{-2} with all safety factors set to unity ((Moan, 2000) (Moan et al., 2017) (Amdahl and Johansen, 2001)).

2.3 Risk analysis for collision scenarios

In order to determine the risk of ship collisions it is necessary to get a picture of the nearby passing ship traffic. Furthermore the likelihood of impact can be determined in terms of a frequency analysis. Collision scenarios are then ranked by its consequences (NORSOK Z-013, 2001).

From an operational point of view it is essential to clarify the orientation and position of ships which are operating close to the platform during loading/unloading. Even though bow impacts are most severe for a platform with respect to the energy level, most ships are oriented with the side or the stern towards the platform. Hence, stern - and side impacts are more likely to occur rather than bow impacts. From a risk point of view, it is necessary to clarify structural damage potential as well as damage to critical elements such as risers and conductors. In order to protect the risers against accidental actions (like ship impacts) the risers and other critical elements should be protected by the structure. For jacket structures this will imply that the critical elements are located along the inside of the jacket legs and braces (NORSOK S-001, 2000).

Chapter 3

Tubular members and joint capacity

A jacket structure consists of numerous tubular members (termed as braces and legs) connected by joints. When subjected to accidental - and environmental actions the joints will transfer loads from one member to adjacent members. The ability to unload and re-distribute loads makes jacket structures in general structurally redundant. Even though loads can be transferred to adjacent members, the members directly in contact with the loads will undergo the largest damages and could even fracture.

The purpose of this chapter is to briefly describe the theory behind deformation of tubular members and joint capacity.

3.1 Deformation of tubular members

According to Søreide (1981), jacket-ship collisions are divided into three categories:

1. Local deformation of brace/leg
2. Global deformation of brace/leg
3. Global deformation of structure

Local deformations like dents will cause a reduction in structural capacity. When the local deformations are large enough the tubular member will undergo global deformations. A further increase will in lead to global deformation of the jacket and, in worst case, cause structural collapse (Søreide, 1981). In jacket-ship impacts, the struck member and its adjacent members will undergo the most severe damages. Collapse of braces will cause a re-distribution of loads and in worst case cause global deformations or damage to critical elements such as risers.

The collapse load R_0 for a tubular member with length l and plastic moment capacity M_P in bending is defined as in Equation 3.1

$$R_0 = 4\frac{M_P}{l}c_1 \tag{3.1}$$

where c_1 is a factor which depends on the boundary conditions. For the ideal pinned and ideal clamped beam elements, c_1 is 1 and 2, respectively. Furthermore, the characteristic strength R_C of a tubular member with a diameter D, thickness t and yield strength f_y is given in Equation 3.2

$$R_C = f_y \frac{t^2}{4}\sqrt{\frac{D}{t}} \tag{3.2}$$

The characteristic strength is commonly used to describe the resistance to denting of tubular members. NORSOK has also introduced a compactness criterion where denting is to be disregarded if Equation 3.3 is fulfilled (Storheim, 2015)

$$f_y t^2\sqrt{\frac{D}{t}} \geq \frac{2}{3}R_0 \tag{3.3}$$

In NORSOK N-004 (2004) the resistance R of a tubular member is expressed in Equation 3.4

$$\frac{R}{R_C} = \left(22 + 1.2\frac{B}{D}\right)\left(\frac{w_d}{D}\right)^{\left(\dfrac{1.925}{3.5 + \dfrac{B}{D}}\right)} \tag{3.4}$$

where w_d is the depth of the dent, B is the width of the contact area (see Figure 3.1) and D is the diameter.

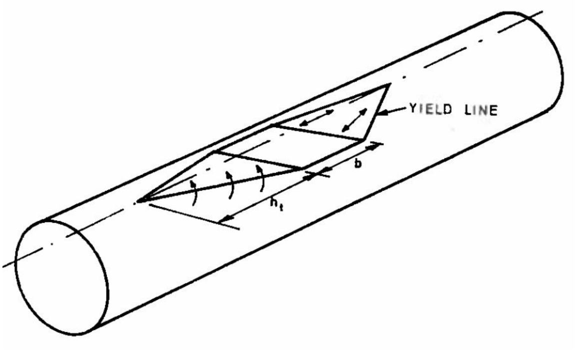

Figure 3.1: Width of contact area of dent (Søreide, 1981)

The resistance curves for $0.0 < B/D < 2.0$ are shown in Figure 3.2. The resistance curves are also implemented in USFOS but with an additional term taking axial effects into account, as can be seen in Equation 3.5

$$\frac{R}{R_C} = \left(22 + 1.2\frac{B}{D}\right)\left(\frac{w_d}{D}\right)^{\left(\dfrac{1.925}{3.5 + \dfrac{B}{D}}\right)} \sqrt{\frac{4}{3}\left(1 - \frac{1}{4}\left(1 - \frac{N}{N_P}\right)\right)} \tag{3.5}$$

where N is the axial force and N_p is the plastic axial capacity. The additional term was proposed by Wierzbicki and Suh in 1988. Figure 3.3 shows how the axial contributions affects the resistance curve for a tubular member with B/D=0.5. However, the curves shown in Figure 3.2 and 3.3 are only walid for $w_d/D > 0.05$

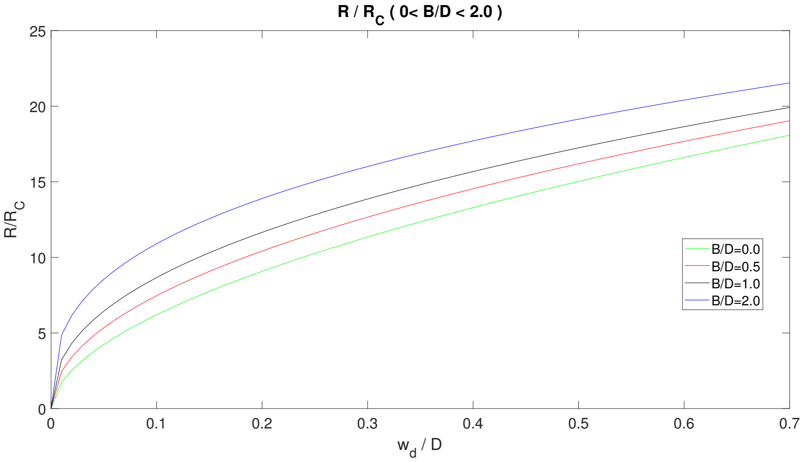

Figure 3.2: Resistance curves for $0 < B/D < 2$ according to NORSOK

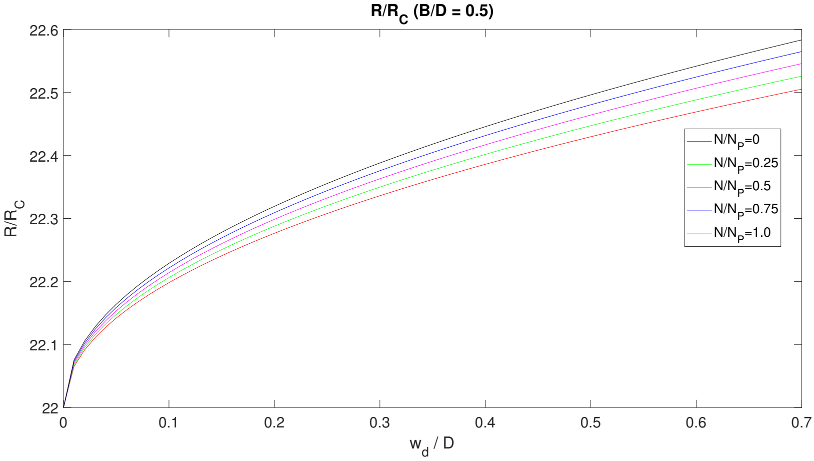

Figure 3.3: Resistance curve for $B/D = 0.5$ with axial effects according to USFOS

A low contact area B implies that the force is more concentrated. If D, R_C and w_d are kept constant, Figure 3.2 and 3.3 shows that the resistance of the tubular member increases with increasing contact area.

3.2 Joint capacity

3.2.1 Joint geometry

Joints must withstand both membrane - and bending forces from adjacent members. The ultimate strength is normally determined by laboratory tests but with the right calibration NLFEA could also be an option. A principle sketch of a joint is shown in Figure 3.4

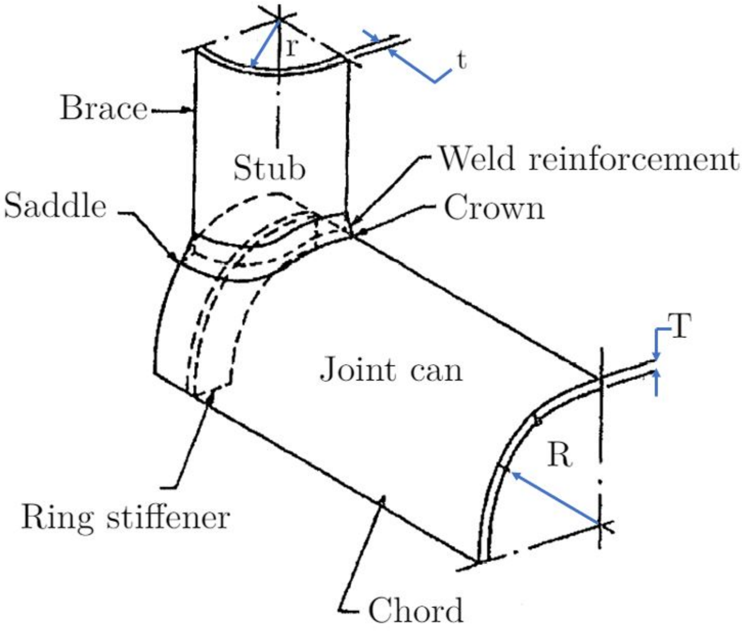

Figure 3.4: Joint definitions (Berge, 2016)

In joint geometry, the main tubular member is denoted *chord* while the remaining tubular members who intersect at the joint is denoted as *braces*. In offshore jacket platforms the chords normally carry the weight of the jacket, while the braces shall balance environmental loads from waves, winds and currents. Based upon the geometry of the chord and the brace, the following joint parameters can be determined:

$$\beta = \frac{d}{D} \tag{3.6}$$

$$\gamma = \frac{D}{2T} \tag{3.7}$$

$$\tau = \frac{t}{T} \tag{3.8}$$

where D and T is the diameter and thickness of the chord, while d and t is the diameter and thickness of the brace.

The *joint can* is the part of the chord at the joint with increased thickness. Likewise, the part of the brace with increased thickness close to the joint is denoted *stub*. The increase in thickness close to the joint is done to increase the capacity (Amdahl et al., 2010). The stress distribution varies from joint geometry and joint types but the maximum stresses are typically located either at the *saddle* or the *crown* (Berge, 2016).

Simple unstiffened tubular joints may be denoted as either type K, type T, type Y and type X. These types are shown in Figure 3.5

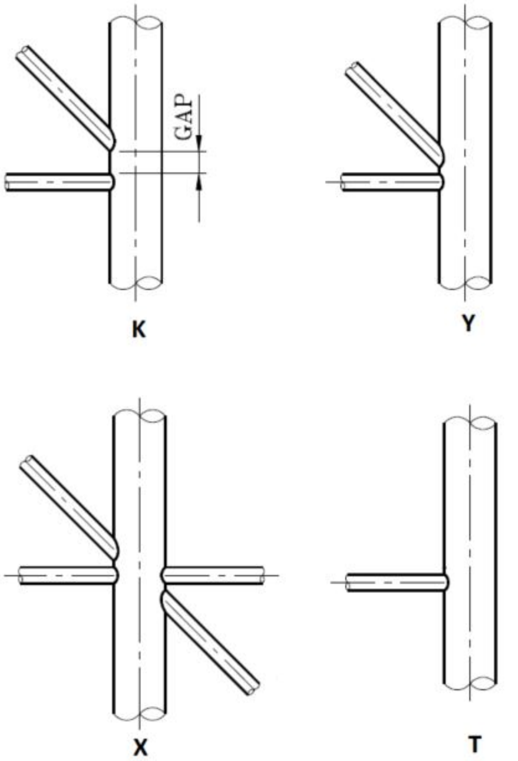

Figure 3.5: Classification of joints (Amdahl et al., 2010)

Typically, in X-joints the axial loads are normally transferred through the chord from one brace to the brace member on the other side. In T-joints and Y-joints the axial brace load are balanced as shear forces in the chord. In K-joints, the axial load is balanced normal to the chord (Amdahl et al., 2010). For complex joints types, the joint is defined as a combination of the different joint types. An example of a 50% K, 50% X joint is shown in Figure 3.6

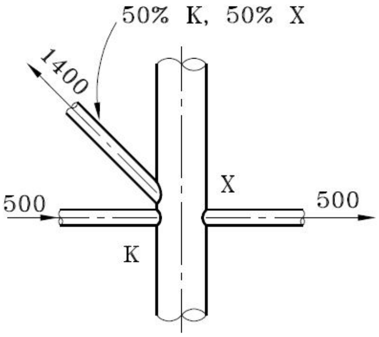

Figure 3.6: 50% K, 50% X joint (Amdahl et al., 2010)

3.2.2 Joint resistance

The following capacity formulas are the same as the ones given in NORSOK N-004 (rev.3) (2013). For further reading it is referred to NORSOK N-004 (rev.3) (2013) and the joint capacity manual for USFOS (USFOS, 2014). Basic formulas for joint axial resistance N_{rd} and joint bending moment resistance M_{rd} are given in Equation 3.9 and 3.10, respectively.

$$N_{rd} = \frac{f_y T^2}{\sin\theta} Q_u Q_f \tag{3.9}$$

$$M_{rd} = \frac{f_y T^2 d}{\sin\theta} Q_u Q_f \tag{3.10}$$

Equation 3.9 and 3.10 express the axial resistance and bending moment resistance, respectively, as they are expressed in the USFOS-manual. In NORSOK N-004 (rev.3) (2013), both values are reduced with a material factor γ_M, as shown in Equation

$$N_{rd} = \frac{f_y T^2}{\gamma_M \sin\theta} Q_u Q_f \tag{3.11}$$

$$M_{rd} = \frac{f_y T^2 d}{\gamma_M \sin\theta} Q_u Q_f \tag{3.12}$$

$\gamma_M = 1.15$ while f_y is the yield strength or yield capacity. If the joint is modelled with a joint can, the joint resistance should be calculated according to Equation 3.13

$$\frac{N_{Rd}}{N_{Rd,can}} = \left(r + (1-r)\left(\frac{T_n}{T_c}\right)^2 \right) \tag{3.13}$$

where $N_{Rd,can}$ is the resistance according to the material and geometry of the chord. In Equation 3.13 r is defined as in Equation 3.14 and must not be confused with the radius of the brace.

$$r = \max\left(1.0, \begin{cases} L_C/2.5D & \beta \leq 0.9 \\ \dfrac{(4\beta-3)L_C}{1.5D} & \beta > 0.9 \end{cases}\right) \tag{3.14}$$

In Equation 3.14 T_n is the chord thickness while T_c is the can thickness. L_C is the effective length of the joint can and is described in NORSOK N-004 (rev.3) (2013). The strength factor Q_u is given according to Table 3.1

Table 3.1: Values for Q_u according to NORSOK N-004 (rev.3) (2013)

Values for Q_u				
Type	**Axial tension**	**Axial compression**	**In-plane bending**	**Out-of-plane bending**
K	$\min\left((16+1.2\gamma)\beta^{1.2}Q_g, 40\beta^{1.2}Q_g\right)$		$(5+0.7\gamma)\beta^{1.2}$	$2.5+(4.5+0.2\gamma)\beta^{2.6}$
Y	30β	(see Equation 3.15)		
X	$6.4\gamma^{0.6\beta^2}$	$\left(2.8+(12+0.1\gamma)\beta\right)Q_\beta$		

where Q_u for axial compression for Y-joints is given as in Equation 3.15

$$Q_u = \min\left(2.8+(20+0.8\gamma)\beta^{1.6}, 2.8+36\beta^{1.6}\right) \tag{3.15}$$

Furthermore, the factors Q_β, Q_g, Q_f and A^2 are given below. Their expressions are given since they describe the joint resistance and to show that they depend on the geometry and material properties, but they will not be further described.

$$Q_\beta = \begin{cases} \dfrac{0.3}{\beta(1-0.833\beta)} & \beta > 0.6 \\ 1.0 & \beta \leq 0.6 \end{cases} \tag{3.16}$$

$$Q_g = \begin{cases} \max\left(1.0, 1+0.2\left(1-\dfrac{2.8g}{D}\right)^3\right) & g/T \geq 0.05 \\ 0.13+0.65\dfrac{tf_{y,b}}{Tf_{y,c}}\gamma^{0.5} & g/T \leq -0.05 \end{cases} \tag{3.17}$$

where $f_{y,b}$ and $f_{y,c}$ is the yield strength of the brace and the chord, respectively.

$$Q_f = 1.0 + C_1\frac{\sigma_{a,Sd}}{f_y} - C_2\frac{\sigma_{my,Sd}}{1.62f_y} - C_3A^2 \tag{3.18}$$

$$A^2 = \left(\frac{\sigma_{a,Sd}}{f_y}\right)^2 + \left(\frac{{\sigma_{my,Sd}}^2 + {\sigma_{mz,Sd}}^2}{1.62{f_y}^2}\right) \tag{3.19}$$

In Equation 3.19 $\sigma_{a,Sd}$, $\sigma_{my,Sd}$ and $\sigma_{mz,Sd}$ is the design axial stress, design in-plane bending stress and design out-of-plane bending stress, respectively. Furthermore, C_1, C_2 and C_3 are coefficients which depends on load type and joint type. Alternatively, A can be expressed as in Equation 3.20

$$A = \sqrt{\left(\frac{P}{N_p}\right)^2 + \left(\frac{M_{ipb}}{M_p}\right)^2 + \left(\frac{M_{opb}}{M_p}\right)^2} \tag{3.20}$$

As already mentioned, an increase in chord - and brace thickness near the joint (can and stub) could increase the joint capacity. As a rule of thumb, γ should be in the range 10-20 (Amdahl et al., 2010). Other reinforcements could be the use of ring stiffeners, as shown in Figure 3.4.

3.2.3 Strength - and failure criteria

In addition to the NORSOK-formulas described above, numerous joint-check criteria are implemented in USFOS. A joint might fail in tension, compression or bending, but quite often due to a combination. For the MSL-criteria, the *strength equation* or *interaction function* is given as

$$\left|\frac{N_{Sd}}{N_{Rd}}\right| + \left(\frac{M_{y,Sd}}{M_{y,Rd}}\right)^2 + \left(\frac{M_{z,Sd}}{M_{z,Rd}}\right)^2 \leq 1 \tag{3.21}$$

where N_{Sd}, $M_{y,Sd}$ and $M_{z,Sd}$ are the axial force, in-plane bending moment and out-of-plane bending moment, respectively while N_{Rd}, $M_{y,Rd}$ and $M_{z,Rd}$ is the corresponding resistance in axial force, in-plane bending moment and out-of-plane bending moment, respectively. NORSOK uses a similar formula for strength check as given in Equation 3.22

$$\left|\frac{N_{Sd}}{N_{Rd}}\right| + \left(\frac{M_{y,Sd}}{M_{y,Rd}}\right)^2 + \left|\frac{M_{z,Sd}}{M_{z,Rd}}\right| \leq 1 \tag{3.22}$$

With respect to capacity and failure mode it is often distinguished between *first crack*, *mean ultimate* and *characteristic ultimate*. Both mean ultimate and characteristic ultimate are based upon test results of joint failure test and they give an indication of the mean capacity of the joint. First crack is based upon test results of when the first crack is formed in the joint and before redistribution takes place (USFOS, 2014). Hence, first crack represents a lower bound or lower capacity of the joint.

For cyclic loading such as storm analyses the risk of collapse due to repeated yielding is high. Hence first crack is preferred for such loads. Ship impacts are instantaneous loads and the risk of repeated yielding is not relevant. A joint or a brace might fail due to ship impact even though the structural integrity is maintained. Hence, mean ultimate and characteristic ultimate may be used for ship impacts.

Joints might also be grouted. Grouted joints do not fail in compression. In USFOS grouted joints are defined with a joint option. In addition, the grout is taken into account by using equivalent chord thickness T (USFOS, 2015b).

The MSL JIP developed capacity formulas which has been implemented in USFOS. Since then, other criteria have emerged. The NORSOK capacity formulas which are given in NORSOK N-004 are nearly identical to the original MSL-equations, while API-RP2A are based upon both the MSL-equations and results based upon FEA ((USFOS, 2014) (NORSOK N-004, 2004)).

Chapter 4

Review of solution algorithms

The purpose of Chapter 4 is to present the theory behind the solution algorithms which are used in LS-DYNA and USFOS. Chapter 4.5 will give a brief description of the stress - and strain definitions used in this master's thesis.

4.1 Equation of motion

The general equation of motion is given in Equation 4.1 on matrix form

$$\mathbf{M}\ddot{\mathbf{r}}(t) + \mathbf{C}\dot{\mathbf{r}}(t) + \mathbf{K}\mathbf{r}(t) = \mathbf{F}(t) \tag{4.1}$$

where **M** is the mass matrix, **C** is the damping matrix and **K** is the stiffness - or internal forces matrix. The product **Kr**(t) is often referred to as the restoring term. **F** contains the external forces. For static analyses, the mass - and the damping term are neglected and the external forces must be balanced by the restoring term. Equation 4.1 may be solved either *explicitly* or *implicitly*. In explicit solvers, the displacements at an incremental step *n* is a function of the displacements, velocities and accelerations at the previos step *n-1* (Moan, 2003). Mathematically, as expressed in Equation 4.2

$$\mathbf{r}_n = \mathbf{r}_n(\mathbf{r}_{n-1}, \dot{\mathbf{r}}_{n-1}, \ddot{\mathbf{r}}_{n-1}) \tag{4.2}$$

An implicit solver uses iterative methods to solve Equation 4.1 at configuration n based upon configuration $n-1$ and $n+1$. LS-DYNA uses an explicit solver which will be descibed further in Chaper 4.2 ((Hallquist, 2006), (DYNAmore, 2018b)). USFOS uses implicit solvers, often combined incremental and iterative methods such as Euler-Cauchy methods and arc-length methods (Søreide et al., 1988). The methods will be demonstrated in Chapter 4.3.2

4.2 LS-DYNA: Central difference time integration

In the following an example of the shifted difference method which is implemented in LS-DYNA will be briefly described. The method is described in more detail by Moan (2003) and by Hallquist (2006)

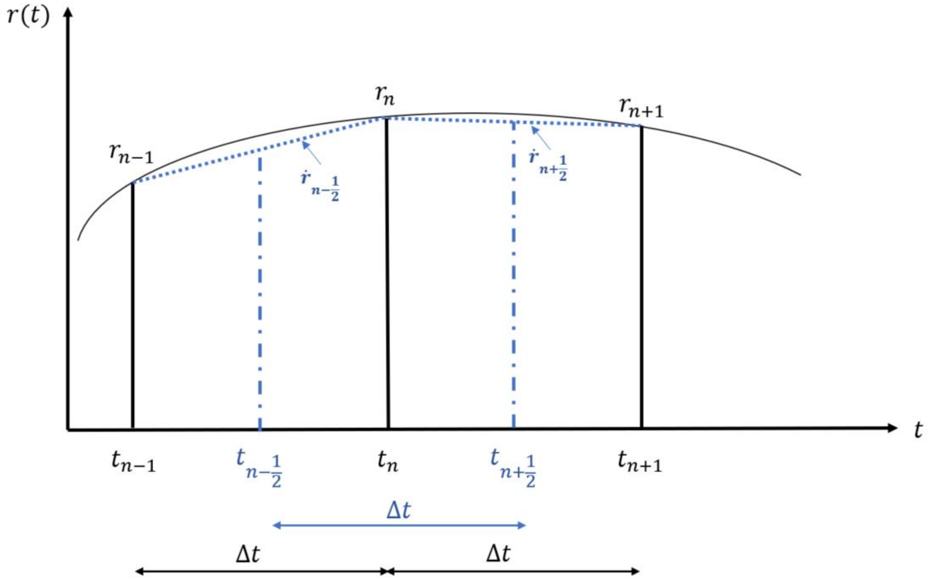

Figure 4.1: Shifted time integration

Figure 4.1 shows the a process r as a function of time t and it is assumed that the time step Δt is small. If the process is shifted with an incremental time step $1/2\Delta T$ towards the right, the slopes at time increment $t_{n-1/2}$ and $t_{n+1/2}$ can be approximated as

$$\dot{r}_{n-1/2} = \frac{r_n - r_{n-1}}{\Delta t} \tag{4.3}$$

$$\dot{r}_{n+1/2} = \frac{r_{n+1} - r_n}{\Delta t} \tag{4.4}$$

Hence, the slope of r at time increment t_n can be expressed as

$$\dot{r}_n = \frac{\dot{r}_{n+1/2} + \dot{r}_{n-1/2}}{2} = \frac{r_{n+1} - r_{n-1}}{2\Delta t} \tag{4.5}$$

Furthermore, the second derivate of r at time increment t_n is

$$\ddot{r}_n = \frac{\dot{r}_{n+1/2} - \dot{r}_{n-1/2}}{\Delta t} = \frac{\frac{r_{n+1} - r_n}{\Delta t} - \frac{r_n - r_{n-1}}{\Delta t}}{\Delta t} = \frac{r_{n+1} + r_{n-1} - 2r_n}{(\Delta t)^2} \tag{4.6}$$

Combining Equation 4.5 and 4.6 gives us the following relations

$$r_{n+1} - r_{n-1} = 2\dot{r}_n \Delta t \rightarrow \dot{r}_n = \frac{1}{2\Delta t}\left(r_{n+1} - r_{n-1}\right) \tag{4.7}$$

$$r_{n+1} + r_{n-1} = 2r_n + \left(\Delta t\right)^2 \ddot{r}_n \rightarrow \ddot{r}_n = \frac{1}{\left(\Delta t\right)^2}\left(r_{n+1} + r_{n-1} - 2r_n\right) \tag{4.8}$$

If Equation 4.7 and 4.8 is inserted into the equation of equilibrium

$$M\left(\frac{1}{\left(\Delta t\right)^2}\left(r_{n+1} + r_{n-1} - 2r_n\right)\right) + C\left(\frac{1}{2\Delta t}\left(r_{n+1} - r_{n-1}\right)\right) + Kr_n = F(t) \tag{4.9}$$

$$\left(\frac{1}{\left(\Delta t\right)^2}M + \frac{1}{2\Delta t}C\right) r_{n+1} + \left(\frac{1}{\left(\Delta t\right)^2}M - \frac{1}{2\Delta t}C\right) r_{n-1} = F(t) - \left(K + \frac{M}{\left(\Delta t\right)^2}\right) r_n \tag{4.10}$$

On matrix form it can be shown that r at incremental time step t_{n+1} is fully described by the previous incremental time steps, with no need to invert the tangent stiffness matrix (Moan, 2003).

In LS-DYNA, the acceleration at configuration n is expressed as (Hallquist, 2006)

$$\mathbf{Ma}^n = \mathbf{P}^n - \mathbf{F}^n + \mathbf{H}^n \tag{4.11}$$

where $\mathbf{M}$, $\mathbf{P}^n$, $\mathbf{F}^n$ and $\mathbf{H}^n$ are the mass matrix, external force vector, stress divergence vetor and the hourglass resistance vector, respectively. By matrix operations, the acceleration is found by Equation 4.12

$$\mathbf{a}^n = \mathbf{M}^{-1}\left(\mathbf{P}^n - \mathbf{F}^n + \mathbf{H}^n\right) \tag{4.12}$$

From the acceleration at configuration n, the velocity at configuration $n + 1/2$ and the displacement at configuration $n + 1$ is found according to Equation 4.13 and 4.14, respectively

$$v^{n+1/2} = v^{n-1/2} + a^n \Delta t^n \tag{4.13}$$

$$u^{n+1} = u^n + v^{n+1/2} \Delta t^{n+1/2} \tag{4.14}$$

Furthermore, kinematic compatibility gives the strains in terms of displacements, as shown in Equation 4.15

$$\boldsymbol{\epsilon} = \begin{bmatrix} \epsilon_x \\ \epsilon_y \\ \epsilon_z \\ \gamma_{xy} \\ \gamma_{yz} \\ \gamma_{zx} \end{bmatrix} = \begin{bmatrix} \frac{d}{dx} & 0 & 0 \\ 0 & \frac{d}{dy} & 0 \\ 0 & 0 & \frac{d}{dz} \\ \frac{d}{dy} & \frac{d}{dx} & 0 \\ 0 & \frac{d}{dz} & \frac{d}{dy} \\ \frac{d}{dz} & 0 & \frac{d}{dx} \end{bmatrix} \begin{bmatrix} u \\ v \\ w \end{bmatrix} = \boldsymbol{\Delta u} \tag{4.15}$$

and from the constitutive equation the stresses are found from the strains. Then the acceleration at the new step is found by equilibrium and the cycle is repeated (DYNAmore, 2018c).

4.3 USFOS: Solution technique

The purpose of Chapter 4.3 is to give a brief description of the solution technique implemented in USFOS. Some definitions regarding nonlinear analysis are presented in Appendix A.3. For further reading, it is referred to (Søreide et al., 1988), Bergan and Syvertsen (1977) and Bell (2015).

4.3.1 Step-by-step method

In the step-by-step method the relation between the incremental change in load ΔR - and displacement Δr is related to the incremental stiffness K_I as

$$K_I^{i-1} \Delta r^i = \Delta R^i \tag{4.16}$$

where the load and displacement at configuration i is given as

$$R^i = R^{i-1} + \Delta R^i \tag{4.17}$$

$$r^i = r^{i-1} + \Delta r^i \tag{4.18}$$

To follow the load curve iterative methods such as the Euler-Cauchy method is used. To avoid large errors an equilibrium correction must be done at every time step. To achieve equilibrium, the *Newton-Raphson method* can be used. A demonstration of the method is given in Figure 4.2.

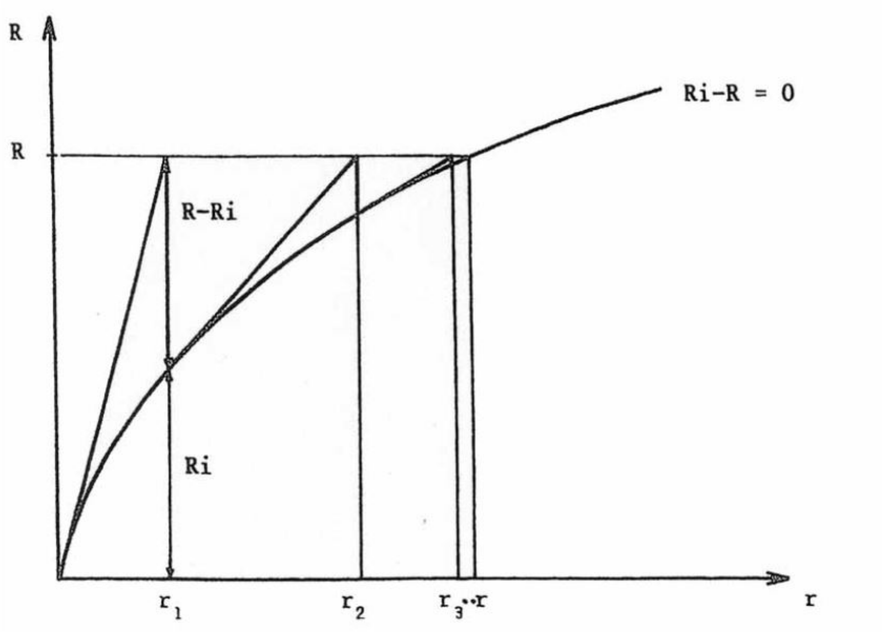

Figure 4.2: Newton-Raphson method (Bergan & Syvertsen, 1977)

The curve in Figure 4.2 represents the equilibrium between external and internal forces. As can be seen iterations are performed until equilibrium is achieved. The tangent stiffness matrix $\boldsymbol{K_I}$ is updated after each iteration step. To gain computational efficiency the *modified Newton-Raphson method* is an alternative. By applying this method the tangent stiffness matrix is only updated once. This can be seen in Figure 4.3. In general, this method requires more iterations than the original Newton-Raphson method, but in return the computational time might be reduced in comparison (Bell, 2015).

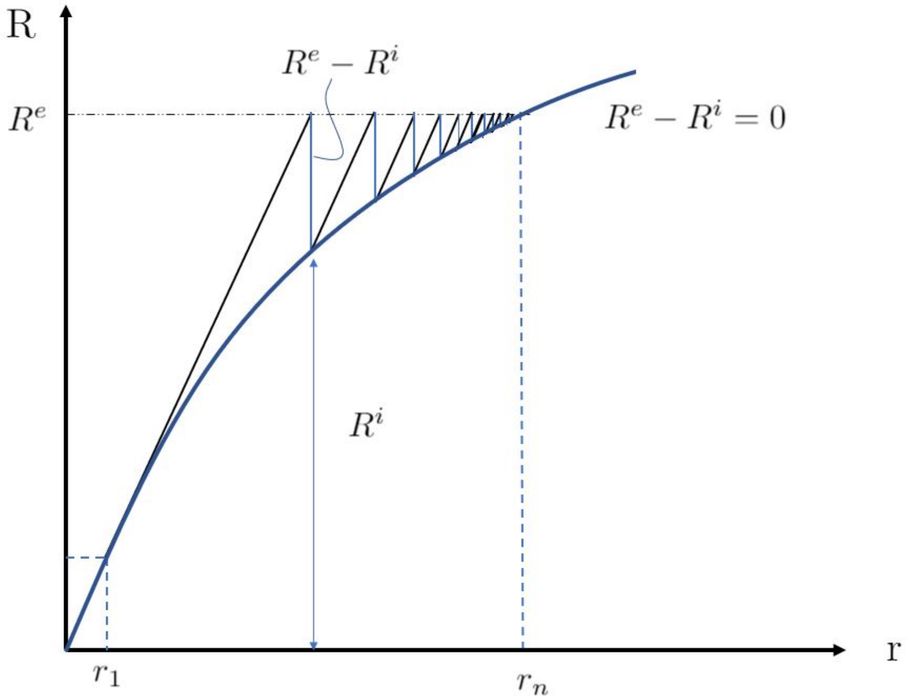
R
$R^e - R^i$
R^e
$R^e - R^i = 0$
R^i
r
r_1
r_n

Figure 4.3: Modified Newton-Raphson method

4.3.2 Arc-length method

When dealing with non-linear problems instability problems with bifurcation points or limit points might occur. Examples of such points are shown in Figure 4.4.

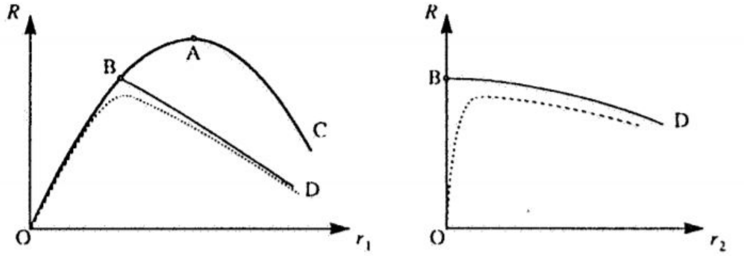

Figure 4.4: Examples of a limit point (A) and a bifurcation point (B) (Søreide et al., 1988)

A limit point (denoted as A) is a point where maximum load is applied while a bifurcation point (denoted as B) is a point from which there are more than one optional solution path to follow. However, the correct path is the path which requires the lowest amount of energy (Søreide et al., 1988)

For pure load-incremental methods such as the Euler-Cauchy methods difficulties will occur if a limit point is reached. In order to follow the curve around a limit point, arc-length methods are suitable. A general presentation is shown in Figure 4.5

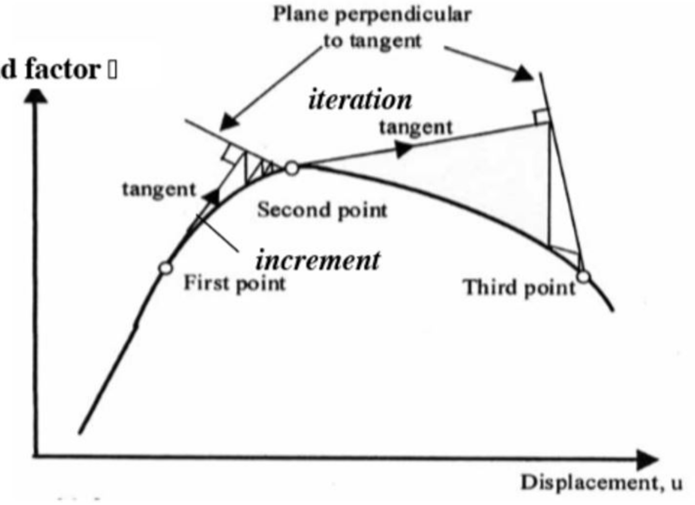
Plane perpendicular to tangent
Load factor
iteration
tangent
tangent
Second point
increment
First point
Third point
Displacement, u

Figure 4.5: Arc-length method (Moan 2003)

As shown in Figure 4.5 the tangent at the first point and a corresponding perpendicular line is used for iteration towards the second point. With the same procedure, it is possible to go beyond the limit point. The arc-length method is implemented in USFOS, which makes the program suitable to study structural response in the post-buckling range (Søreide et al., 1988).

4.4 Explicit versus implicit solvers

Since explicit solvers do not require iterations and inversion of matrices they are suitable for large equation systems. However, explicit solvers are only stable for small time steps. In comparison, implicit solvers are stable for large time steps (DNVGL RPC208, 2016). For explicit FE-solvers the time step is determined from the largest natural frequency of the element. To ensure stability in explicit solvers, information cannot propagate through more than one element during one time step ((Cook et al., 2002) (Moan, 2003)).

Given a two-noded bar element with a uniform cross section area A, elastic modulus E and length L as well as an uniformly distributed mass M. If the mass is lumped, the highest undamped eigenfrequency can be found by

$$M\ddot{\boldsymbol{u}} + K\boldsymbol{u} = \mathbf{0} \tag{4.19}$$

$$\det\left\{\frac{EA}{L}\begin{bmatrix}1 & -1\\ -1 & 1\end{bmatrix} - \omega^2\frac{\rho AL}{2}\begin{bmatrix}1 & 0\\ 0 & 1\end{bmatrix}\right\} = \mathbf{0} \tag{4.20}$$

$$\omega_{max} = \sqrt{\frac{4EA}{\rho AL^2}} = \frac{2}{L}\sqrt{\frac{E}{\rho}} \tag{4.21}$$

Hence, stability is ensured as long as the time step Δt_{cr} does not exceed

$$\Delta t = \frac{2}{\omega_{max}} = \frac{2}{\left(\frac{2}{L}\sqrt{\frac{E}{\rho}}\right)} = L\sqrt{\frac{\rho}{E}} \tag{4.22}$$

In order to increase the time step and hence reduce computational time, *mass scaling* can be performed. With this method, the mass of small elements are increased. Higher mass implies higher density which according to Equation 4.22 increases the critical time length. In LS-DYNA a selective mass scaling is optional. Selective mass scaling implies that the user spesifies a minimum time step length and if an element has a critical time step which is lower than this value LS-DYNA will add a non-physical mass to the element.

4.5 Strain and stress definitions

Figure 4.6 shows a bar element with an initial cross section area and volume A_0 and V_0, respectively. A force F is applied and the bar is elongated to a final length $l = l_0 + \Delta l$. The final cross section area and volume are A and V, respectively.

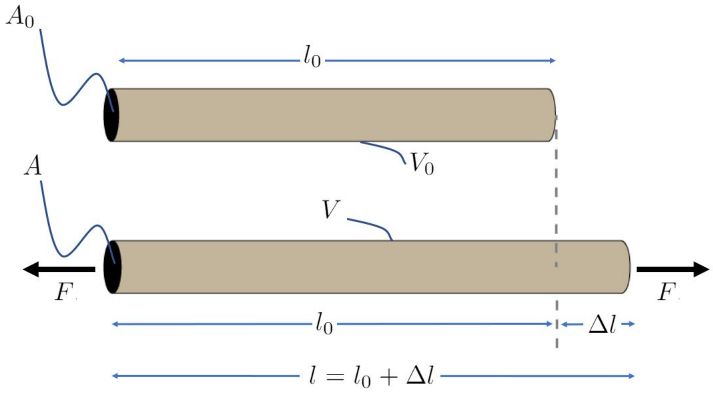

Figure 4.6: Bar subjected to a load F

Mathematically, the *true strain* ϵ is defined as in Equation 4.23

$$\epsilon = \int_{l_0}^{l} \frac{1}{l'} dl' = \ln(l_0 + \Delta l) - \ln l_0 = \ln \frac{l_0 + \Delta l}{l_0} = \ln\left(1 + \frac{\Delta l}{l_0}\right) = \ln(1 + e) \quad (4.23)$$

where the *engineering strain e* is defined as the change in length divided by the initial length. Engineering strain e refers to the initial volume V_0 and initial area A_0, whereas the true strain refers to the deformed volume V and deformed area A. The corresponding stress component to engineering strain is 1^{st} *order Piola-Kirchhoff stress* while the natural strain is related to *Euler-Cauchy stress*. 1^{st} *order Piola-Kirchhoff stress* and *Euler-Cauchy stress* are often referred to as *engineering stress* and *true stress*, respectively. Another strain component, *Green strain* E is defined as

$$E = \frac{l^2 - {l_0}^2}{2{l_0}^2} \quad (4.24)$$

Green strain corresponds to 2^{nd} *order Piola-Kirchhoff stress.*

When dealing with incremental methods it is common to differ between *total Lagrangian approach* and *updated Lagrangian approach*. In the total Lagrangian approach configuration n is referred to the inital configuration (initial area A_0 and initial volume V_0). Hence, Green strain E and 2^{nd} *order Piola-Kirchhoff stresses* are used. The updated Lagrangian approach describes configuration n based upon the previous configuration $n - 1$ (deformed area A and deformed volume V). In the updated Lagrangian approach, true strain ϵ and true stress are used.

The relationship between *true stress* σ_{true} and *engineering stress* σ_{eng} is given in Equation 4.25

$$\sigma_{eng} = \frac{\sigma_{true}}{1 + e} \tag{4.25}$$

The formulation in USFOS is based upon updated Lagrangian formulation. For small strains the 2^{nd} *order Piola-Kirchhoff stresses* approached the true stress (Søreide et al., 1988)

Chapter 5

Review of previous work

In ship collision analysis a distinction is made between *external mechanics* and *internal mechanics*. During a ship collision the interacting bodies will change velocity and direction. Based upon conservation of energy, the difference between the kinetic energy before the collision $E_{k,0}$ and the kinetic energy after the collision E_k equals the amount of energy which is dissipated as strain energy E_S

$$E_{k,0} = E_k + E_S$$

The strain energy is used as input into the internal mechanics, which deals with how the internal energy is dissipated in the interacting objects. According to Storheim (2015) Minorsky was the first to distinguish between external and internal mechanics of ship collisions in 1959.

Minosky studied ship impacts and proposed a linear relationship between energy absorbed and the resistance factor. According to Amdahl (1983) Minorskys results from 1958, which were based upon the assumption that most of the energy was absorbed plastically, gave a good prediction for high energy collisions.

A study for low-energy collisions between two ships was performed in the 1970s. The bow of the striking ship was assumed to be rigid meaning that the entire collision energy was assumed absorbed as plastic deformation energy in the struck ship. Another simplification was that the collisions were right angled, and only the compartment between the neighbouring frames of the hull absorbed the collision force. According to Hysing (1978) equilibrium in collision direction (see Figure 5.1) gives a collision load as expressed in Equation 5.1

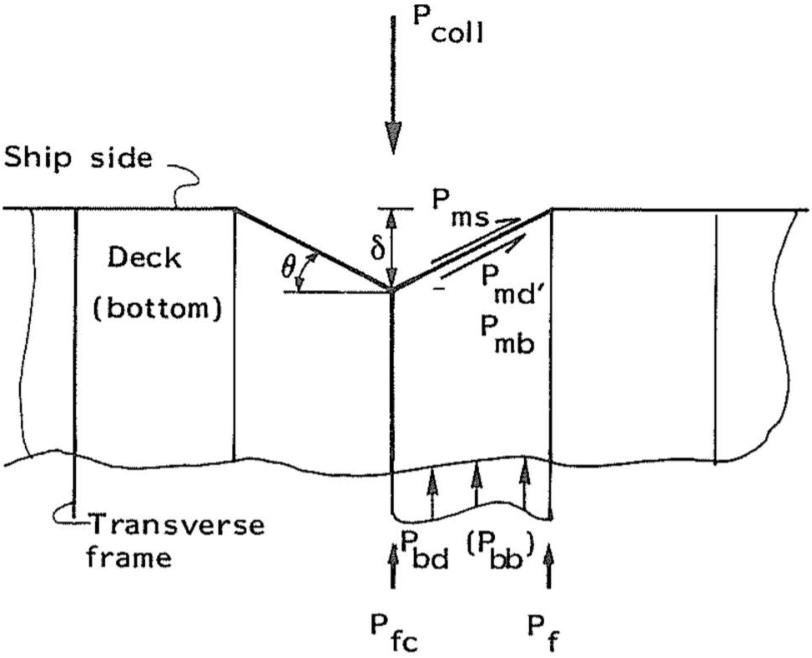

Figure 5.1: Model for low energy collision scenarios (Hysing, 1978)

$$P_{coll} = 2\left(P_{md}\sin\theta + \left(P_{md} + P_{mb}\right)\sin\theta\right) + P_{bd} + P_{bb} + P_{bf}) \tag{5.1}$$

The reaction force

$$P_f = \left(P_{ms} + P_{md} + P_{mb}\right)\sin\theta \tag{5.2}$$

is increased until is has reached the buckling load value of the girder. The results fitted quite well to the force-deformation curves in the recommended practise.

A study of impacts between supply vessels and offshore structures was carried out by Amdahl in 1983 in addition to deformation behaviour of tubular bracings. As reference vessel, a 5000 tonnes displacement vessel was used. Two tests for tubular members were performed, both free – and fixed to horizontal motion. Every test specimen were fixed against rotation. The experiments were compared with simulations in the program IMPACT which assumed strain hardening. For the horizontally free – and horizontally fixed specimens, collapse took place at the end (compression side) due to local buckling and near the welds due to fracture, respectively. It was concluded that plastic method theory gave good understanding to the deformation even though it was also concluded to take the effect of local indentation into consideration (Amdahl, 1983).

With the increase in supply vessel displacement and new technology in combination with human failures, the risk of high energy collisions emerged. Until then, supply vessel impacts were mainly characterized as a drifting issue. High-energy ship collisions with jacket legs were analysed by Amdahl and Johansen in 2001. The collisions were in the range of 40-50MJ since risk analysis had shown that collisions with this amount of energy were a potential hazard to platforms designed for collision in the range of 11MJ-14MJ. Since the jacket brace is not capable of dissipating the total collision energy, a strength design was favourable, meaning that the brace locally should be designed to be able to crush the bow (Amdahl and Johansen, 2001).

Amdahl and Skallerud described the analysis prosedure for a ship collision in 2002. The ship was modelled as a spring, with zero elongation as initial condition. Furthermore, the spring was elongated while the load intensity was reduced. The contact between ship and installation depends on the type of installation . The ship collision was considered as a SDOF-motion (Amdahl and Skallerud, 2002).

Another high-energy ship-jacket platform collision study was performed in 2014 by Travanca and Hao. The extensive work included a selection of three jackets: A three-legged, a four-legged and an eight-legged jacket. In addition, different ship types were used and different collision scenarios at leg, joint and brace were performed. This was done in order to demonstrate yielding of adjacent members to the collision area. It was also shown that the thickness of the member affected by the collision could give good estimates of the relatively strength of the jacket as a global system (Travanca and Hao, 2014).

A study of columns structures subjected to ship side-collisions was done by Reny Watan in her master thesis from 2011. Watan studied a combination of boundary conditions (e.g.: fixed, clamped, axial flexibility) and the design conditions. The study concluded that the use of fixed columns was a valid assumption, since the effect from the actual axial flexibility played a minor role for the deformation process of the column. The column stiffness was found from ship impact analyzes in *USFOS* and based upon the simplified calculations in *DNVGL-RP-C204* (Watan, 2011).

In recent years, NLFEA has proven to be a good tool for ship collision analyses. An extensive work with NLFEA-studies of ship collisions with offshore structures and icebergs was performed by Martin Storheim in his PhD-thesis from 2015. Storheim compared experimental results with results obtained with NLFEA and studied the material behaviour and different fracture criteria. His findings and recommendations regarding ship collision analysis in LS-DYNA have been valuable input for this master's thesis.

A NLFEA-optimization study of the strength of unstiffened columns were done by Kjetil Qvale in his master thesis from 2012. The focus was on columns subjected to supply vessel beam collisions. It was concluded that the effect of thickness was more crucial to the column strength than the effect of ring stiffeners (Qvale, 2012).

With the frequent use of NLFEA in ship collision analysis a FE-library of structural ship models were included in the latest version of *DNVGL-RP-C208: Determination of structural capacity by non-linear finite element analysis methods* in 2016. As mentioned in the introduction the FE-models do not represent an actual OSV but are meant to be representative for the a vast varity of the OSV on the NCS.

As an alternative to the single degree-of-freedom ship collision analyzes, Zhaolong Yu focused on 6DOF collision analyzes in his PhD-thesis from 2017. Yu used two models which were based upon a hydrodynamic maneuvring model and linear potential flow theory, respectively. According to Yu, few attempts have been reported in the literature but the accuracy of a coupled model is more accurate compared to the decoupled model where external - and internal mechanics are treated seperately (Yu, 2017).

Chapter 6

Material theory

6.1 DNVGL-RPC208: Proposed material model

The purpose of this section is to describe the material model implemented in *DNVGL-RP-C208: Determination of structural capacity by non-linear finite element analysis methods*. Figure 6.1 shows the true stress-strain curve for plastic strain with its corresponding parameters.

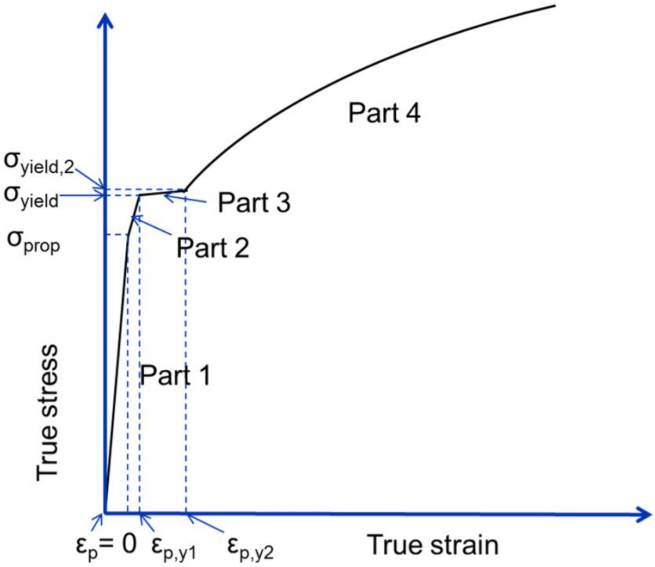

Figure 6.1: Stress-strain curve (DNVGL RPC208, 2016)

Up to $\epsilon_{p,y2}$ the stress-strain relationship follows a piecewise-linear relationship. The yield plateu is located within $\epsilon_{p,y1} < \epsilon < \epsilon_{p,y2}$. After $\epsilon_{p,y2}$ the stress-strain relationship follows a hardening model which is given in Equation 6.1 (DNVGL RPC208, 2016)

$$\sigma = K \cdot \left(\epsilon_p + \left(\frac{\sigma_{yield2}}{K} \right)^{\frac{1}{n}} - \epsilon_{p_y 2} \right) \tag{6.1}$$

where $K = \sigma_{UTS} \left(\frac{e}{n} \right)^n$ and $n = \ln 1 + \epsilon_{UTS}$. The parameters in Equation 6.1 depend upon material type, thickness and resistance. Data sets for low resistance (5% fractile) - and high resistance (95% fractile) are present in the recommended practice. The low resistance values for S355 and S235 are shown in Table 6.1

Table 6.1: Low resistance values for S235 and S355 (DNVGL RPC208, 2016)

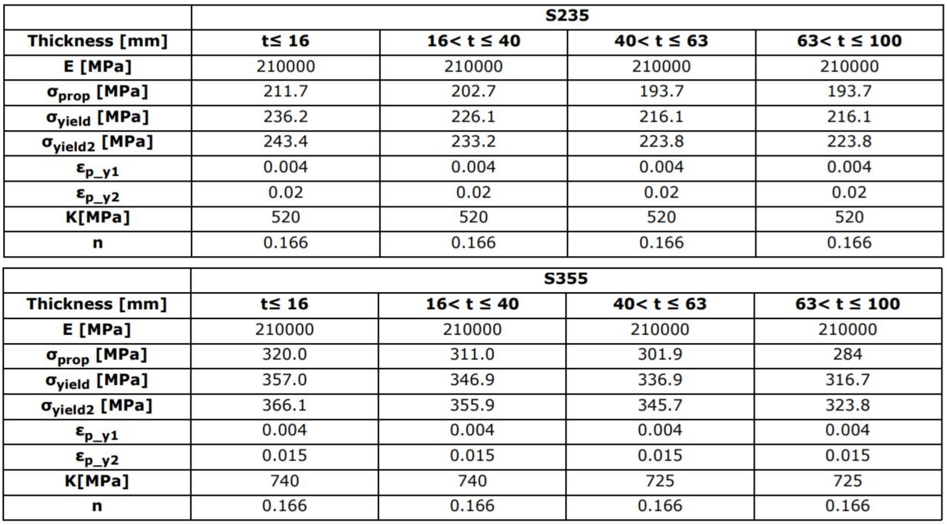

	S235			
Thickness [mm]	**t≤ 16**	**16< t ≤ 40**	**40< t ≤ 63**	**63< t ≤ 100**
E [MPa]	210000	210000	210000	210000
σ_{prop} [MPa]	211.7	202.7	193.7	193.7
σ_{yield} [MPa]	236.2	226.1	216.1	216.1
σ_{yield2} [MPa]	243.4	233.2	223.8	223.8
ε_{p_y1}	0.004	0.004	0.004	0.004
ε_{p_y2}	0.02	0.02	0.02	0.02
K[MPa]	520	520	520	520
n	0.166	0.166	0.166	0.166

	S355			
Thickness [mm]	**t≤ 16**	**16< t ≤ 40**	**40< t ≤ 63**	**63< t ≤ 100**
E [MPa]	210000	210000	210000	210000
σ_{prop} [MPa]	320.0	311.0	301.9	284
σ_{yield} [MPa]	357.0	346.9	336.9	316.7
σ_{yield2} [MPa]	366.1	355.9	345.7	323.8
ε_{p_y1}	0.004	0.004	0.004	0.004
ε_{p_y2}	0.015	0.015	0.015	0.015
K[MPa]	740	740	725	725
n	0.166	0.166	0.166	0.166

It is desirable that the material model represents non-linear behaviour and thus calibration against experimental/empirical data is needed. The recommended practice also recommends that one of three methods should be followed in the analysis: (1) governing parameters should be conservative, (2) validation against design values or (3) validation against tests. (1) implies that the material parameters should be selected in order to give a safe-side estimate (DNVGL RPC208, 2016).

6.2 Elastic-plastic material behaviour

There are three basic principles that govern elastic-plastic material behaviour: a *yield criterion*, a *hardening rule* and a *flow rule*. The principles will be briefly described through Figure 6.2.

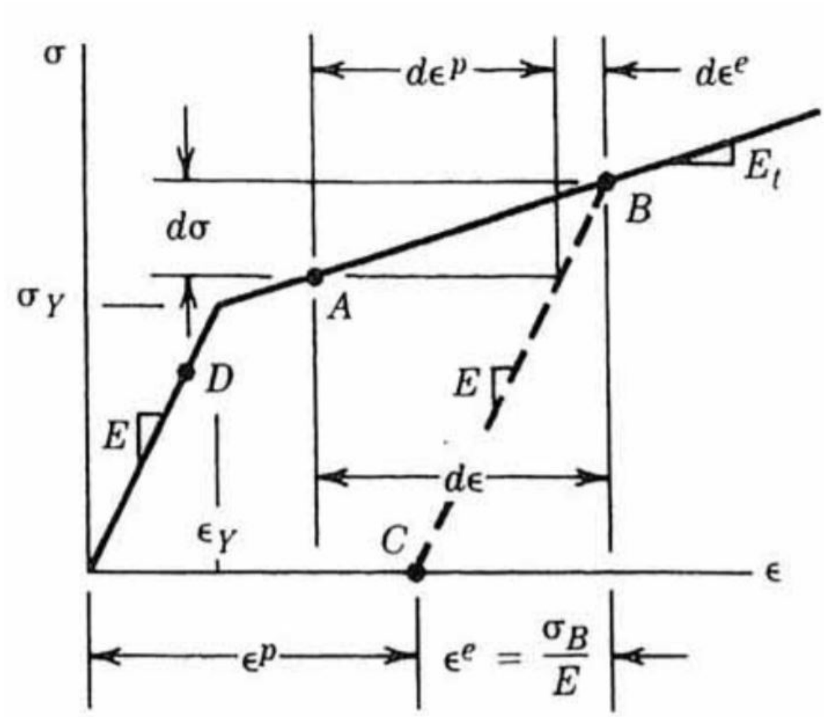

Figure 6.2: Idealized stress-strain plot (Cook et al., 2002)

In principle, the strain ϵ consists of an elastic part ϵ_e which is reversible and a plastic part ϵ_p as described in Equation 6.2

$$\epsilon = \epsilon_e + \epsilon_p \tag{6.2}$$

$Reversible$ means that the material will obtain its initial shape (before loading) if the loading is removed. The *yield criterion* states that plastic deformations starts to occur when the stress exceeds the yield stress, as stated in Equation 6.3

$$|\sigma| > |\sigma_Y| \tag{6.3}$$

Until yield the behaviour is elastic and the yield stress σ_Y and yield strain ϵ_Y are marked in Figure 6.2. The *hardening rule* describes how the yielding changes by the historical plastic flow. The stress-strain curve transitions from a linear to a non-linear behaviour which is shown as a change in slope after point D in Figure 6.2. If unloading occur at point B the stress will decrease linearly from point B towards point C where the stress is equal to zero. However, due to the plastic history the material will have a permanent plastic strain ϵ^p at zero stress as shown in Figure 6.2. If loading is applied once more the stress will increase linearly until point B is reached. Furthermore, varying stress between 0 and σ_B will cause a varying elastic strain between point B and point C. This leads to the *flow rule* which accounts for historic plastic flow and that an increase in strain increment $\delta\epsilon$ will lead to an increase in stress increment $\delta\sigma$ (Moan, 2003). Mathematically, this is explained by the *consistency condition* as expressed in Equation 6.4

$$f = \sigma - \sigma_Y = 0 \tag{6.4}$$

$$\delta f = \frac{\delta f}{\delta \sigma}\delta\sigma - \frac{\delta f}{\delta \epsilon_p}\delta\epsilon_p = \frac{\delta f}{\delta \sigma}\delta\sigma - H'\delta\epsilon_p = 0 \tag{6.5}$$

An increase in strain increment must cause an increase in stress increment in such a way that the consistency condition as expressed in Equation 6.4 is always satisfied.

6.3 Tensile fracture

According to NORSOK N-004 (2004) and Amdahl and Skallerud (2002) the critical strain ϵ_{cr} depends on *strain rate*, *presence of strain concentrations*, *defects* and *material toughness*. Due to defects, welds will normally achieve lower fracture toughness than expected based upon the material. It is therefore desirable to achieve the larger plastic strains outside the welds. Geometrical properties (e.g.: cross section dimensions) and material properties (e.g.: ductility, yield - and tensile strength) will affect the critical strain outside welds where defects is to be disregarded. NORSOK has proposed critical strains for steel type S235 and S355 to be 0.2 and 0.15, respectively. The values are chosen in order to give reasonable results with a bi-linear stress-strain curve (NORSOK N-004 (rev.3), 2013).

In FEA the critical strain depends on the mesh size. Recommendations are given in DNVGL-RPC208 and it is recommended that the tensile failure should be calibrated against a known solution (DNVGL RPC208, 2016). In NORSOK N-004 (rev.3) (2013) the critical average strain ϵ_{cr} is recommended according to Equation 6.6

$$\epsilon_{cr}(l_e) = \left(0.02 + 0.65\frac{t}{l_e}\right)\frac{355}{f_y} \tag{6.6}$$

where t is the plate thickness and l_e is the element of the element. It is recommended that the mesh size at impact zone should be at least 5 times the thickness ((NORSOK N-004 (rev.3), 2013) (Vredeveldt et al., 2013)).

Chapter 7

Collision scenarios

Based upon a study of the nearby vessel activity, dimensions of a representative vessel for collision analysis were determined (see Table 7.1)

Table 7.1: Dimensions of representative vessel

Dimensions	
Displacement	7500 tonnes
Length	83 m
Breadth	17 m
Draught	6 m

Based upon data given in Table 7.1 and data described in Chapter 2.1 the representative vessel corresponds to the following energy levels for ALS-design

$$E_{C,stern} = \frac{1}{2}7.5Mkg \cdot 1.1 \cdot (2m/s)^2 = 16.5MJ$$

$$E_{C,side} = \frac{1}{2}7.5Mkg \cdot 1.4 \cdot (2m/s)^2 = 21.0MJ$$

$$E_{C,bow} = \frac{1}{2}7.5Mkg \cdot 1.1 \cdot (3m/s)^2 = 37.1MJ$$

The collision scenarios are visualized in the following chapters. Figure 7.2, 7.4, 7.6 and 7.8 shows the dimensions between jacket elevation $+25'$ (located 3,5 meters above the mean water level) and a ship with length 80 meters. The jacket rows is also specified. Figure 7.3, 7.5, 7.7 and 7.9 shows the scenario in LS-PrePost with jacket legs and notation of relevant members. Furthermore, Figure 7.1 shows the size of the representative vessel in comparison with the jacket-platform model. The mean water line is marked with a blue line.

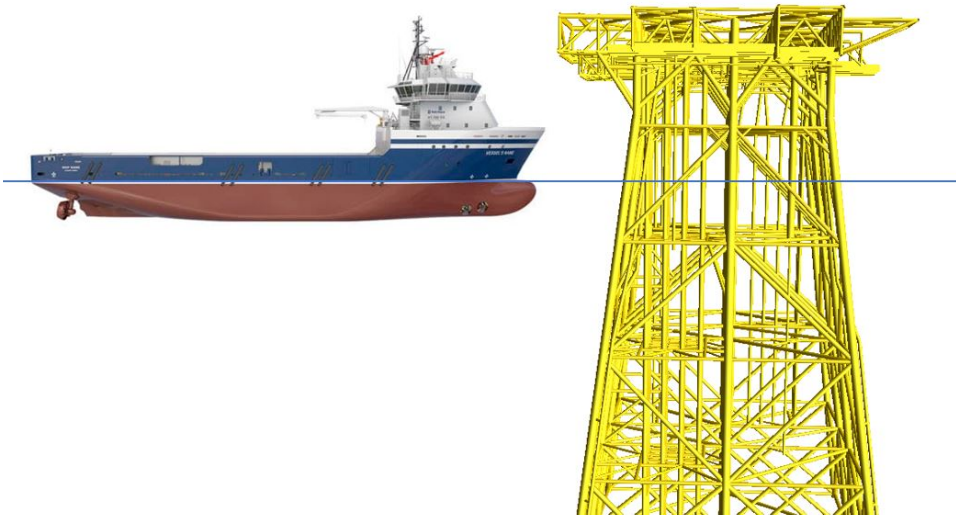

Figure 7.1: Comparison between representative vessel and jacket platform

7.1 Scenario 1: Stern collision against leg C2 and C3

The main focus of scenario 1 is to investigate potential damage to the water injection riser and the gas pipeline behind the brace between leg C2 and C3. For the stern collisions against leg C2 and C3, the collision angle was 42.7 degrees and 45.4 degrees, respectively.

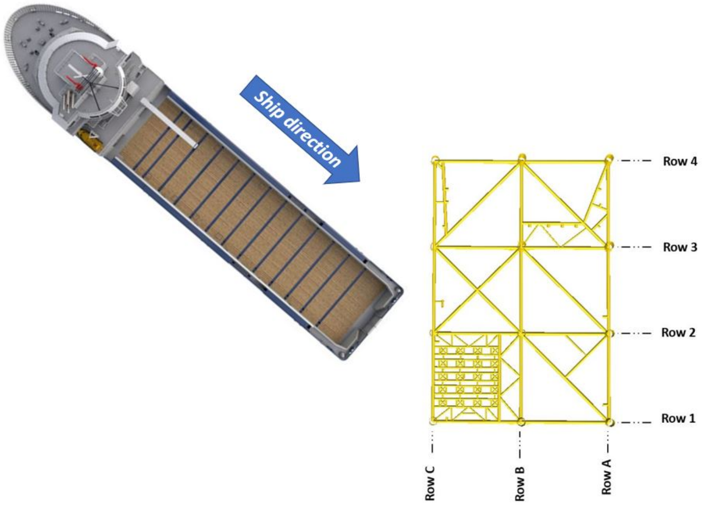
Ship direction
Row 4
Row 3
Row 2
Row 1
Row C
Row B
Row A

Figure 7.2: Side collision against leg C2 and C3

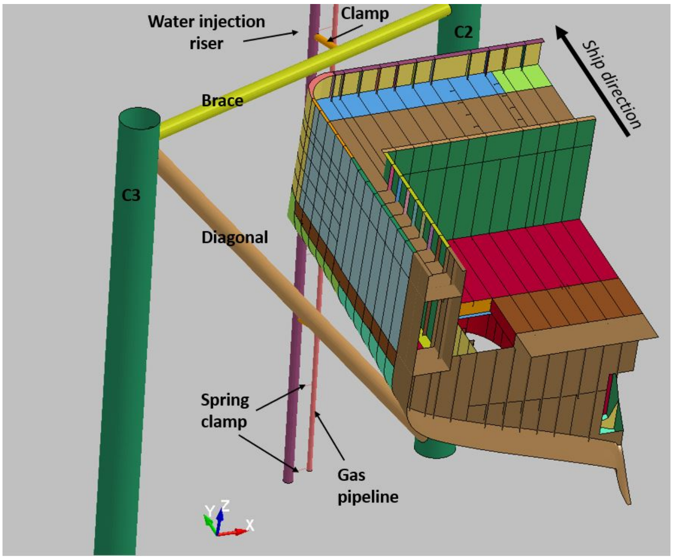
Water injection riser
Clamp
C2
Ship direction
Brace
C3
Diagonal
Spring clamp
Gas pipeline
Y
Z
X

Figure 7.3: Scenario 1 shown in LS-PrePost

7.2 Scenario 2: Side collision against leg A4

The main focus of scenario 2 is to investigate the residual load carrying capacity of the jacket platform if leg A4 is damaged. The collision angle is 45 degrees.

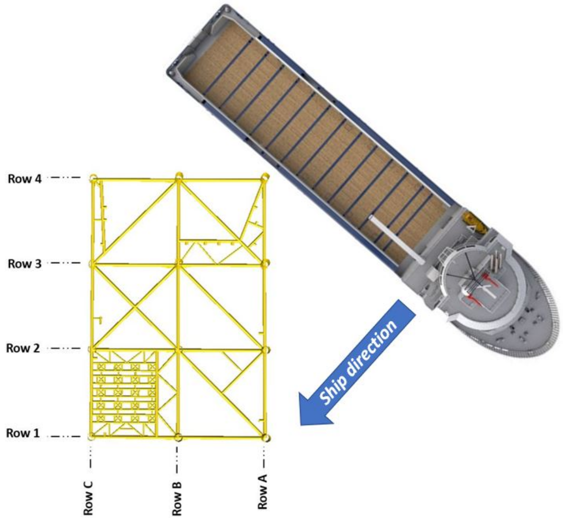
Row 4
Row 3
Row 2
Row 1
Row C
Row B
Row A
Ship direction

Figure 7.4: Side collision against leg A4

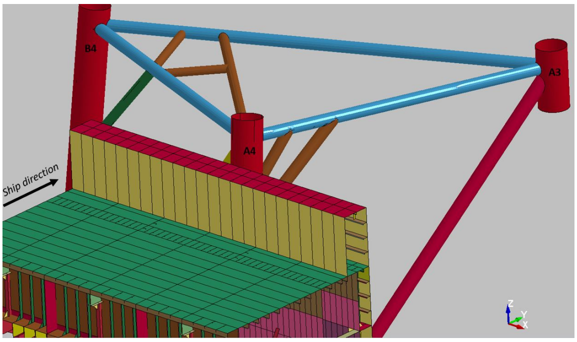
B4
A3
A4
Ship direction
Z
Y
X

Figure 7.5: Scenario 2 shown in LS-PrePost

7.3 Scenario 3: Stern collision against leg A1 and A2

The main focus of scenario 3 is to investigate potential damage to the gas pipeline or oil pipeline behind the brace between leg A1 and A2. The collision angle is 14 degrees.

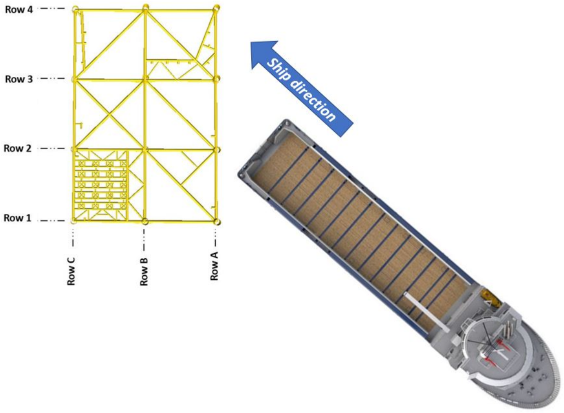
Row 4
Row 3
Row 2
Row 1
Row C
Row B
Row A
Ship direction

Figure 7.6: Stern collision against leg A1 and A2

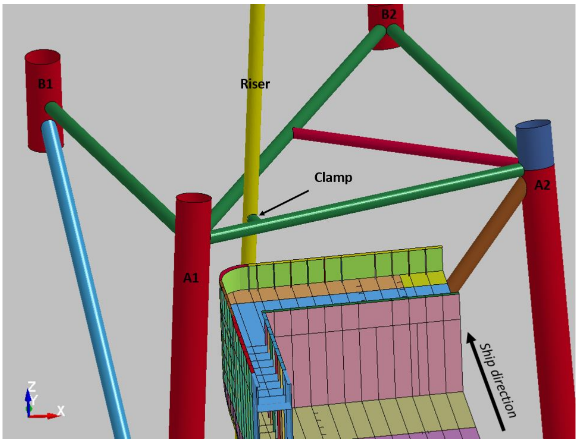
B2
B1
Riser
Clamp
A2
A1
Ship direction
Z
X

Figure 7.7: Scenario 3 shown in LS-PrePost

7.4 Scenario 4: Bow collision against conductor area

The main focus of scenario 4 is to investigate potential damage of the conductor area due to a bow impact. The scenario is a head-on impact.

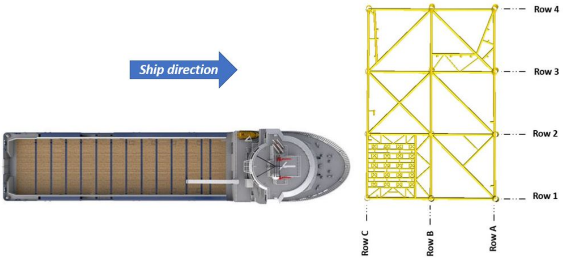
Ship direction
Row 4
Row 3
Row 2
Row 1
Row C
Row B
Row A

Figure 7.8: Bow collision against conductor area

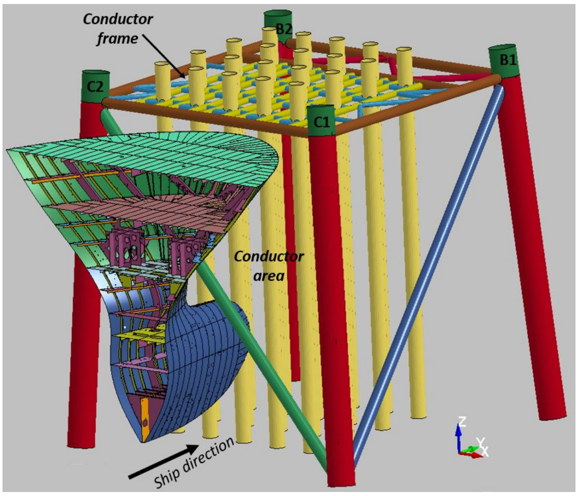
Conductor frame
B2
B1
C2
C1
Conductor area
Ship direction
Z
Y
X

Figure 7.9: Scenario 4 shown in LS-PrePost

7.5 Discussion of global ship motions

The local analyses in LS-DYNA are decoupled which means that global (rigid body) ship motions caused by impact or enviornmental loads are disregarded.

Potential global motions of the ship for Scenario 1 could be that the ship rotates about either leg C2 and C3, which could cause a secondary impact along Row C (see Figure 7.2). Depending on where along the ship side the ship will hit leg A4, a potential side collision along Row A or Row 4 could be possible scenarios for a secondary impact (see Figure 7.4). A secondary impact caused by Scenario 3 could be a side impact along Row A. However, a secondary side impact depends on the collision angle and the amount of water which must be "moved" by the ship. The probability of secondary impacts would have required information regarding the hydrodynamics, such as added mass. Such information have not been taken into consideration and is therefore not accounted for throughout this master's thesis. However, the reader should be aware of that the results of decoupled analyses might not be realistic.

For the bow impact in Scenario 4 there are only a diagonal member protecting the conductors. It is believed that this diagonal is not strong enough to resist a ship impact and it could be that the decoupled method is valid for Scenario 4.

Chapter 8

Method

The method of this master's thesis is summarized in the following steps:

1. **Local analysis in LS-DYNA:** The purpose of the local analysis in LS-DYNA is to investigate the energy dissipation between the ship and the jacket platform. Furthermore, the local deformations shall be studied. Local deformations includes (1) force-deformation behaviour of the ship, (2) deformation behaviour of the jacket and (3) the potential damage to critical elements.
2. **Output from LS-DYNA as input in USFOS:** In USFOS the ship shall be represented by a nonlinear spring. The force-deformation behaviour of the ship obtained from LS-DYNA shall be used as input. Furthermore, the global jacket response shall be compared with the response simulated in LS-DYNA.
3. **Comparison between LS-DYNA and USFOS:** The response of the sturctural jacket sub-model is compared with the response of the jacket in USFOS. Results in LS-DYNA and USFOS shall be discussed in view of both old - and new requirements.

A flow-chart of the method is shown in Figure 8.1

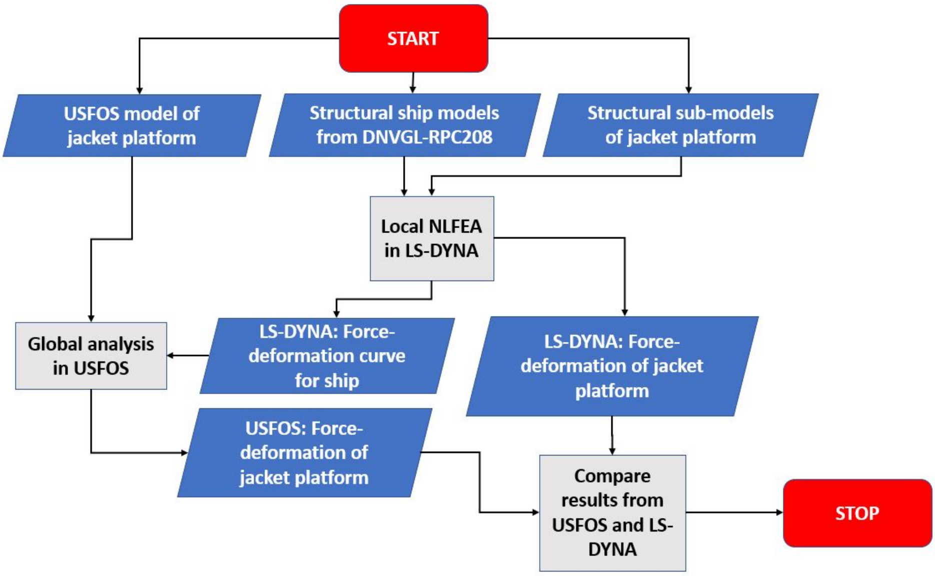
START
USFOS model of jacket platform
Structural ship models from DNVGL-RPC208
Structural sub-models of jacket platform
Local NLFEA in LS-DYNA
Global analysis in USFOS
LS-DYNA: Force-deformation curve for ship
LS-DYNA: Force-deformation of jacket platform
USFOS: Force-deformation of jacket platform
Compare results from USFOS and LS-DYNA
STOP

Figure 8.1: Flow chart of method

The analyses in LS-DYNA are performed quasi-statically. The ship is pushed towards the jacket with a constant speed. A major drawback with this method is that internal - and external mechanics are decoupled. In a realistic case the ship motion will be affected by the struck object or even environmental loads such as wind and waves. Hence, *secondary impacts* will probably occur, as described in Chapter 7.5.

Dynamic analyses in USFOS are performed with the *SURFIMP*-command. (This command is briefly described in Appendix D, while recommendations are described in Appendix E). The nonlinear spring which shall represent the ship is modelled between a jacket node (impact site) and a node with a nodal mass and initial velocity (ship) and the collision energy is determined according to Equation 2.1. For static analyses the nodal mass and initial velocity are replaced with a load which is applied incrementally. In addition, the static command *BIMPACT* is a frequent used command where the collision energy is given as input.

In USFOS secondary impacts could be applied statically with a combination of *BIMPACT* and *MULT_IMP*. The collision energy is specified with BIMPACT and the ship impact will act on the structure until the energy is dissipated. If a member fractures the remaining energy will be transferred to the next element until the given energy is absorbed by the jacket-plattform. Hence the user must guess the most likely collision path of the ship and range the elements in a given order.

Chapter 9

Structural analysis models

9.1 Global platform model for USFOS analysis

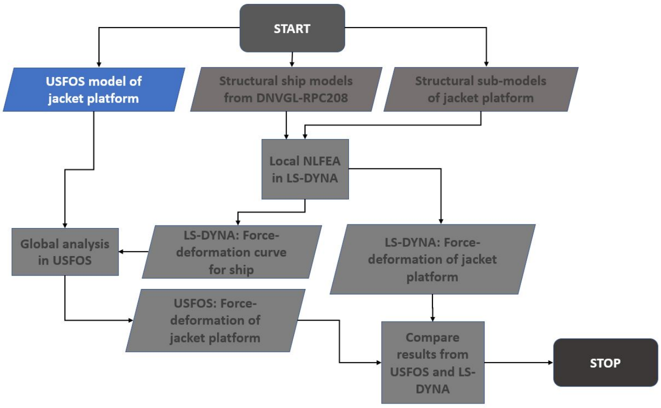
START
USFOS model of jacket platform
Structural ship models from DNVGL-RPC208
Structural sub-models of jacket platform
Local NLFEA in LS-DYNA
Global analysis in USFOS
LS-DYNA: Force-deformation curve for ship
LS-DYNA: Force-deformation of jacket platform
USFOS: Force-deformation of jacket platform
Compare results from USFOS and LS-DYNA
STOP

The reader should notice that the received USFOS-model was originally made for storm analyses. Only minor modifications have been made, which are described in Chapter 9.1. The purpose of this chapter is therefore to give a brief description of the model and the modifications done in order to perform ship impact analyses. The reader should also be aware that the USFOS-model is not modelled by the author.

The platform is shown in Figure 9.1. It is 90 meters between topside and seabed, while the water depth is 72 meters.

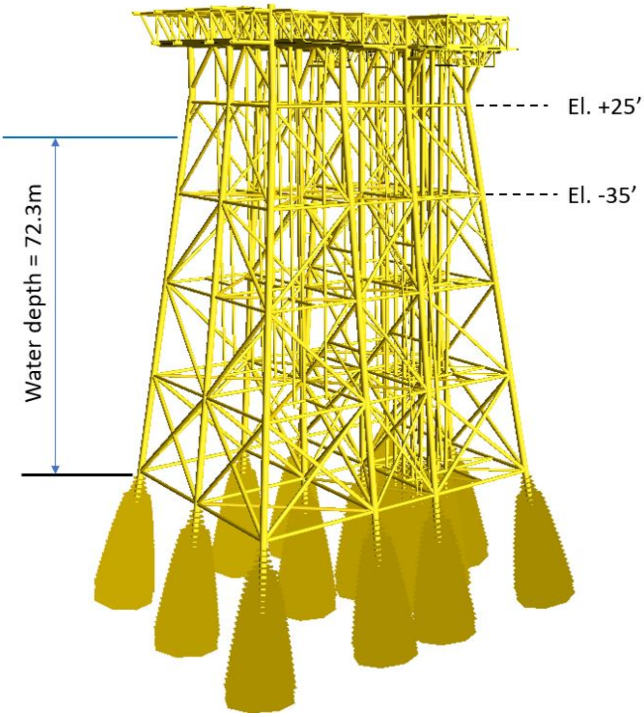

Figure 9.1: Jacket platform with soil layers

Material

The jacket platform is mainly made out of steel St52-3N, also denoted NV-36 and S355. Some elements are made out of steel St.37, also denoted NV-NS and S235. This includes the gas pipeline between leg C1 and C2 and its clamp towards the water injection riser.

Furthermore, the yield stress is thickness dependent, as described in Chapter 6.1.

Element modelling

Close to the mean water level there are many short elements. This might have to do with complex geometry close to elevation +25' (due to joints) but it might also have something to do with hydrodynamic coefficients with respect to splash zone (see Chapter 9.1). Furthermore, at elevation +25' all the joints are modelled with a joint can.

Boundary conditions

The jacket model is modelled with soil layers which shall represent the seabed. No modifications have been made to these layers.

Hydrodynamic coefficients

A jacket-platform is a surface piercing structure which consists of numerous tubular members. According to NORSOK N-003 hydrodynamic forces on such structures should be calculated by Morison's equation, which is expressed in Equation 9.1

$$dF = \rho \frac{\pi D^2}{4} C_M a_x dz + \frac{1}{2} \rho C_D D |u_x| u_x dz \tag{9.1}$$

where ρ is the density of the sea water, D is the diameter of the cylinder, C_M is the mass coefficient, C_D is the drag coefficient, while a_x and u_x is the acceleration - and velocity of the water particles in x-direction, respectively (Morrison et al., 1950).

According to NORSOK N-003 (2017) the drag - and mass coefficient for rough members should be 1.05 and 1.2, respectively. For smooth members, the drag - and mass coefficient should be 0.65 and 1.6, respectively. Roughness might be caused by marine growth which often is the case for members located in the splash zone. Marine growth will also cause an increase in element mass.

Hence, all tubular members which are located in the splash zone (between elevation (+25') and topside) are defined as rough members, while the members located between the seabed and mean water level are defined as smooth members.

Modifications

Originally, the received jacket platform was made for storm analysis. Hence a few modifications have been made:

1. **Bridge removal:** A bridge was included in the received jacket model. In a ship impact analysis the bridge will only contribute with elements to the global model which will not have any influence on the structural integrity. Hence, the bridge was removed and replaced with nodal masses (equal to half of the bridge weight) so that the platform's centre of gravity is maintained.

2. **Small elements:** Another issue was USFOS analysis termination due to failure of small elements close to topside. Since these elements have no influence on the structural integrity of the jacket platform the yield stress is increased in order to avoid analysis termination due to failure of such elements.

3. **Discretization of elements:** As will be described in Appendix E there were some problems with the USFOS-command *SURFIMP (Attach)* close to joints. This was solved by *discretization* (see Figure 9.2). A new node is defined at a impact site and the original element is divided in two.

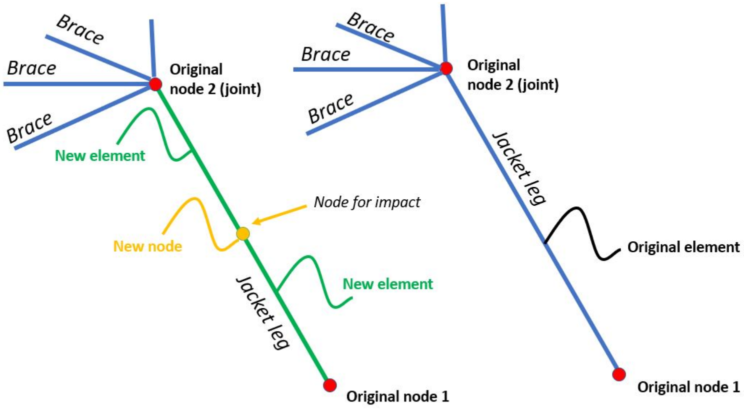
Brace
Brace
Brace
Original node 2 (joint)
New element
Node for impact
New node
New element
Jacket leg
Original node 1
Brace
Brace
Brace
Original node 2 (joint)
Jacket leg
Original element
Original node 1

Figure 9.2: Example of discretization

The effect of the discretization mentioned above might influence the buckling load, which is described in Equation 9.2

$$P_{cr.} = \frac{\pi^2 EI}{(kl)^2} \tag{9.2}$$

where k is a factor which represents the boundary conditions. If a long element is discretized into many smaller elements it was belived to have an influence of the overall load-carrying capacity of the structure. However, USFOS is based upon energy methods and even in case of discretization USFOS will still take the overall length into account. However, finer discretization will cause a problem with yield hinges moving back and forth, a typical *bicycle chain*-effect.

Close to joints in the received USFOS-model there was a problem with short elements, as seen in Figure 9.3. The elements 5458, 5457, 5456 and 5455 have a length of 1.524m, 1.118m, 0.619m and 0.928m, respectively. With respect to fracture strain criteria in USFOS, small elements will in particular be sensitive to small contractions and elongations. Hence, fracture criteria were not applied to shorter elements.

The physical jacket platform has inserted piles which are grouted. This was already taken into account by equivalent thickness and cross section area in the USFOS-model.

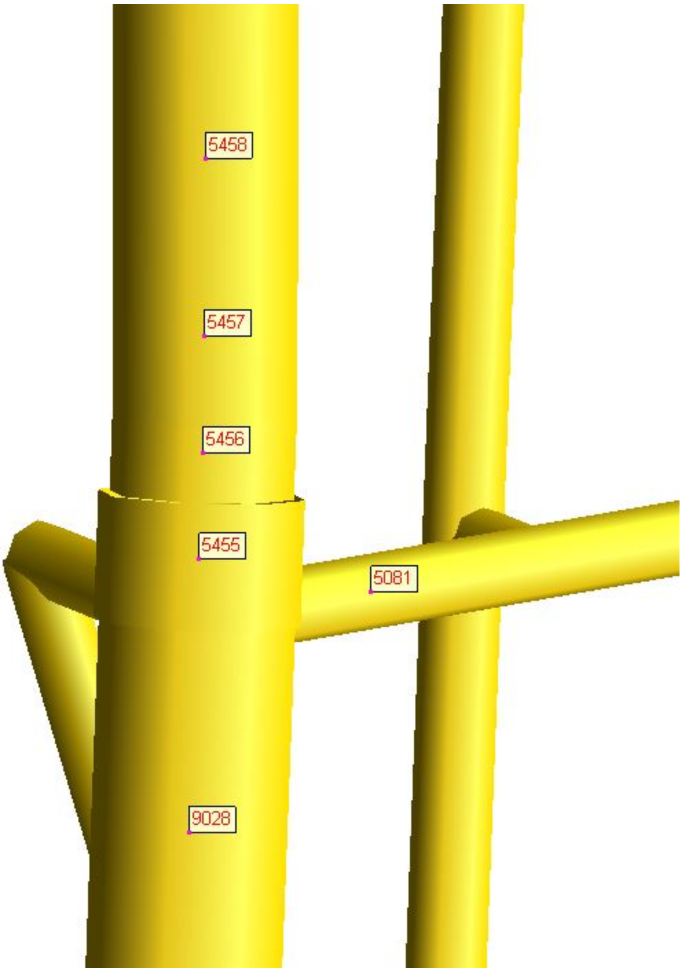
5458
5457
5456
5455
5081
9028

Figure 9.3: Example of small elements in USFOS-model

9.2 Ship models for LS-DYNA analysis

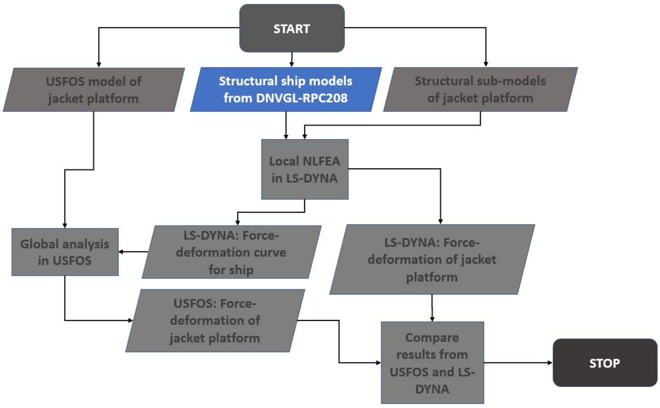
START
USFOS model of jacket platform
Structural ship models from DNVGL-RPC208
Structural sub-models of jacket platform
Local NLFEA in LS-DYNA
Global analysis in USFOS
LS-DYNA: Force-deformation curve for ship
LS-DYNA: Force-deformation of jacket platform
USFOS: Force-deformation of jacket platform
Compare results from USFOS and LS-DYNA
STOP

The structural ship models which are included in the latest version of DNVGL-RPC208 are used in the NLFEA in LS-DYNA. The purpose of this chapter is to give a brief description of the structural models, which are described in more detail in DNVGL 2015-0984 (2016) and DNVGL RPC208 (2016). The structural models have not been made by the author. Hence, only descriptions and citations to relevant documents will be provided.

9.2.1 Material model

All structural ship models use the material model which is described in DNVGL-RPC208 (see Chapter 6.1). All structural models are built with steel type NV-NS (S235) and NV-36 (S355), see Figure 9.4. The mean values are used as material parameters.

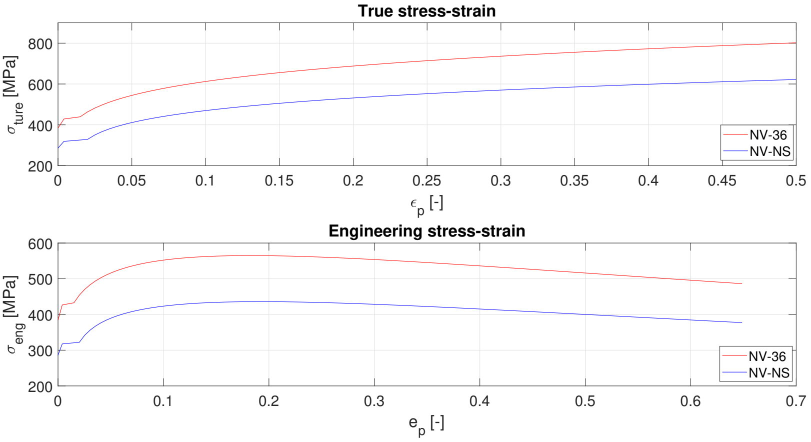

Figure 9.4: True - and engineering stress-strain for NV36 and NVNS

9.2.2 Boundary conditions

Figure 9.5 shows the boundary conditions used for the bow model during the LS-DYNA analyses. In order to keep the bow moving along y-direction the nodes marked in red (the rear end) are only allowed to move in y-direction. Furthermore, the same nodes are given a prescribed velocity of 3m/s. In addition, all the nodes in the bow model is given an initial velocity of 3m/s to avoid deformation lag and shear in the bow-model. The inital velocity decays quick and the bow will therefore not behave as a rigid body. For the side model three control nodes (marked in Figure 9.6) are given a prescribed motion and restriction to only move along the y-axis. These nodes are further coupled to other nodes along the boundary of the structural model.

The stern model is shown in Figure 9.7. Only half of the stern is modelled. All the nodes which lies in the geometric symmetry plane are only allowed to move along the global x-direction. Furthermore, a rigid part which is located in the back of the model are given a prescribed velocity in the x-direction.

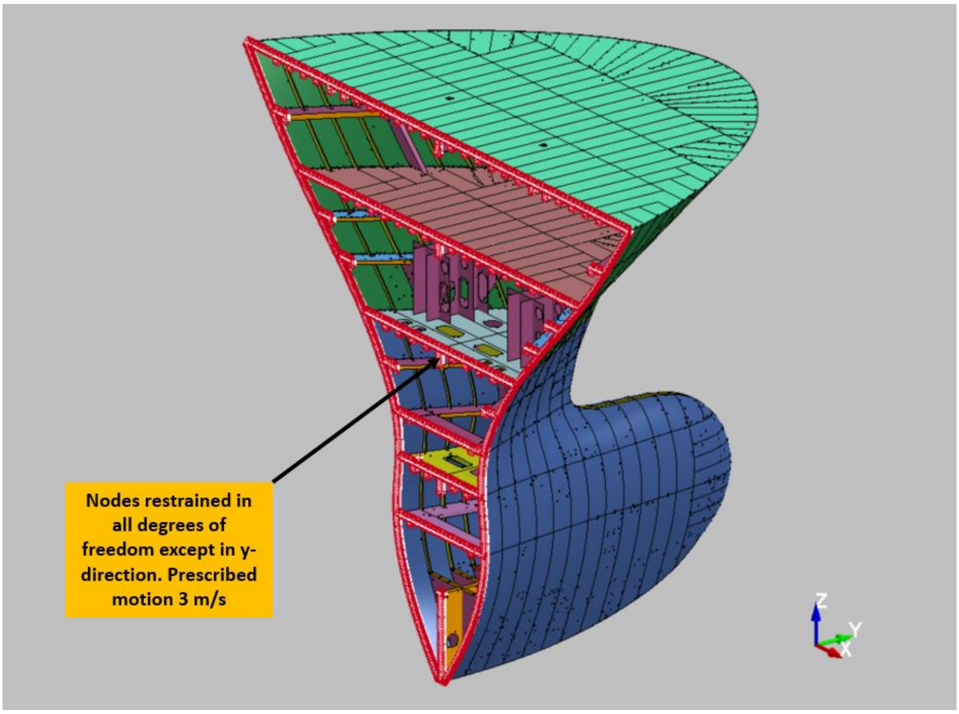
Nodes restrained in all degrees of freedom except in y-direction. Prescribed motion 3 m/s
Z
Y
X

Figure 9.5: Boundary conditions for bow structural model

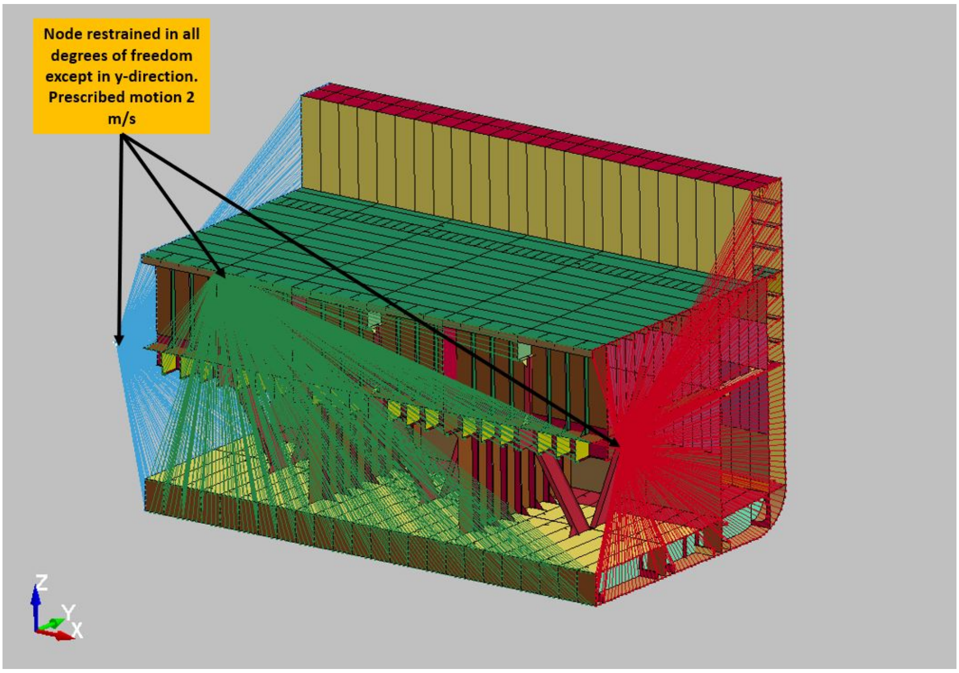
Node restrained in all degrees of freedom except in y-direction. Prescribed motion 2 m/s
Z
Y
X

Figure 9.6: Boundary conditions for side structural model

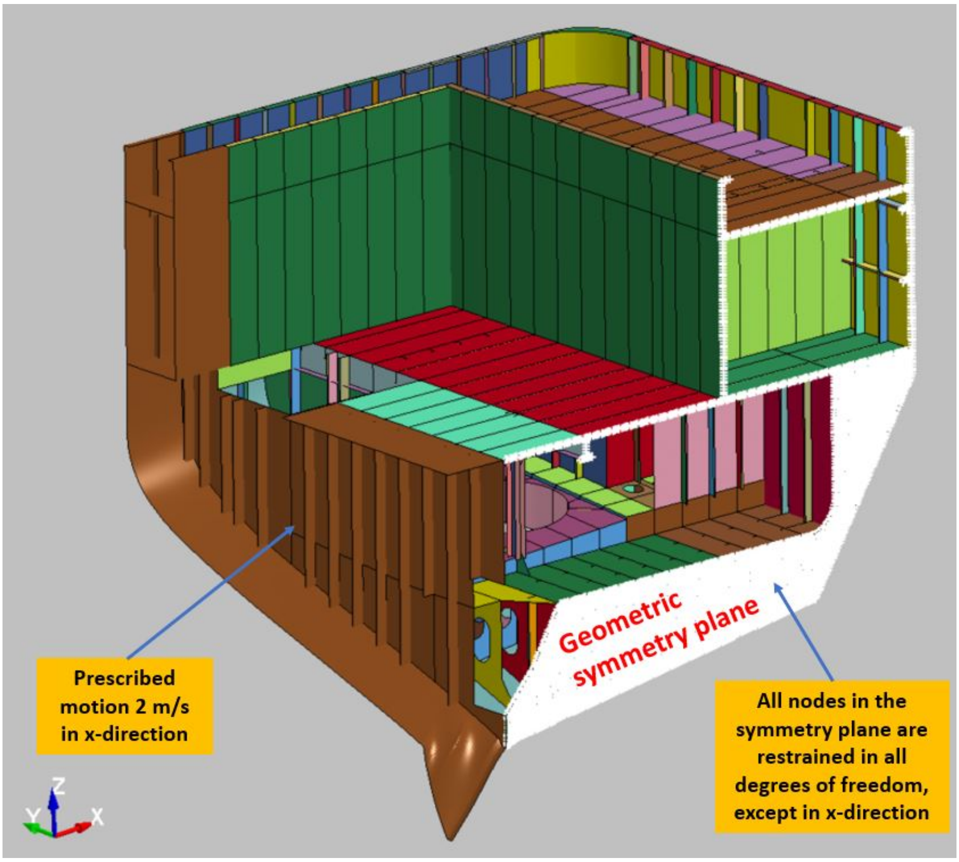

Geometric symmetry plane
Prescribed motion 2 m/s in x-direction
All nodes in the symmetry plane are restrained in all degrees of freedom, except in x-direction
Z
Y
X

Figure 9.7: Boundary conditions for stern structural model

9.2.3 Structural failure

According to DNVGL 2015-0984 (2016) the tensile failure criterion is determined through calibration tests. As a result, the principle failure strain for S235 and S355 is set to 0.177 and 0.174, respectively. However, only the stern - and the side model were given a failure criterion. Since the stability failure load for the bow was close to the failure load the failure criterion was not applied to the bow model (DNVGL 2015-0984, 2016).

9.2.4 Element type

In the LS-DYNA analysis the Belytschko-Lin-Tsay element was used (see Figure 9.8).

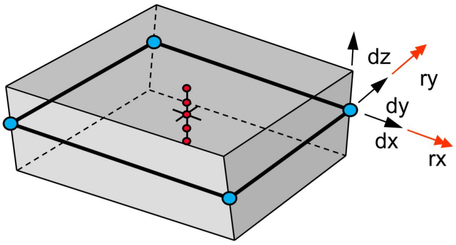

Figure 9.8: Belytschko-Lin-Tsay element Haufe et al. (2013)

As seen in Figure 9.8 the element is a four-noded element. Reduced integration and five through-thickness integration points are used. According to Haufe et al. (2013) and Hallquist (2006) the element is computer efficient.

Furthermore, the element is formulated with Reissner-Mindlin theory (thick-plate theory) in terms of velocity strains and Cauchy stresses. The displacements are defined from the displacements of the mid-surface plane as described in Equation 9.3

$$v = v^m - \hat{z}e_3 \times \theta \tag{9.3}$$

where v^m is the mid-surface velocity, while $\hat{z}$ and θ is the angular velocity and the distance in the fiber direction, respectively (Hallquist, 2006). As described by Haufe et al. (2013) the element does not pass the patch test and is not recommended for coarse mesh due to warpage. However, as argued by Storheim (2015) it is not clearly specified what is meant by a coarse mesh.

9.2.5 Dimensions and mesh size

The dimensions of the bulbous bow, side - and stern corner structural model are shown in Figure B.1, B.2 and B.3

For the structural models the mesh size is approximately in the range 40mm to 55mm (DNVGL 2015-0984, 2016). Both the bulbous bow and stern corner have a mesh size in the range of 50mm - 60mm. In the JIP the structural capacity of the bow model was determined through a collision with a rigid wall, while the side and stern corner were determined through collisions against rigid cylinders with diameters of 1.5m and 10m, respectively. Hence, it was desirable to have a finer mesh at impact area. The middle part of the side model has a fine mesh (50mm) while the rest of the model has a coarser mesh size (170mm), see Figure 9.9.

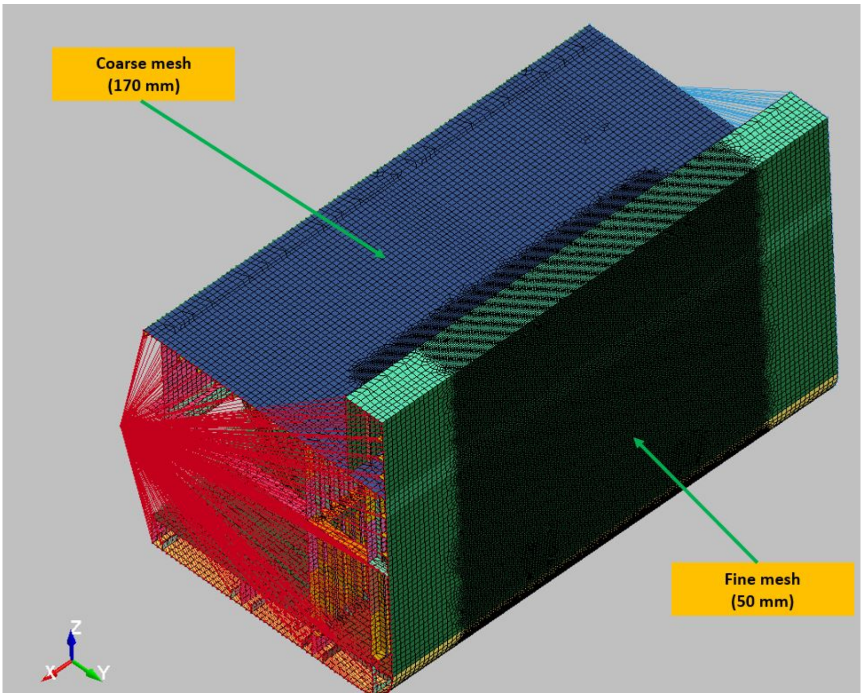
Coarse mesh
(170 mm)
Fine mesh
(50 mm)
Z
X
Y

Figure 9.9: Mesh for structural side model

9.3 Jacket submodels for LS-DYNA analysis

The purpose of this chapter is to describe the structural sub-models of the jacket platform. All structural sub-models are modelled by the author. The sub-models were sketched and meshed in *SESAM GeniE* and then converted to *LS-PrePost*. Node merging and model clean-up were carried out in *LS-PrePost*. The critical elements will be described in Chapter 9.3.5

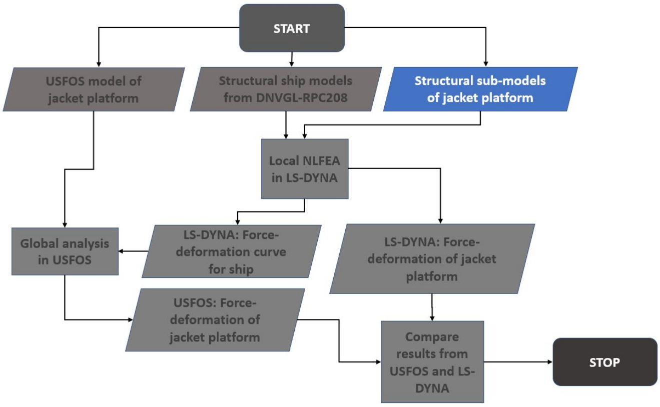
START
USFOS model of jacket platform
Structural ship models from DNVGL-RPC208
Structural sub-models of jacket platform
Local NLFEA in LS-DYNA
Global analysis in USFOS
LS-DYNA: Force-deformation curve for ship
LS-DYNA: Force-deformation of jacket platform
USFOS: Force-deformation of jacket platform
Compare results from USFOS and LS-DYNA
STOP

One structural sub-model of the jacket platform was modelled for each collision scenario. Due to the size, the sub-models are valid for local NLFEA only. In order to study the global response due to joint rotations it would have been desirable with a larger sub-model, e.g. the entire model between elevation $(+25')$ and $(-35')$ (see Figure 9.1). However, this was not done both due to storage and converting of file, but also due to problems with *SESAM GeniE* when the models became to large.

The dimensions are partly based upon structural drawings and partly upon the global USFOS model. All structural sub-models of the jacket platform are shown thorugh Figure 9.10 - 9.13.

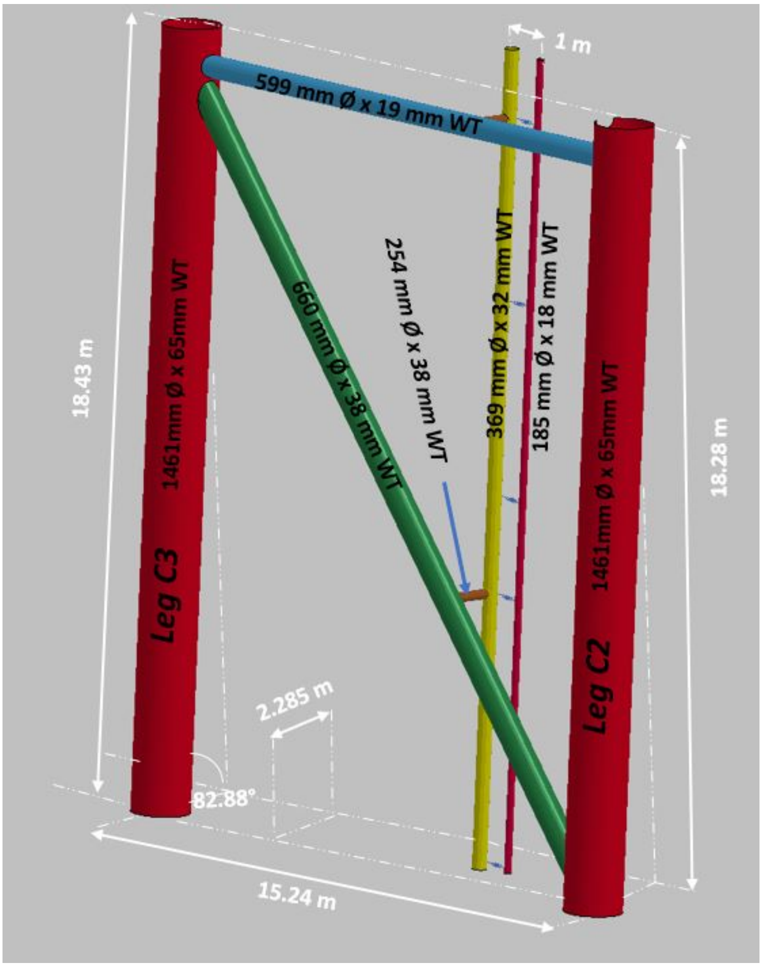
1 m
599 mm Ø x 19 mm WT
18.43 m
1461mm Ø x 65mm WT
Leg C3
660 mm Ø x 38 mm WT
254 mm Ø x 38 mm WT
369 mm Ø x 32 mm WT
185 mm Ø x 18 mm WT
1461mm Ø x 65mm WT
Leg C2
18.28 m
2.285 m
82.88°
15.24 m

Figure 9.10: Dimensions of structural jacket sub-model for collision scenario 1

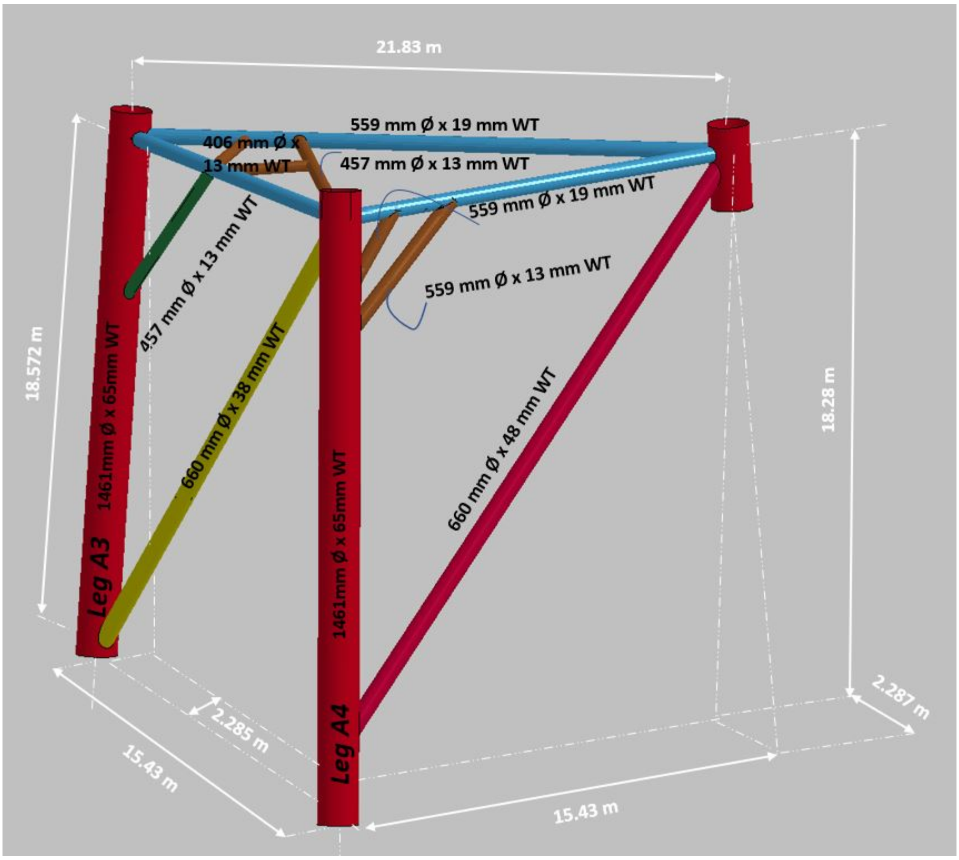
21.83 m
559 mm Ø x 19 mm WT
406 mm Ø x 13 mm WT
457 mm Ø x 13 mm WT
559 mm Ø x 19 mm WT
457 mm Ø x 13 mm WT
559 mm Ø x 13 mm WT
18.572 m
1461mm Ø x 65mm WT
Leg A3
660 mm Ø x 38 mm WT
1461mm Ø x 65mm WT
660 mm Ø x 48 mm WT
18.28 m
Leg A4
2.285 m
15.43 m
15.43 m
2.287 m

Figure 9.11: Dimensions of structural jacket sub-model for collision scenario 2

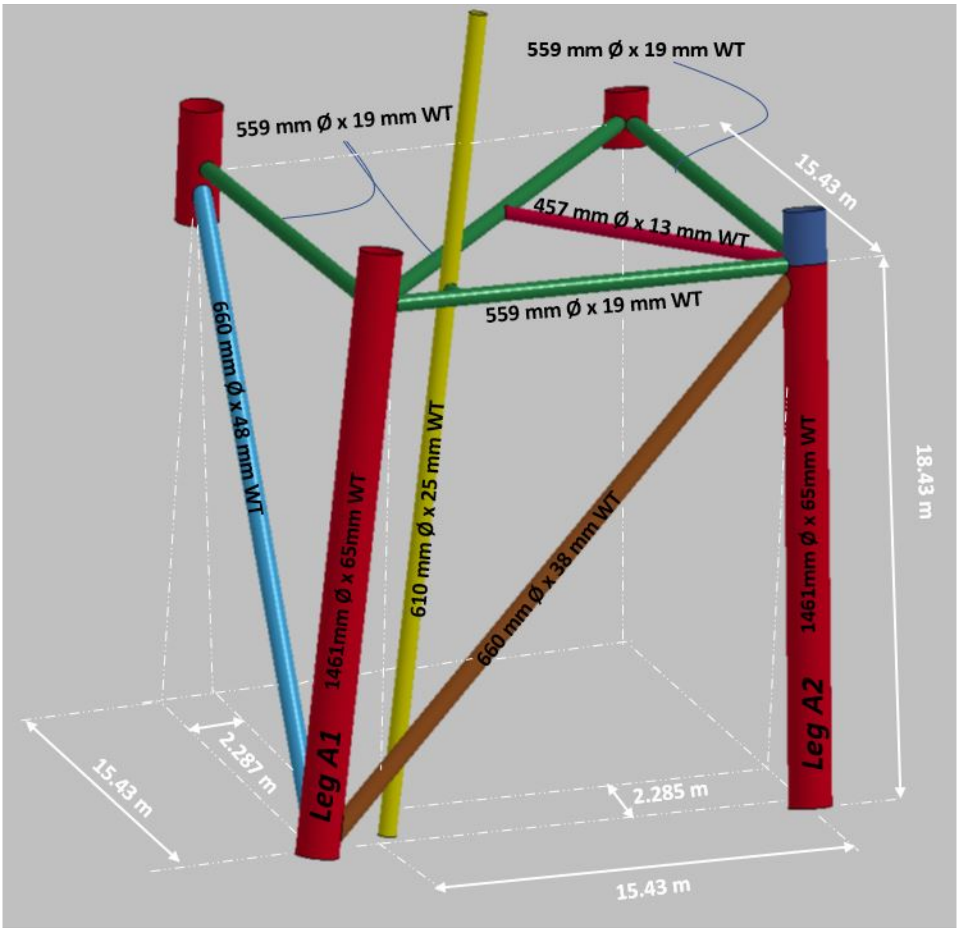
559 mm Ø x 19 mm WT
559 mm Ø x 19 mm WT
15.43 m
457 mm Ø x 13 mm WT
559 mm Ø x 19 mm WT
660 mm Ø x 48 mm WT
1461mm Ø x 65mm WT
610 mm Ø x 25 mm WT
660 mm Ø x 38 mm WT
1461mm Ø x 65mm WT
18.43 m
Leg A1
Leg A2
15.43 m
2.287 m
2.285 m
15.43 m

Figure 9.12: Dimensions of structural jacket sub-model for collision scenario 3

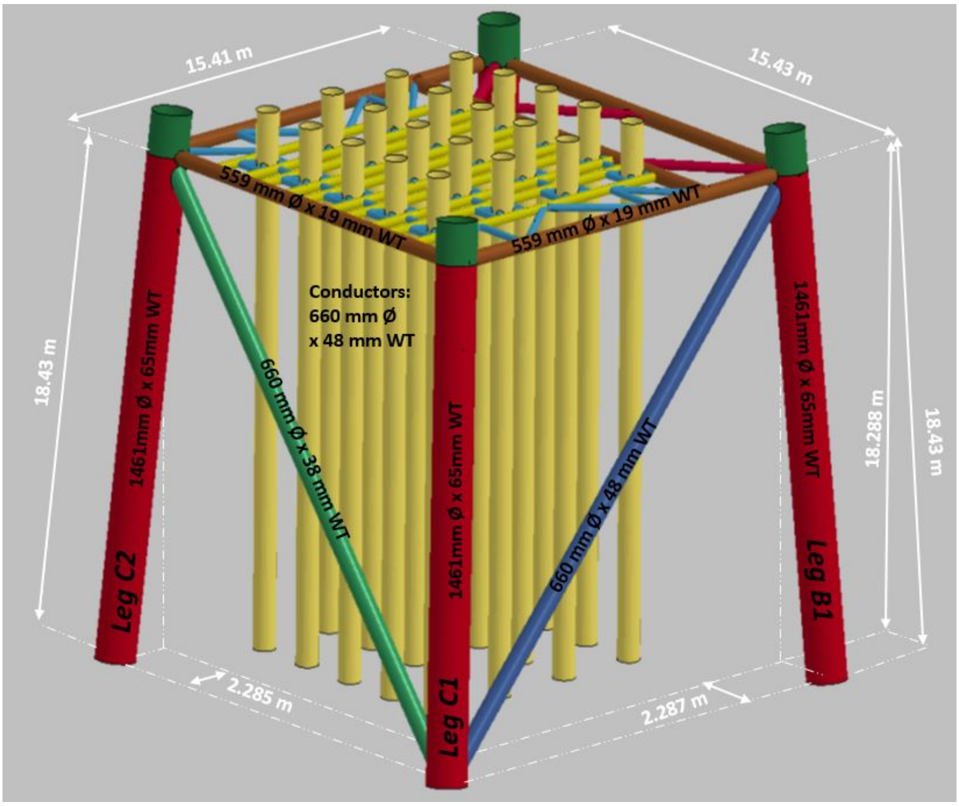
15.41 m
15.43 m
559 mm Ø x 19 mm WT
559 mm Ø x 19 mm WT
Conductors:
660 mm Ø
x 48 mm WT
18.43 m
1461mm Ø x 65mm WT
Leg C2
660 mm Ø x 38 mm WT
1461mm Ø x 65mm WT
Leg C1
660 mm Ø x 48 mm WT
1461mm Ø x 65mm WT
Leg B1
18.288 m
18.43 m
2.285 m
2.287 m

Figure 9.13: Dimensions of structural jacket sub-model for collision scenario 4

9.3.1 Inaccuracies

Due to time limitations and lack of experience by the author, there are some inaccuracies that have to be taken into account regarding the structural sub-models of the jacket platform:

1. **Joint cans and brace stubs:** The structural sub-models contain neither joint cans or brace stubs. Hence, it is assumed that the sub-models will appear softer than initially anticipated, since the joint can and brace stub will cause a more rigid behavior of the joint as a whole. A solution could have been to adjust the thickness close to the joint, but this was not done due to the inaccuracies it would have caused with the already modelled diameter of the leg.

2. **Welds and imperfections:** Welds and imperfections are not taken into account.

3. **Conductor frame:** The conductor frame was based upon the global USFOS-model. However, in reality the conductor frame is rather compact with small stiffened plates keeping the conductors in place.

9.3.2 Boundary conditions

For all of the structural sub-models the jacket legs are fixed in the lower end. However, to avoid spurious membrane forces and to trig both the buckling - and denting behaviour the jacket legs were permitted to move vertically (global z-direction) in the upper end. However, the upper end of the jacket legs were fixed against translation in global x- and y-direction and against rotations. The choice of boundary conditions were inspired by LS-DYNA simulations of ship impact towards the leg of the Grane plattform done by Johansen and Amdahl (2000).

9.3.3 Element type and mesh size

Belytschko-Lin-Tsay element (see Figure 9.8) with reduced integration and 5 number of through thickness integration points are used. The mesh size for the structural sub-models are mainly 100mm x 100mm and uniform mesh is used for each part. Smaller - and badly shaped elements were eliminated by node-merging in LS-PrePost.

9.3.4 Material

As described in Chapter 9.1, the jacket is mainly made out of steel St53-2N (S355), while some critical members are made of St37 (S235).

In LS-DYNA, the chosen material type for the structural jacket sub-models is the same which was used for the structural ship models in LS-DYNA:
MAT_MODIFIED_PIECEWISE_LINEAR_PLASTICITY.
The advantage of this material type is that the user can specify both a stress-strain curve and a failure criterion (DYNAmore, 2018a) (The failure criterion will be further described in Chapter 9.3.6). Based upon recommendations by Storheim (2015) materials with physical yield values and a smooth stress-strain curve should be used for NLFEA in LS-DYNA. The material is defined with an elastic modulus E, density ρ, Poisson's ratio ν and a yield stress σ_y. When yield is reached, the stress-strain relationship will follow the user-defined stress-strain curve. Thus, σ_{prop} (see Figure 6.1) was given as yield stress into the material model.

Stress-strain curves for the materials used in the structural jacket sub-model is shown in Figure 9.14 and 9.15 compared with NV-NS and NV-36 which is used in the structural ship models. Since the jacket platform is the structure of concern the low resistance values for S355 and S235 are used (see Table 6.1). The curves in Figure 9.14 are used as input in LS-DYNA while the curves in Figure 9.15 are the same curves converted into engineering stress - and strain, according to Equation 4.23 and 4.25.

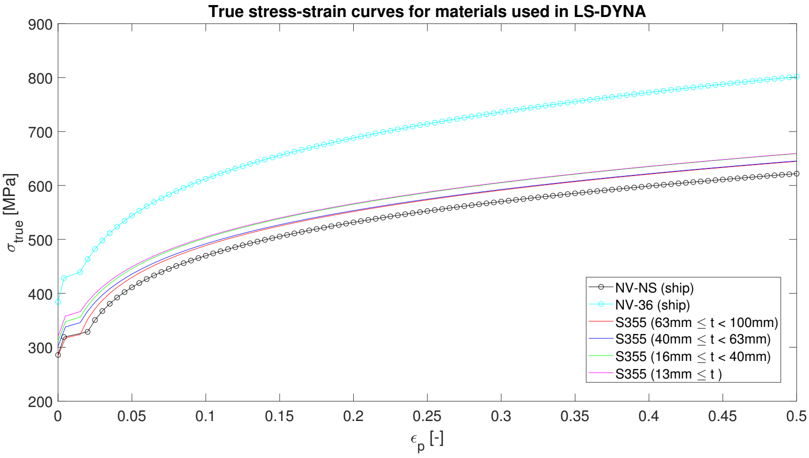

Figure 9.14: True stress-strain curves for materials used in LS-DYNA structural model

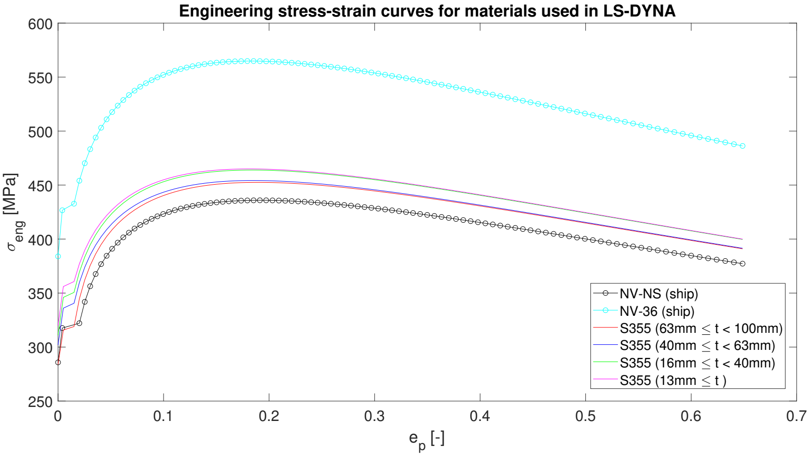

Figure 9.15: Engineering stress-strain curves for materials used in LS-DYNA structural model

9.3.5 Description and modelling of critical elements

The purpose of this chapter is to describe the critical elements which shall be included in the local analyses. A physical presentation will be followed by a modelling part where the choices of modelling is presented. The risers are shown in Figure 9.16

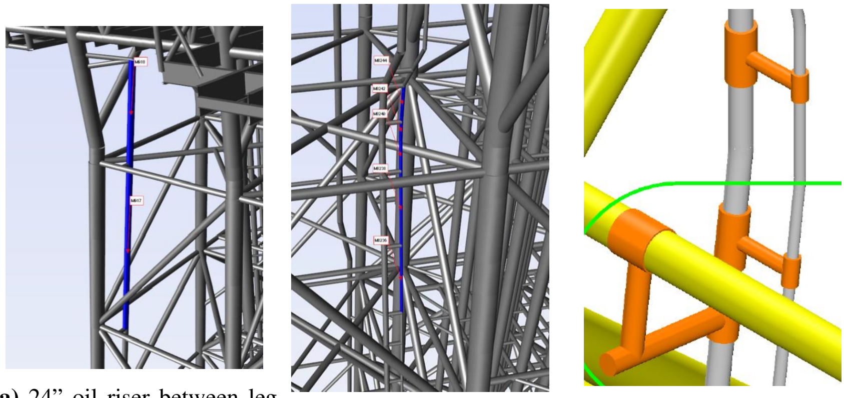

(a) 24” oil riser between leg A1 and A2

(b) 6” gas pipeline between leg C2 and C3

(c) Clamp for risers between leg C2 and C3

Figure 9.16: Critical elements

The risers are connected to the jacket structure by clamps, which can be seen in Figure 9.16c. Based upon recieved information, the risers are able to move vertically thorugh the clamp, even though the vertical motions are small and almost negligible. According to the global USFOS-model the clamps are made in steel type St.37

A major inaccuracy regarding the critical elements is that internal pressure is not taken into account. The 24” riser (see Figure 9.16a has an internal pressure of 20 bar, while the 6” riser (see Figure 9.16b) has an internal pressure of 140 bar. For the gas pipeline in circumferential direction this equals an circumferential stress $\sigma_\theta = 36MPa$. With a yield stress $f_y = 225MPa$ the internal pressure cause an utilization of 15%.

Both internal pressure and temperatur will affect the ultimate stress, see Appendix A - A.2. However, the temperature effects are not considered but the reader should be aware of that such contributions might affect the ultimate capacity.

As mentioned in Chapter 9.3.1 the risers are connected to the jacket platform by clamps and even free to move vertically through these clamps. The modelling of the clamps and configurations of the critical elements were done through *trial-and-error*. Due to lack of modelling knowledge in GeniE by the author and some computer difficulties the clamps between risers and jacket were modelled with shell elements with equivalent diameter and thickness (see Figure 9.17a). The clamps between the water injection riser and the gas riser between leg C2 and C3 (see Chapter 7.1) were modelled as a spring with stiffness k_{clamp}

$$k_{clamp} = \frac{E_{clamp} A_{clamp}}{L_{clamp}}$$

where E_{clamp}, A_{clamp} and L_{clamp} is the elastic modulus, cross section area and length of the clamp, respectively.

For the conductors there are two potential failure modes: (1) local deformations which can cause local fracture/rupture and (2) global deformations which can cause the conductors to be pulled out of the wellheads at the seabed. However, due to the modelling (see Chapter 9.3.1) the conductors were perfectly connected to the frame and the motions will therefore be controlled by the frame. The upper part of the conductors was attached to the conductor frame while the lower part was fixed in all degrees of freedom but with the permission to move vertically. Internal pressure in the conductors is not taken into account. Based upon received information the conductors are normally open towards the atmosphere and the area between the conductor and outer casing is grouted, which gives a high bending capacity.

The structural sub-models of the jacket were not made large enough to reach topside. In addition to both time limitations and lack of experience by the author and problems with *SESAM GeniE* due to small element sizes deck penetrations and flanges was not taken into account.

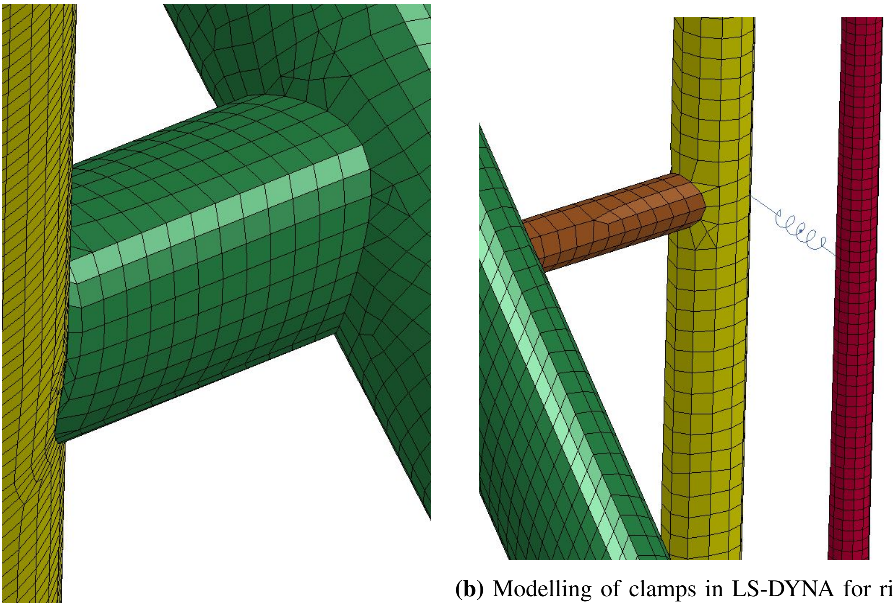

(a) Clamp modelling for 24” riser

(b) Modelling of clamps in LS-DYNA for risers between leg C2 and C3

Figure 9.17: Critical elements

9.3.6 Structural failure

As failure criterion a major plane strain was chosen. This is the same failure criterion which was used for the structural side - and stern model (see Chapter 9.2.3). Since the failure major plane strain for the structural stern - and side model were mainly 0.17 the failure criterion for the jacket sub-models was set to 0.15 to be on the conservative side. However, as mentioned in Chapter 6.3 the choice of fracture criteria in FEA is a complex procedure which depends on element length. A mesh convergence study was not carried out for the NLFEA in LS-DYNA which is a big source of error. Even though NORSOK N-004 (rev.3) (2013) recommends a critical strain of 15% for S355 such values shall not be chosen without considering geometrical properties of the structure. Unfortunately this was not given that much prioritization by the author and when it was discovered, there was no time to redo the analyses in LS-DYNA.

Chapter 10

Local collision analysis (LS-DYNA)

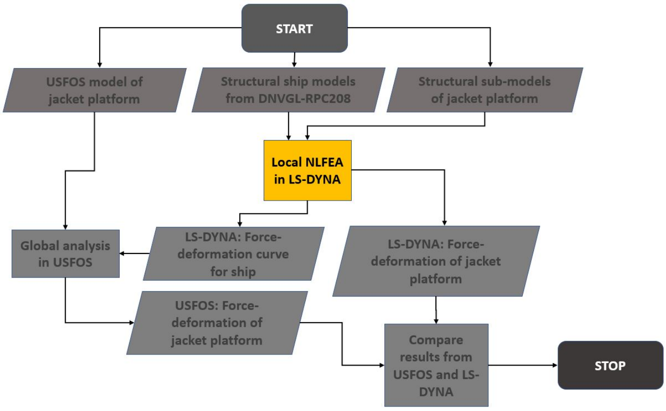
START
USFOS model of jacket platform
Structural ship models from DNVGL-RPC208
Structural sub-models of jacket platform
Local NLFEA in LS-DYNA
Global analysis in USFOS
LS-DYNA: Force-deformation curve for ship
LS-DYNA: Force-deformation of jacket platform
USFOS: Force-deformation of jacket platform
Compare results from USFOS and LS-DYNA
STOP

10.1 Summary of LS-DYNA results

Table 10.1 gives a summary of the achieved energy levels for each scenario and information regarding the energy dissipation.

In scenario 1 against leg C2 and scenario 3 the total collision energy level was not reached, due to choice of collision angle, ship direction and limitations in the analysis setup. However, for these simulations it was desirable to study the damage potential on risers.

Table 10.1: Summary of LS-DYNA results

Scenario	**Energy level reached**	**Energy dissipation**		**Comment**
1	16.5 MJ	Jacket Ship	2.5 MJ 14.5 MJ	Stern collision against leg C2
1	10.1 MJ	Jacket Ship	9MJ 1.1 MJ	Stern collision against leg C3
2	21 MJ	Jacket Ship	15.68 MJ 5.38 MJ	Side collision against leg A4
3	11.43 MJ	Jacket Ship	10.5MJ 0.93MJ	Stern collision against leg A2
4	37.13 MJ	Jacket Ship	7.13MJ 30 MJ	Bow collision against conductor area

With NLFEA-results from LS-DYNA it is possible to study the local deformations of both the structural sub-models of the jacket and the structural ship models.

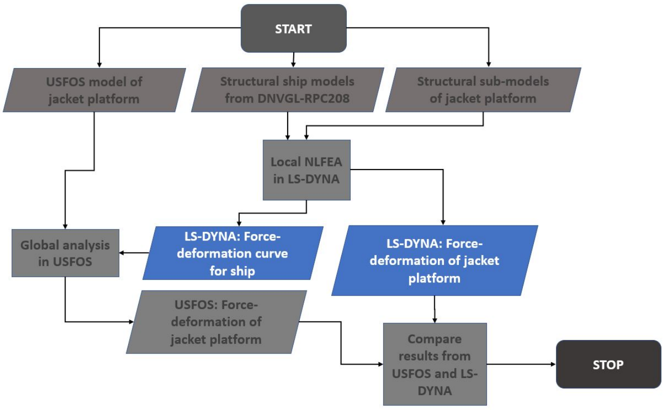
START
USFOS model of jacket platform
Structural ship models from DNVGL-RPC208
Structural sub-models of jacket platform
Local NLFEA in LS-DYNA
Global analysis in USFOS
LS-DYNA: Force-deformation curve for ship
LS-DYNA: Force-deformation of jacket platform
USFOS: Force-deformation of jacket platform
Compare results from USFOS and LS-DYNA
STOP

10.2 Scenario 1: Stern collision against leg C2 and C3

Figure 10.1 shows the force-deformation curve for the stern during the collision against leg C2, while the corresponding energy absorption for jacket and ship is shown in Figure 10.2.

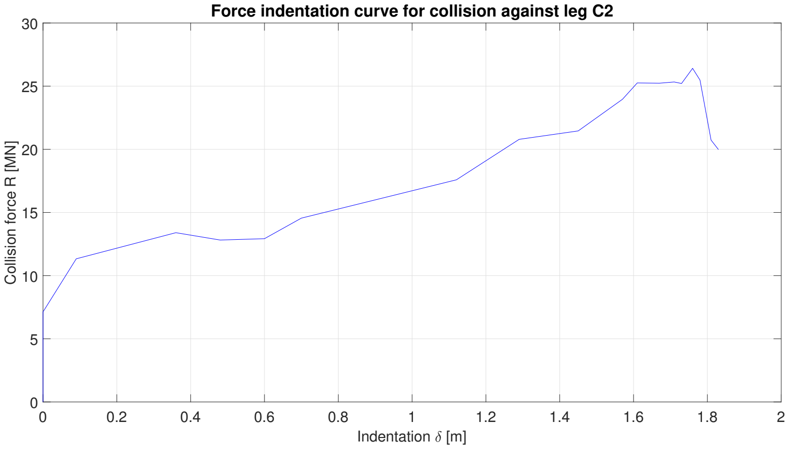

Figure 10.1: Force-deformation curve for stern (Collision against leg C2)

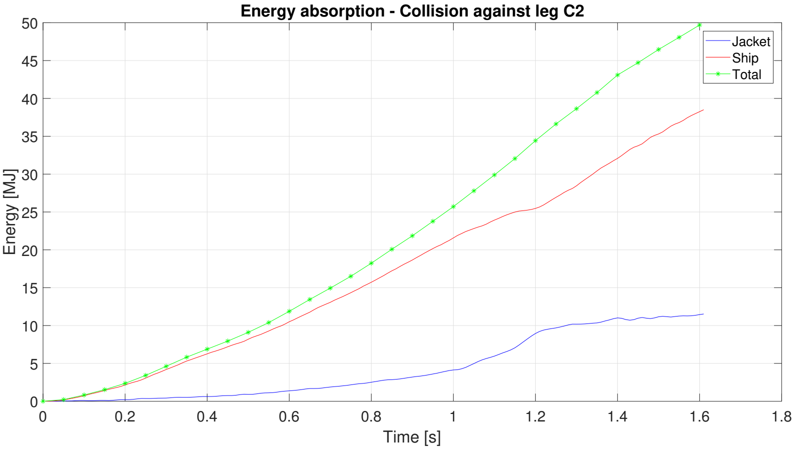

Figure 10.2: Energy absorption for collision against leg C2

For the collision against leg C2 (see Figure 10.2) the stern contribute to a major part of the energy dissipation. This is because the stern is crushed towards the jacket leg. However, there are uncertainties with respect to the boundary conditions. The collision takes place close to the geometric symmetry plane of the stern corner (see Figure 9.7). As a result, the ship may appear softer than it would have done in reality. However, it is clear that with the angle of attack there is a severe damage potential to the risers between leg C2 and C3.

For the collision against leg C3 the stern first hits the diagonal which collapses in a three-hinge mechanism. The dent caused by the diagonal is small and the collision against leg C3 has therefore not been presented in terms of force-deformation curves. Instead, Figure 10.3 shows the force versus time curve for stern collision against leg C3.

It is not clear what is causing the drop at t=0.7 sec. due to inaccurate boundary conditions of the gas pipeline, but the gas pipeline undergoes large deformations during impact with the stern. Fracture occurs in the clamp near the brace at t=1 sec. At t=1.25 second, the water injection riser fractures close to the upper boundary. The deformations are large, but due to inaccurate boundary conditions it is questionable if the riser would rupture in reality. At t=1.8 sec. the diagonal between leg C2 and C3 fractures close to leg C3, which causes the drop in Figure 10.3. According to energy measure in LS-DYNA, the diagonal absorbs 5MJ before it fractures. However, due to tension forces in the clamp between the diagonal and the water injection pipeline the diagonal has already been utilized at the middle before it is struck by the stern.

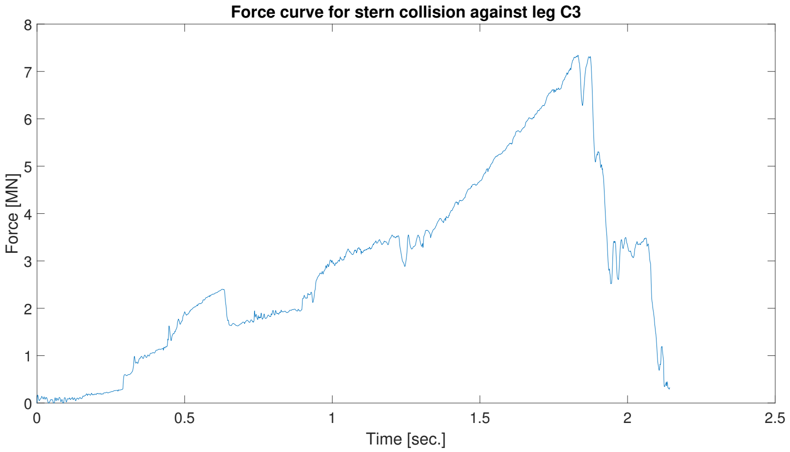

Figure 10.3: Force-time curve for stern against leg C3

The energy absorption for the collision against leg C3 is shown in Figure 10.4. In Figure 10.4 it can be seen that the jacket platform absorbs most of the collision energy. This is reasonable based upon the deformations and it seems reasonable since the diagonal participates in the collision. As the diagonal collapses in a three-hinge mechanism approximately 10MJ has been absorbed by both objects. It is believed that the remaining part of the collision energy will be absorbed by jacket leg C3, but as mentioned the simulation terminated before the desirable energy level was reached.

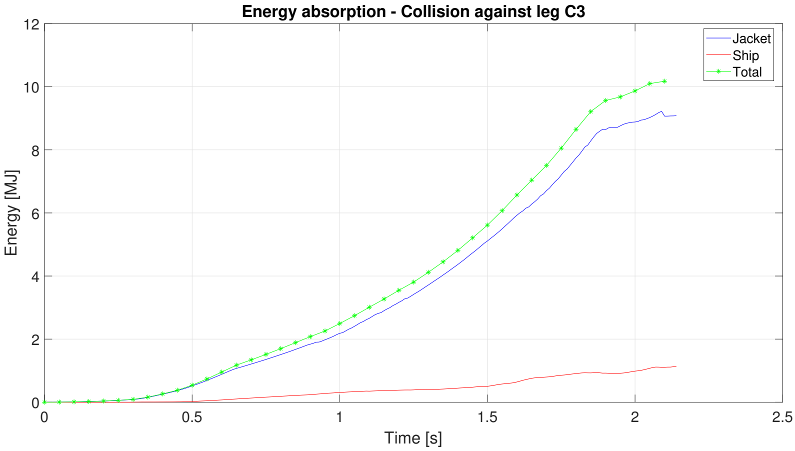

Figure 10.4: Energy absorption for collision against leg C3

At the given attack angles of the stern, the risers face severe damage before the stern hits either leg C2 or leg C3. Especially the clamp between the diagonal and water injection riser is subjected to high stresses which can cause damages on both diagonal and risers. To model the clamp between the two risers as an axial spring turned out to not be a good idea, since the global deformations of the gas pipeline became to large. In addition the spring is connected between one node at each riser which is causing non-physical hot spots at the risers. Hence, more accurate modelling of the clamps are recommended in order to achieve a more credible result but due to time limitations and lack of experience by the author it was not possible to model the riser clamp more accurate. After the analysis was performed, the author became aware of that Storheim (2015) had not recommended use of axial springs in NLFEA in LS-DYNA. However, it is demonstrated that a stern corner collision against both leg C2 and leg C3 is able to cause severe damages to the risers.

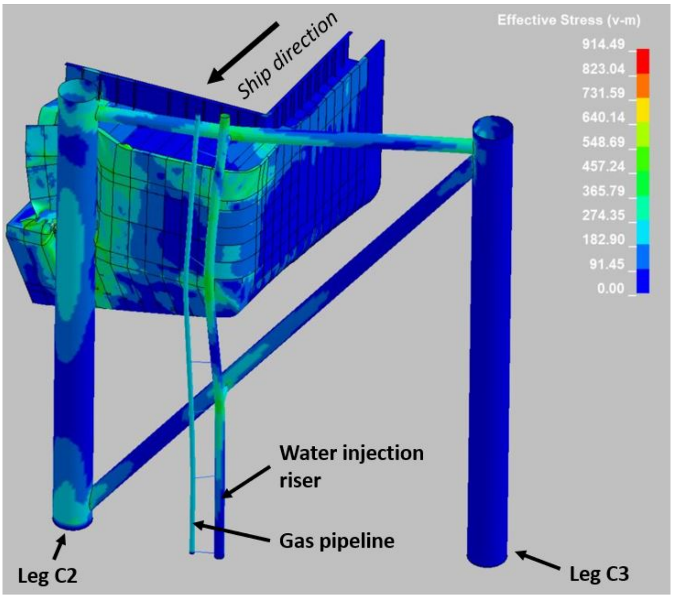
Ship direction
Effective Stress (v-m)
914.49
823.04
731.59
640.14
548.69
457.24
365.79
274.35
182.90
91.45
0.00
Water injection riser
Gas pipeline
Leg C2
Leg C3

Figure 10.5: von-Mises plot of the collision against leg C2 when the entire collision energy is absorbed

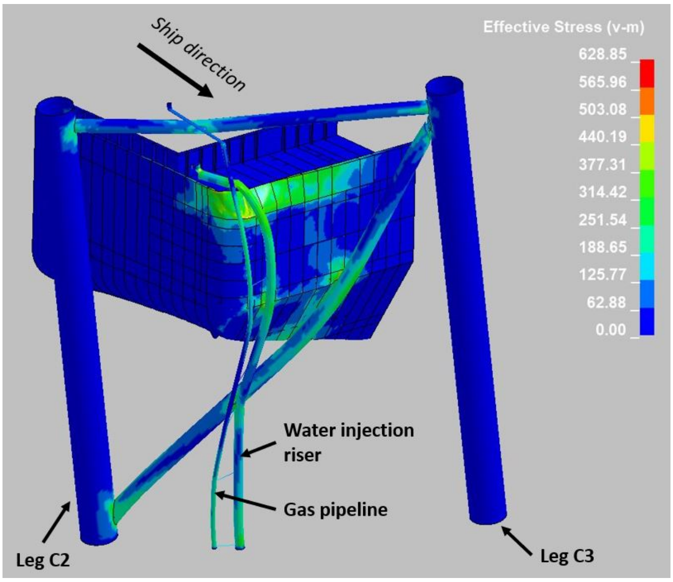
Ship direction
Effective Stress (v-m)
628.85
565.96
503.08
440.19
377.31
314.42
251.54
188.65
125.77
62.88
0.00
Water injection riser
Gas pipeline
Leg C2
Leg C3

Figure 10.6: von-Mises plot of the collision against leg C3

10.3 Scenario 2: Side collision against leg A4

The force-deformation curve for the side collision against leg A4 is shown in Figure 10.7. There is only one contact point between the ship and the jacket, and the collision energy is therefore transferred through this point. As can be seen, a major part of the collision energy is dissipated as deformation energy in the jacket. The collision force is transferred to adjacent members which as a result undergo global deformations (see Figure 10.12 and 10.11). Since deformations occur not only in leg A4 but in adjacent braces as well it is believed that the force-deformation behaviour of the jacket presented in Figure 10.7 is too conservative, since the collision force is plotted towards the dent depth in jacket leg A4 and deformations in adjacent members are not considered. If time had allowed it would have been desirable to establish an expression for an equivalent force-deformation relationship for the jacket platform, but this has not been done.

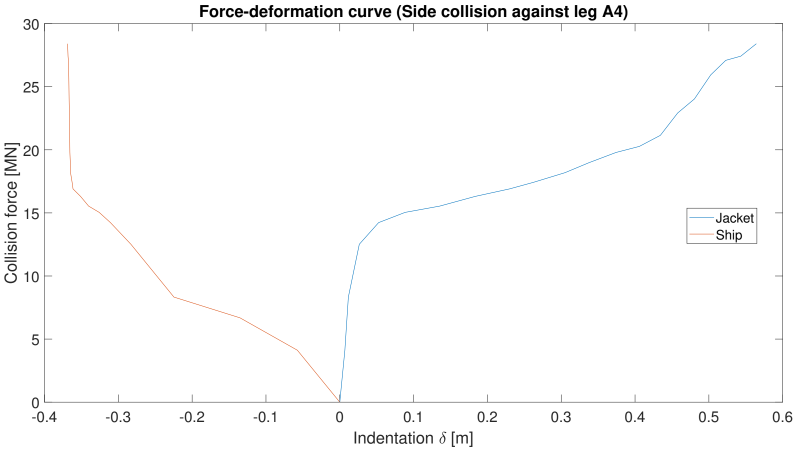

Figure 10.7: Force-deformation curve for side collision against leg A4

A time-dependent energy-absorption plot is shown in Figure 10.8. In total, 15.68 MJ and 5.32 MJ of the collision energy are absorbed by the jacket and the ship, respectively.

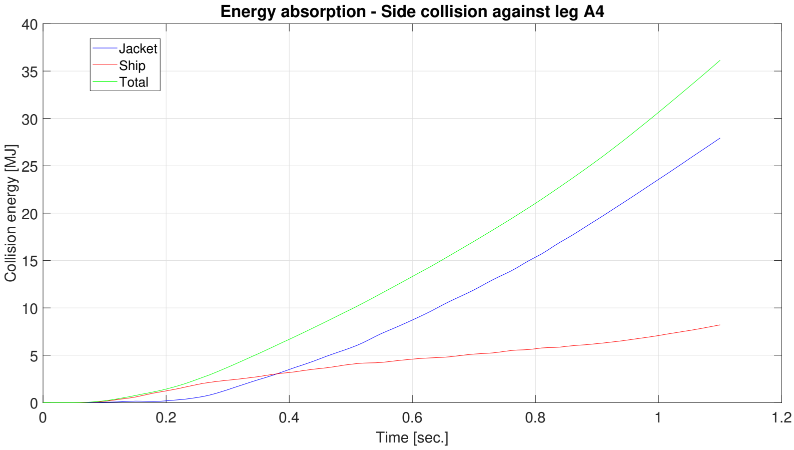

Figure 10.8: Energy absorption for collision against leg A4

As seen in Figure 10.8 the ship dissipates most of the energy until T=0.4 seconds. During the first part of the collision, the collision energy contributes to local deformations of a plate in the ship model which can be seen in Figure 10.9 - 10.10. At T=0.4 seconds the plate (and hence the ship) becomes strong enough and deformations starts to take place in the jacket leg. It is believed that there are the membrane forces in the plate in the structural side model that cause the high slope at the end of the force-deformation curve for the ship (see Figure 10.7).

First the leg undergoes local deformations in terms of denting which results in global deformations which can be seen in Figure 10.11-10.12 As a result, the brace between leg A4 and A3 deforms in compression.

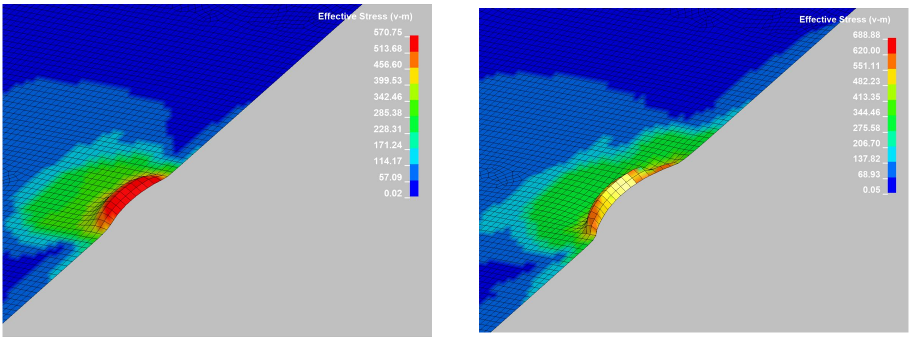
Effective Stress (v-m)
570.75
513.68
456.60
399.53
342.46
285.38
228.31
171.24
114.17
57.09
0.02
Effective Stress (v-m)
688.88
620.00
551.11
482.23
413.35
344.46
275.58
206.70
137.82
68.93
0.05

(a) T=0.1sec.

(b) T=0.1sec.

Figure 10.9: Local damage of plate in structural side model (0.1s<T<0.15s)

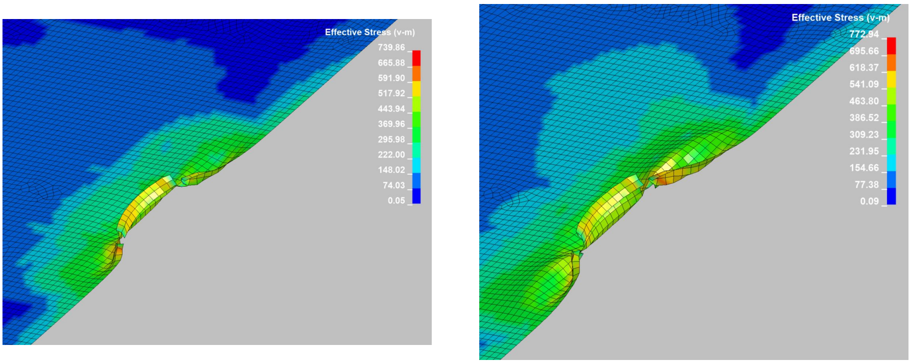
Effective Stress (v-m)
739.86
665.88
591.90
517.92
443.94
369.96
295.98
222.00
148.02
74.03
0.05
Effective Stress (v-m)
772.94
695.66
618.37
541.09
463.80
386.52
309.23
231.95
154.66
77.38
0.09

(a) T=0.2sec.

(b) T=0.3sec.

Figure 10.10: Local damage of plate in structural side model (0.2s<T<0.3s)

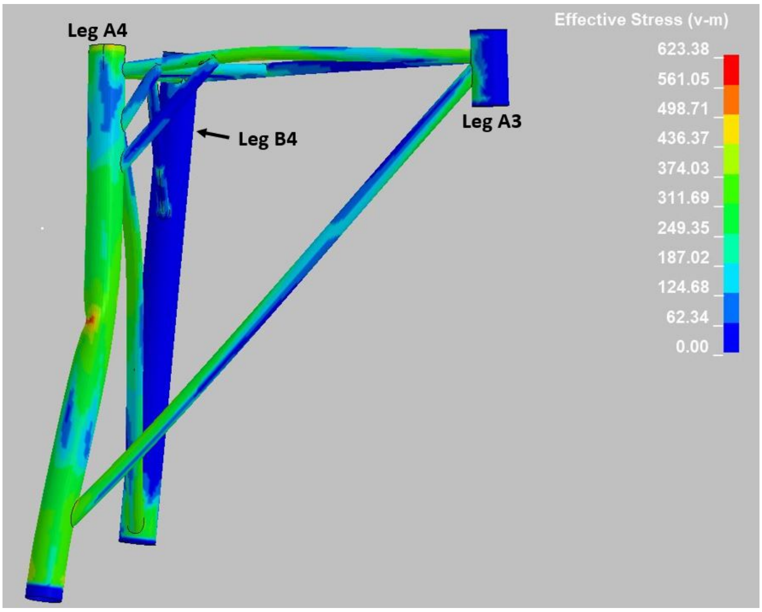
Leg A4
Leg B4
Leg A3
Effective Stress (v-m)
623.38
561.05
498.71
436.37
374.03
311.69
249.35
187.02
124.68
62.34
0.00

Figure 10.11: Jacket after collision seen from right

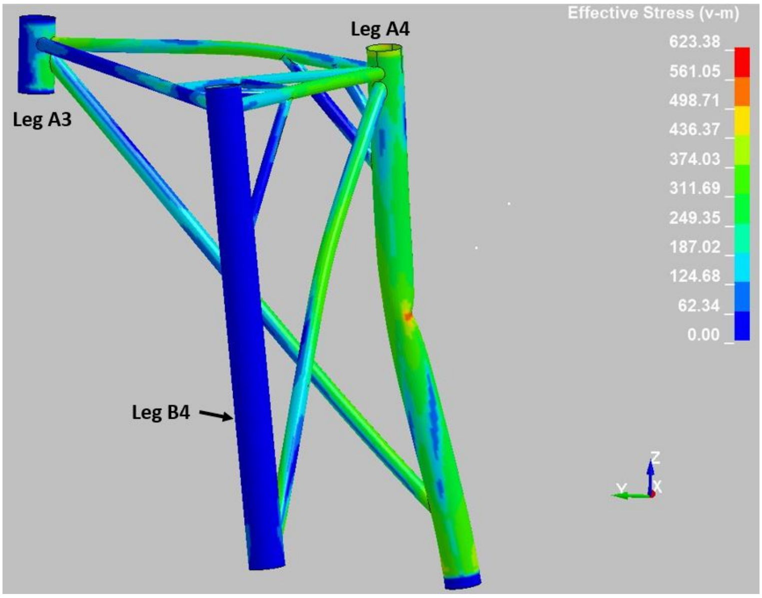
Leg A3
Leg A4
Leg B4
Effective Stress (v-m)
623.38
561.05
498.71
436.37
374.03
311.69
249.35
187.02
124.68
62.34
0.00
Z
Y
X

Figure 10.12: Jacket after collision seen from left

10.4 Scenario 3: Stern collision against leg A1 and A2

The force - and energy curves are shown in Figure 10.13

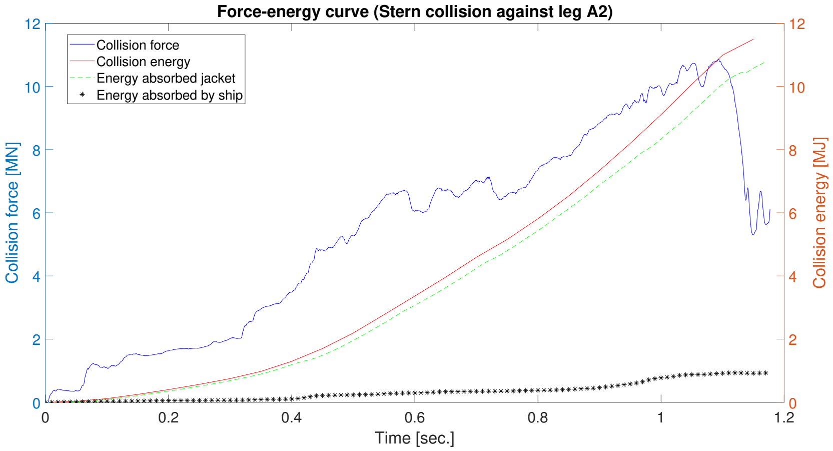

Figure 10.13: Force - and energy for stern collision against leg A1 and A2

As for the collision against C3, the simulation does not reach the critical limit of 16.5MJ. A closer investigation of the collision shows that there are two contact points: one between stern and riser and one between diagonal and stern, see Figure 10.14. Denting takes place in both the riser and the diagonal but the dents are relatively small and it has been chosen to not present them in terms of force-deformation curves.

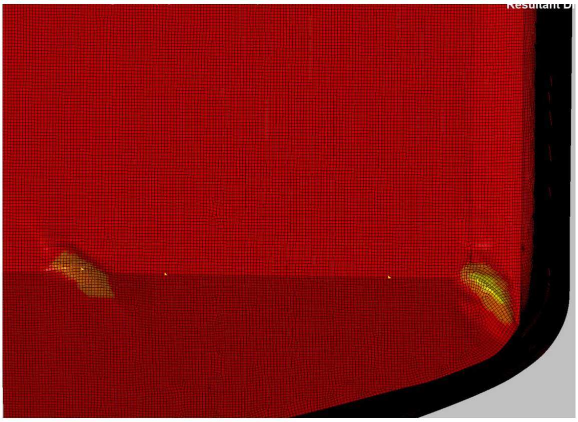

Figure 10.14: Dents in stern caused by diagonal (left) and riser (right)

Figure 10.13 shows that most of the collision energy is dissipated by the jacket. Axial forces in the riser due to the ship is causing axial forces in the clamp which again results in shear forces in the brace. As a result, fracture occurs in the brace close to the clamp. Almost instantaneously fracture occurs in the brace close to leg A1 (see Figure 10.15). This is causing the flat area between $0.6s < T < 0.8s$ in Figure 10.13. It must be mentioned that the clamp is assumed to be perfectly welded to the brace, and the dimensions are based upon equivalent geometrical - and material paramters from the USFOS-model. It is questionable if deformations of the riser could cause rupture of the brace and a fracture in the clamp between the riser and the brace might also be possible. The sudden drop in the force curve in Figure 10.13 is caused by fracture in the diagonal close to leg A2 (see Figure 10.16). At this point, 11.43 MJ has been absorbed in both objects. Most likely the remaining energy will be absorbed by leg A2 when the stern eventually hits this leg.

Due to inaccurate modelling it is believed that the clamp between the brace and the riser might appear stronger than in reality. It might be more likely that the clamp will fail (due to axial tension forces) but without more accurate modelling of the clamp it is hard to say. However, the simulation shows that the stern is capable of performing severe damage to the riser before it hits leg A2.

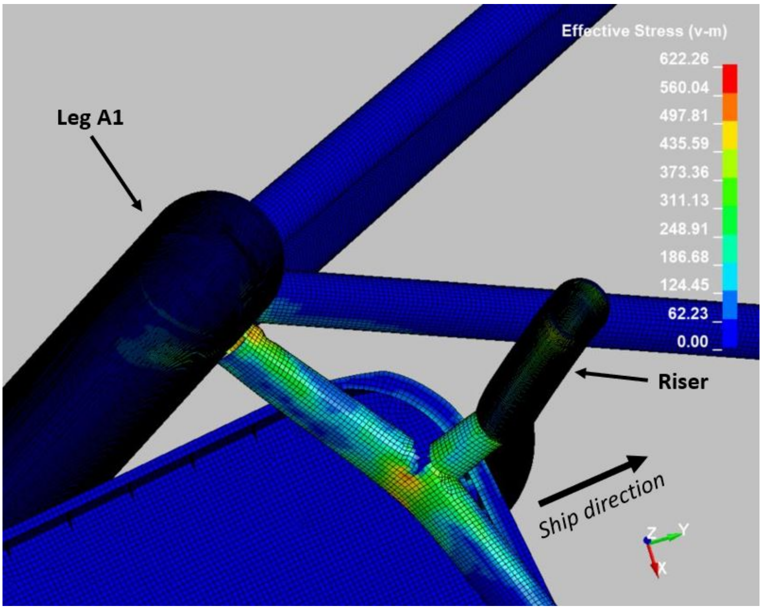

Figure 10.15: Fracture in brace close to clamp and close to leg A1

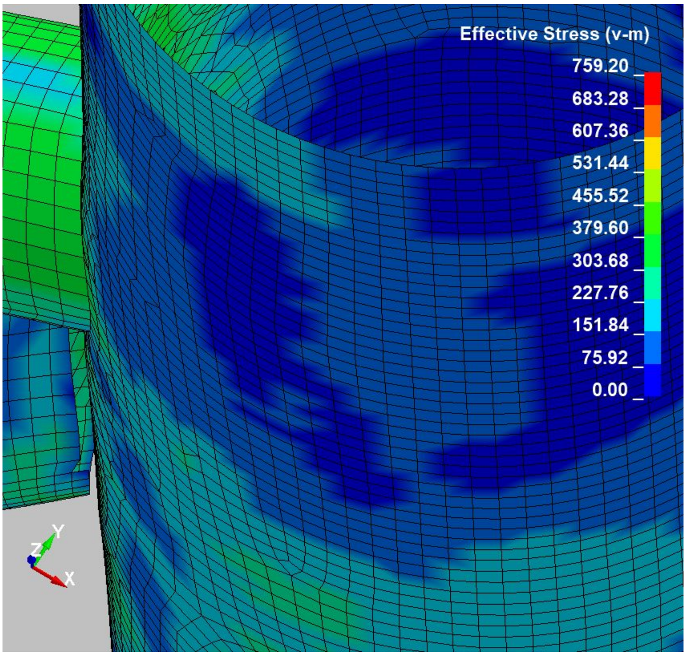
Effective Stress (v-m)
759.20
683.28
607.36
531.44
455.52
379.60
303.68
227.76
151.84
75.92
0.00
Y
Z
X

Figure 10.16: Fracture diagonal

10.5 Scenario 4: Bow collision against conductor area

Since the bow - without the additional mass from the rest of the ship - is pushed towards the jacket with a constant velocity the initial velocity is irrelevant for the force-displacement curve. A ship travelling at 5m/s will each second travel the same distance as a ship travelling at 3m/s will do each 1.67 second.

Figure 10.17 shows the force versus time for bow impact against the conductor area. In Figure 10.17 the red line shows the collision force as a function of time when the bow travels with a speed of 5m/s. The green line shows the same force-curve only delayed with a factor of 1.67, while the blue line is the collision force as a function of time when the bow travels with a speed of 3m/s. Due to sampling frequency there are some deviations between the *actual* 3m/s force-time curve and the *approximated* 3m/s force-time curve. However, due to coinciding results and in order to save computer time a run with 5m/s was chosen to be a good option, as can be seen in Figure 10.18. Figure 10.18 shows that it is possible to achieve the same force-deformation curve regardless of initial velocity, since the force-deformation curve does not depend on time.

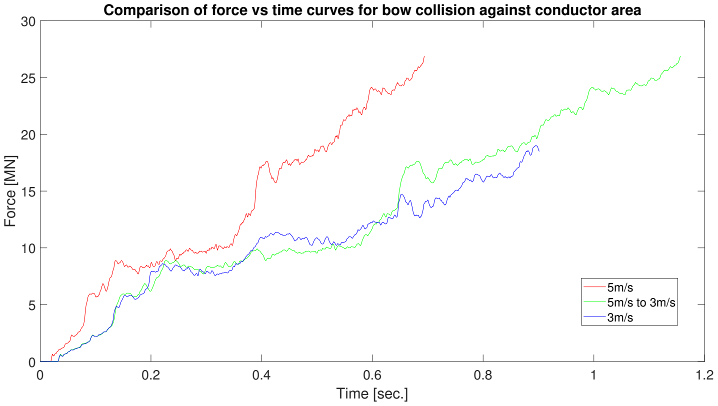

Figure 10.17: Comparison for force-time curves for forecastle at 5m/s and 3m/s

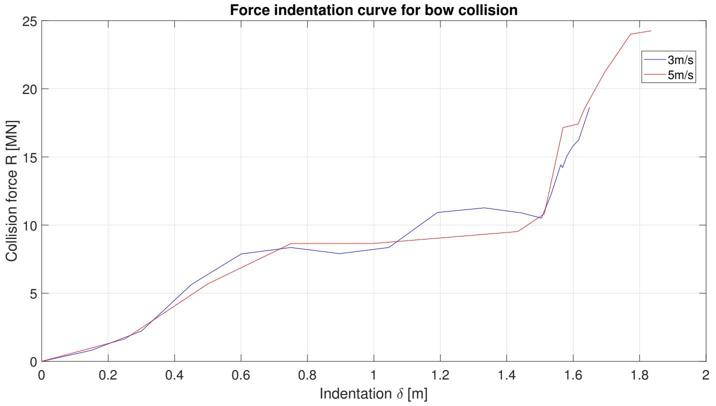

Figure 10.18: Comparison between force-deformation curves for forecastle in bow at 5m/s and 3m/s

The force-deformation curves shown in Figure 10.18 have some similarities with the force-deformation curves shown in Figure 2.3. As explained in Chapter 2.1 the curve in Figure 2.3 was based upon ships with raked bows. In scenario 4 the forecastle undergoes the largest deformations while the bulb is passing between the conductors with small but significant deformations. Raked bows will appear softer than bulbous bows due to the reinforced design of the bulb. Even though there are some contributions from the deformation of the bulb, the bow collision towards the conductor area might be considered as a raked bow impact since it is mainly the forecastle which participates in the energy dissipation.

The energy absorption is shown in Figure 10.19 and it is seen that the ship contributes to a major part of the energy dissipation.

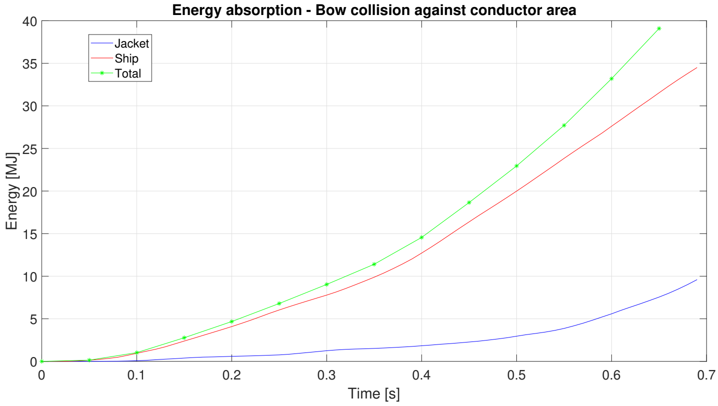

Figure 10.19: Energy absorption for bow collision against conductor area

With the forecastle above – and the bulb underneath the diagonal, the conductors in front undergoes large global deformations. The compactness criterion (see Equation 3.3) is fulfilled for the conductors, which implies that denting can be disregarded. The bow undergoes the most severe damages during the collision, as can be seen in Figure 10.20. The diagonal member have some local and global deformations and seems to collapse as a three-hinge mechanism, see Figure 10.21.

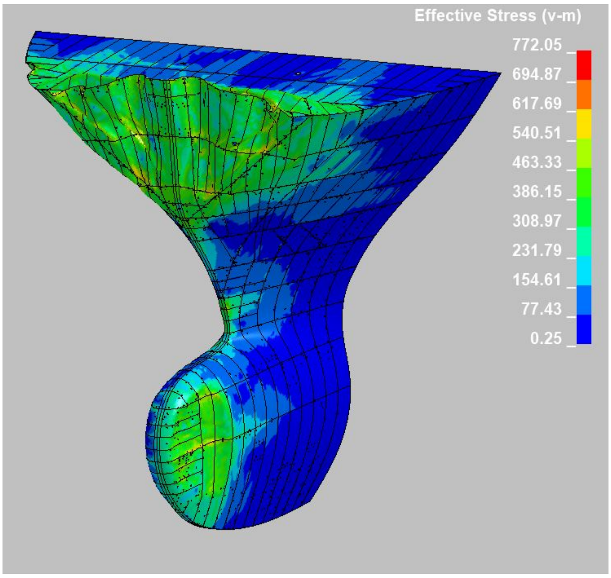
Effective Stress (v-m)
772.05
694.87
617.69
540.51
463.33
386.15
308.97
231.79
154.61
77.43
0.25

Figure 10.20: Bow model after collision

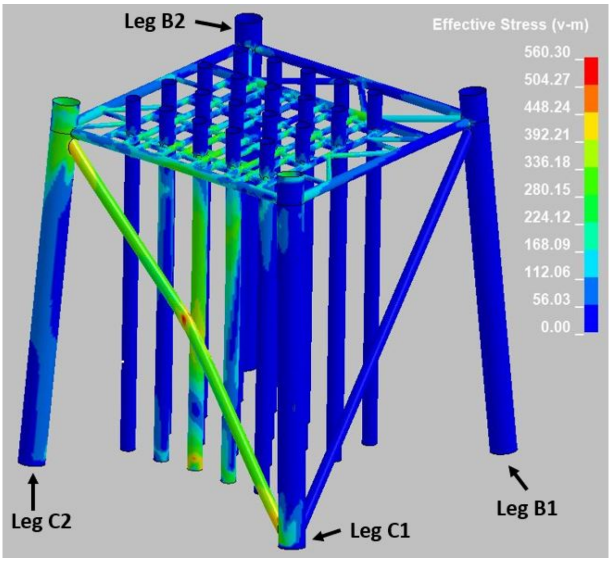
Leg B2
Effective Stress (v-m)
560.30
504.27
448.24
392.21
336.18
280.15
224.12
168.09
112.06
56.03
0.00
Leg C2
Leg B1
Leg C1

Figure 10.21: Jacket model after collision

Chapter 11

Global collision analysis (USFOS)

The analyses from LS-DYNA have provided information regarding the local deformations and energy dissipation. This information shall be used as input for the global analyses in USFOS. To the extent possible, ship impact analyses shall be performed both statically and dynamically and the most suitable method shall be judged.

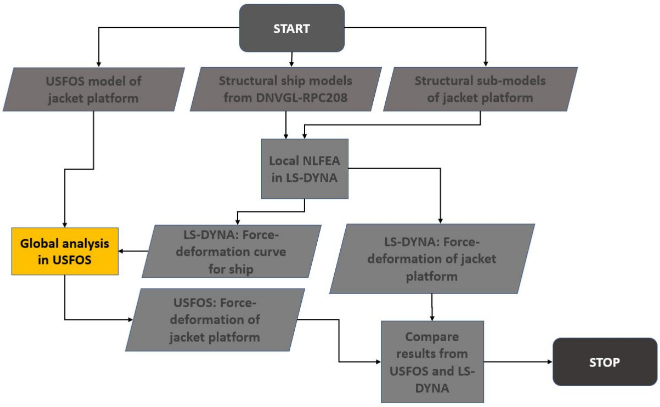
START
USFOS model of jacket platform
Structural ship models from DNVGL-RPC208
Structural sub-models of jacket platform
Local NLFEA in LS-DYNA
Global analysis in USFOS
LS-DYNA: Force-deformation curve for ship
LS-DYNA: Force-deformation of jacket platform
USFOS: Force-deformation of jacket platform
Compare results from USFOS and LS-DYNA
STOP

11.1 Summary

Table 11.1 shows a summary of the current and old collision energy requirements for ship collisions compared with the results obtained with USFOS. By new requirement, it is referred to the requirements presented in Chapter 7

Table 11.1: Summary of USFOS analyses

Case	Description	Requirement [MJ]		Analysis	USFOS Command	Energy dissipation [MJ]	
		Old	New			Jacket	Ship
1	Stern collision against leg C2	11	16.5	Dynamic	SURFIMP (Attach)	11.7	4.2
	Stern collision against diagonal and leg C3			Static	BIMPACT	16.5	-
2	Side collision against leg A4	14	21	Dynamic	SURFIMP Attach	12.3	6.7
				Static	SURFIMP Loadcase	16	-
				Static	BIMPACT	21	-
3	Stern collision against leg A2	11	16.5	Static	BIMPACT	16.5	-
4	Bow collision against conductor area	11	37.13	Static	BIMPACT	9.5	-

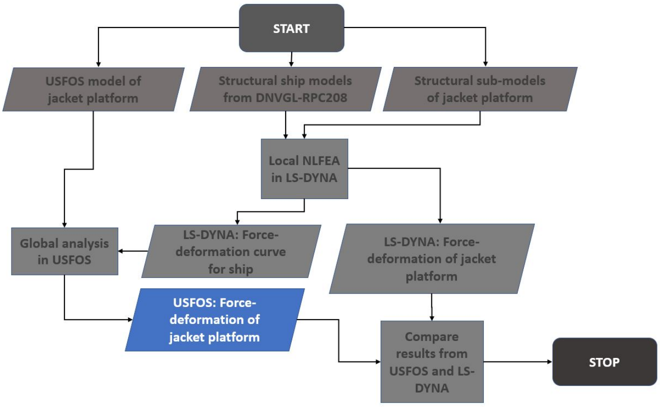
START
USFOS model of jacket platform
Structural ship models from DNVGL-RPC208
Structural sub-models of jacket platform
Local NLFEA in LS-DYNA
Global analysis in USFOS
LS-DYNA: Force-deformation curve for ship
LS-DYNA: Force-deformation of jacket platform
USFOS: Force-deformation of jacket platform
Compare results from USFOS and LS-DYNA
STOP

11.2 Scenario 1: Stern collision against leg C2 and C3

11.2.1 Dynamic analysis

From the LS-DYNA anlysis it was possible to achieve a force-deformation curve for the stern from the stern collision against leg C2. The stern collision against leg C2 was carried out dynamically with the *SURFIMP*-command. Figure 11.1 shows the force-deformation curves for the ship and jacket. The negative force in Figure 11.1 are difficult to explain. A tension force occur instantaneous at t=10.8 seconds and vanish after 0.1 seconds (In comparison, the ship impact is over at t=7.8 seconds). The same happens for the dent depth in the jacket leg but a dent depth of 0.8 meters ($w_d/D = 0.6$) 3.5 seconds after impact is not reasonable.

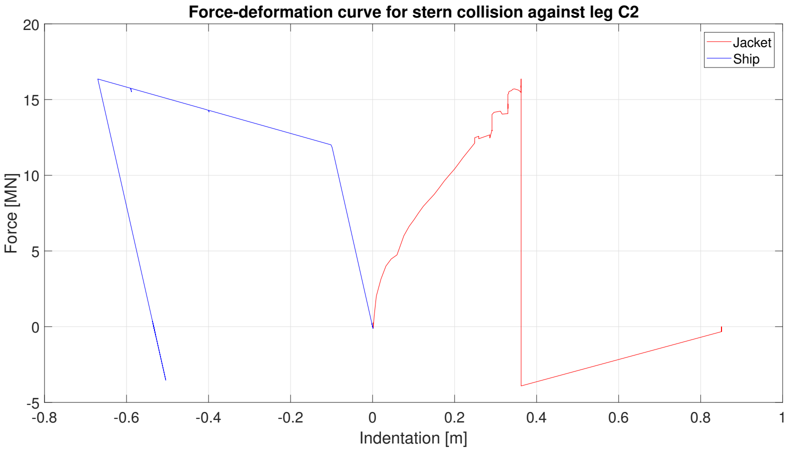

Figure 11.1: Force deformation plot for dynamic side collision against leg C2

Figure 11.2 shows the global energy. Gravitational loads causes an initial energy absorption of 6.7MJ. The ship collision lasts for approximately 2 seconds and when maximum energy is reached unloading takes place. Based upon Figure 11.2 the jacket dissipates 11.7 MJ while the ship dissipates 4.2MJ. Hence, it was difficult to track the impact energy. During discussions with supervisor it was concluded that the effects in the global energy plot might be caused by other things than the ship impact, e.g. displacement of topside and unloading and reloading of adjacent members. Hence, the energy values based upon the global energy plot in USFOS must be taken with a grain of salt, but based upon the observations the energy absorption seem reasonable.

The second peak in Figure 11.2 is caused by the 100year wave in the residual strength check. The 100-year wave does not cause structural collapse of damaged jacket platform.

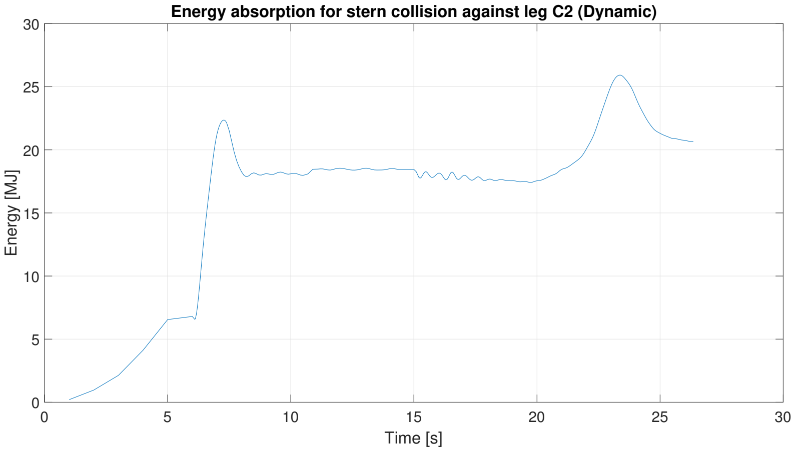

Figure 11.2: Energy absorption for dynamic side collision against leg C2

11.2.2 Static analysis

The collision against leg C3 was done statically, due to two contact points and some challanges with the dynamic SURFIMP-command for more than one contact point. Figure 11.3 shows the result from the static ship collision performed in USFOS. The first 6.3 MJ (38.1%) of the collision energy is absorbed by the diagonal before fracture occurs. The energy is then transfered to the leg which absorbs the rest of the collision energy.

This result is conservative. No force-deformation curve for the ship has been used and hence the entire collision energy has been dissipated by the jacket structure. Another insecurity is the choice of extent. An extent of 0.2 meters has been used in the leg, while 0.1 has been used for the diagonal. The extent in the diagonal is reasonable, since the stern corner hits the diagonal with its edge which results in a rather small contact area. The diagonal deforms as a three-hinge mechanism and a small contact area is therefore reasonable. The extent of 0.2 for the leg C3 is harder to justify, since no contact was observed in the LS-DYNA analysis. The stern corner is mainly in contact with the bulwark which is unsupported in the upper end. Hence, it is not reasonable to think that the extent is as high as 3 meters and the value was lowered. However, when the extent exceeded 0.2 meters for the leg, the analysis was terminated due to large rotational angles in the topside. A low extent yields a more concentrated collision (see Equation 3.5)

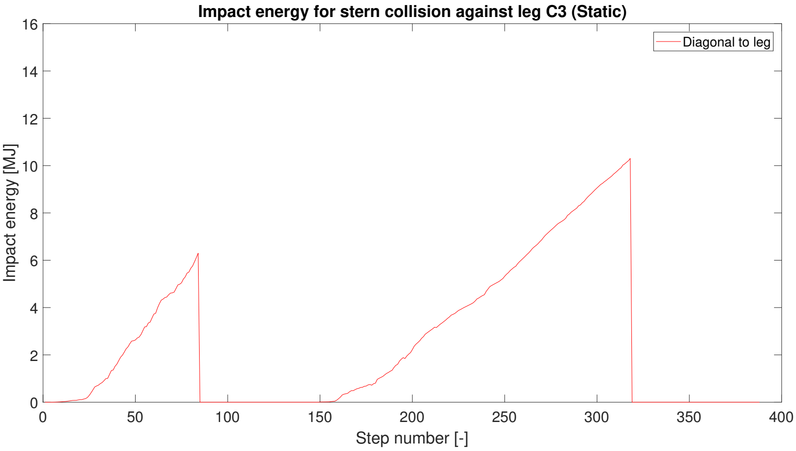

Figure 11.3: Impact energy for collision against leg C3

The joint check shows that neither joint exceed the ductility limit or peak axial, but as expected all the joints close to the impact area exceed first yield. Figure 11.4 shows the platform after impact with the checked nodes marked. The jacket platform survived the residual strength check in damaged condition.

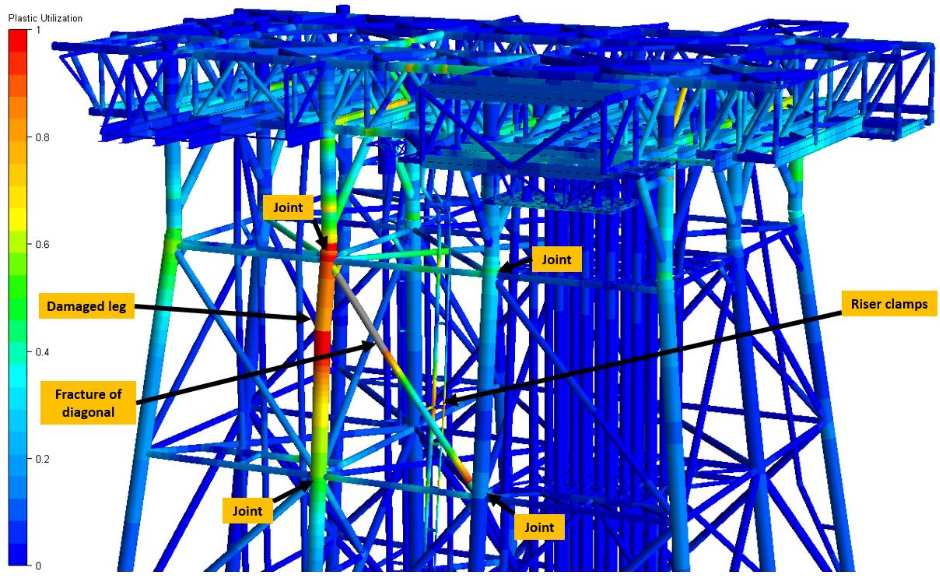
Plastic Utilization
1
0.8
0.6
0.4
0.2
0
Joint
Joint
Damaged leg
Riser clamps
Fracture of diagonal
Joint
Joint

Figure 11.4: Plastic utilization of jacket after impact

11.3 Scenario 2: Side collision against leg A4

11.3.1 Dynamic analysis

A force-deformation curve from the dynamic side collision analysis against leg A4 is shown in Figure 11.5 compared with the force-deformation curves from LS-DYNA. Furthermore, the corresponding energy-plot is shown in Figure 11.6. The force-deformation curve for the ship in USFOS follows a user-defined curve based upon the results from LS-DYNA while the corresponding force-deformation curve for the jacket is given by the dent-depth in leg A4. The area under the jacket force-deformation curve from USFOS represents the denting energy, or the energy which participate in the denting process in leg A4. The force-deformation curve of the jacket is lower in USFOS than the force-deformation curve obtained with LS-DYNA, which is reasonable since it was observed during the LS-DYNA analysis that deformation also occurred in adjacent members. Hence, the entire collision force contributed to more deformation than only denting in leg A4. After maximum indentation is obtained (the energy-level is reached) unloading takes place in both jacket platform and ship. During unloading the force-deformation curve of the ship has the same slope as the first part of the force-deformation curve. This is also questionable. It would have been interesting to compare this result with a similar userdefined force-deformation curve with a steeper slope in the start, but due to time limitations this was not carried out.

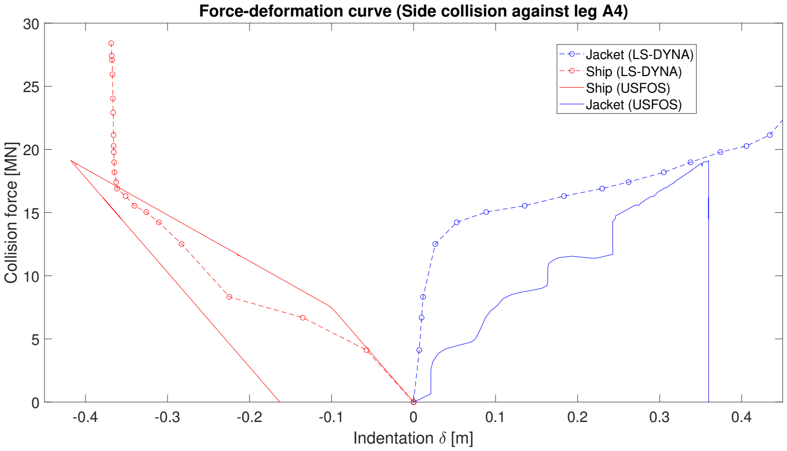

Figure 11.5: Force deformation plot for dynamic side collision against leg A4

The ship impact takes place at t=6 seconds and has a duration of 2 seconds. As seen in Figure 11.6 the energy level in the jacket drops with roughly 6 MJ. This is believed to be the energy dissipated by the ship, which is in agreement with the results obtained from LS-DYNA, see Table 10.1. The second peak in Figure 11.6 is caused by the 100-year wave. In the dynamic analysis the jacket survives the wave without loss of structural integrity.

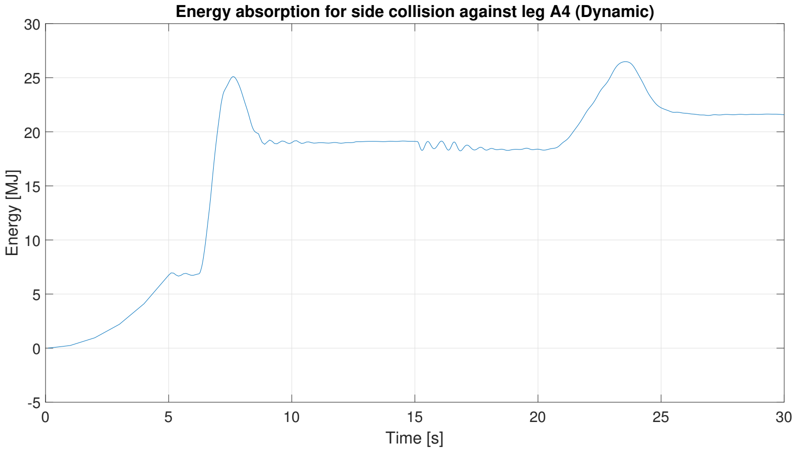

Figure 11.6: Energy absorption for dynamic side collision against leg A4

11.3.2 Static analysis

A comparison between static - and dynamic SURFIMP was performed. Figure 11.7 compare the force-deformation curves of the jacket from LS-DYNA with the corresponding force-deformation curves from USFOS obtained with static - and dynamic analysis. The deviations between the two USFOS-curves are rather small. For the static SUFRIMP-command, the nodal mass and initial velocity are replaced by a nodal load which is applied incrementally. This is the reason for why there are no signs of unloadning in the static force-deformation curve.

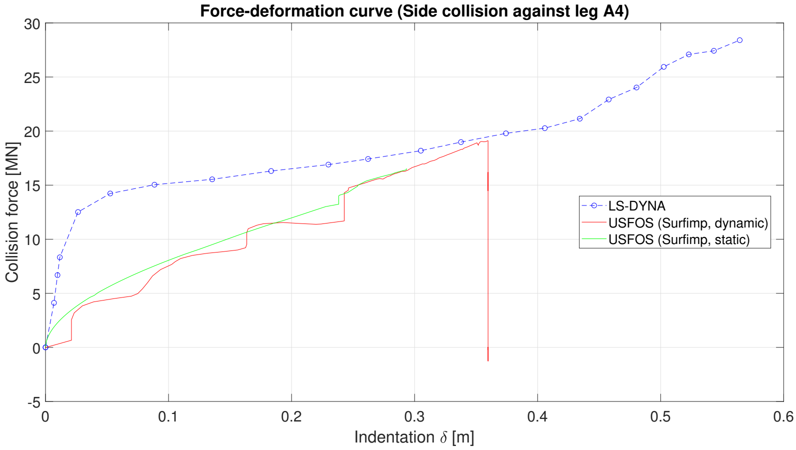

Figure 11.7: Comparison of force-deformation curves for scenario 2

Based upon the LS-DYNA analysis, the jacket absorbed 15.38MJ of the total collision energy. Figure 11.8 shows the global energy of the jacket as a function of step number. Unlike the dynamic analysis there is no unloading, but the jacket absorbs 16MJ without structural collapse.

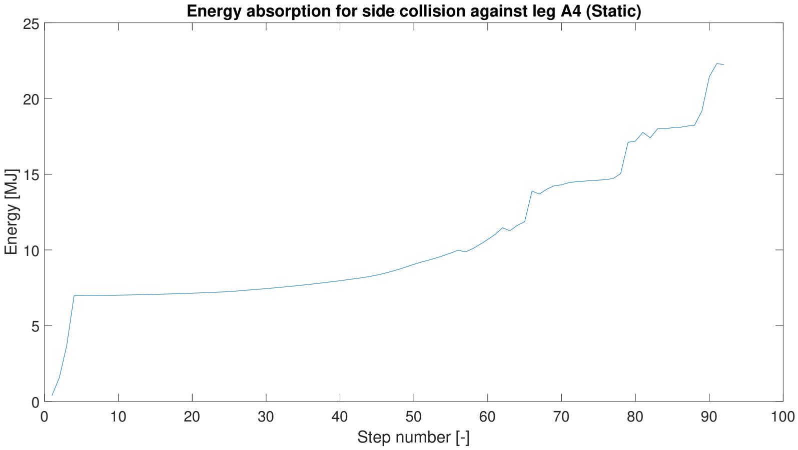

Figure 11.8: Energy absorption for jacket

11.3.3 BIMPACT analysis

A comparison was made with a BIMPACT analysis was performed. The impact energy is shown in Figure 11.9. When 8.13 MJ of the collision energy is dissipated by the jacket fracture occur in element 9015 (see Figure 11.11). The forces is re-distributed and unloading takes place. The contact point is moved to a $2nd$ contact point (see Figure 11.10) and the remaining collision energy is dissipated.

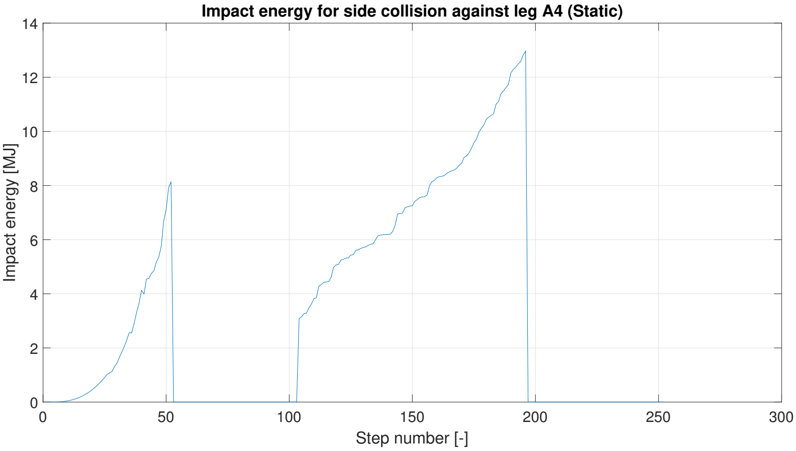

Figure 11.9: Impact energy for side collision against leg A4

However, two uncertainties must be mentioned: (1) load incremental step for static analyses and (2) fracture criterion. For static analyses the load is applied incrementally and close to collapse the change in load increments must be small enough to capture the collapse behaviour. The external loads must be balanced by the restoring term and the system might experience a *load shock* close to a limit point. The choice of load increments must therefore be judged by calibration in USFOS. When a fracture criterion is applied to element 9015 (see Figure 11.11), element 9015 will fail in compression when 8.13 MJ of the collision energy is dissipated by the jacket. Unloading takes place and the remaining amount of energy is dissipated by the jacket through a new contact point. Without fracture criteria applied to element 9015, element 9013 and 9018 fails in compression when 12MJ is dissipated by the jacket. Due to numerical problems close to adjacent joints no unloading – or redistribution of the energy takes place, and the analysis was terminated.

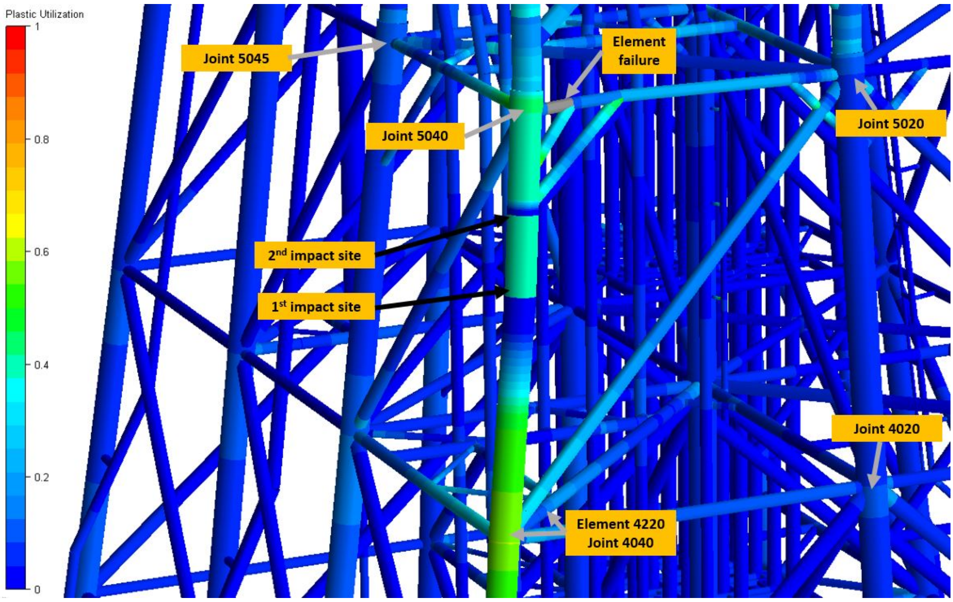
Plastic Utilization
1
0.8
0.6
0.4
0.2
0
Joint 5045
Element failure
Joint 5040
Joint 5020
2nd impact site
1st impact site
Joint 4020
Element 4220
Joint 4040

Figure 11.10: Plastic utilization after collision

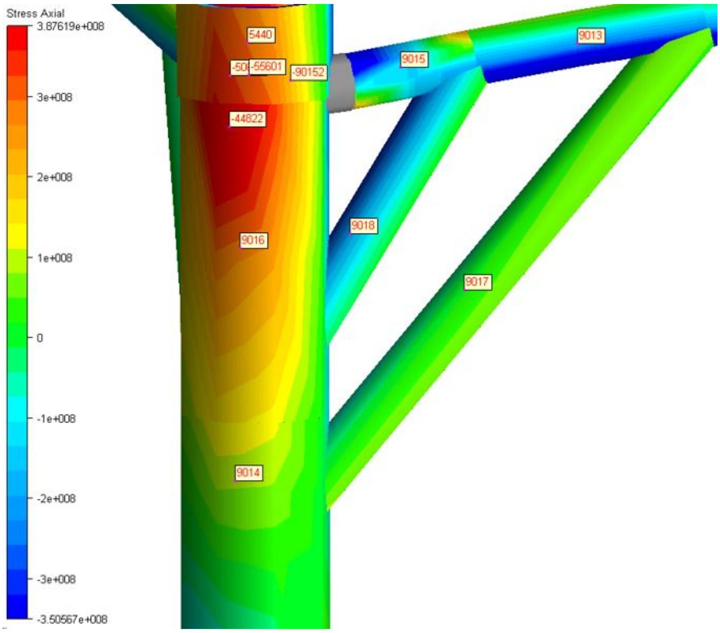
Stress Axial
3.87619e+008
3e+008
2e+008
1e+008
0
-1e+008
-2e+008
-3e+008
-3.50567e+008
5440
-50
-55601
-90152
-44822
9016
9014
9015
9013
9018
9017

Figure 11.11: Element numbers close to impact site for scenario 2

A joint check (NORSOK Rev.03, mean and grouted joints) shows that neither joints exceeds the axial peak or ductility limit. However, for a non-grouted joint check joint 4040 (brace 4220) exceeds the axial peak. The remaining adjacent joints exceeds first crack with utilizations in the range of 0.18 – 0.804. Without fracture criteria on element 9015, element 9013 and 9018 fails in compression when 12MJ of the collision energy is dissipated by the jacket. Due to numerical problems close to adjacent joints no unloading – or redistribution of the energy takes place, and the analysis is stopped.

11.3.4 Discussion between static and dynamic analysis

The motion of the jacket at site of impact relative to the motion of the ship was studied to investigate potential dynamic effects. It was discovered that at the instant of unloading both the jacket and the ship changed direction, see Figure 11.12. Hence the inertia contributions are negligible which justifies that static analyses are acceptable. The deviation between the red and blue on the range 6 sec. < T < 7.6 sec. describes the deformation of the ship. The deviation after t=8 sec. has no physical meaning since the non-linear spring has zero stiffness in tension.

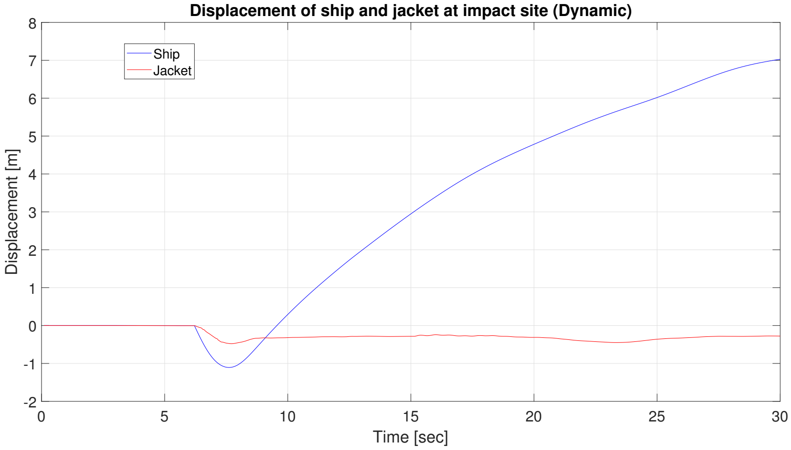

Figure 11.12: Comparison of jacket - and ship displacement

Figure 11.13 and 11.15 shows the plastic utilization and axial stress, respectively for the jacket platform at maximum energy for the dynamic analysis. It can be seen that the jacket undergoes large deformations. The permanent damages of the jacket can be seen in Figure 11.14. The axial stress distribution at maximum energy is shown in Figure 11.15. The response is similar to the results obtained with LS-DYNA with compressional forces in the diagonals and the brace between leg A4 and B4.

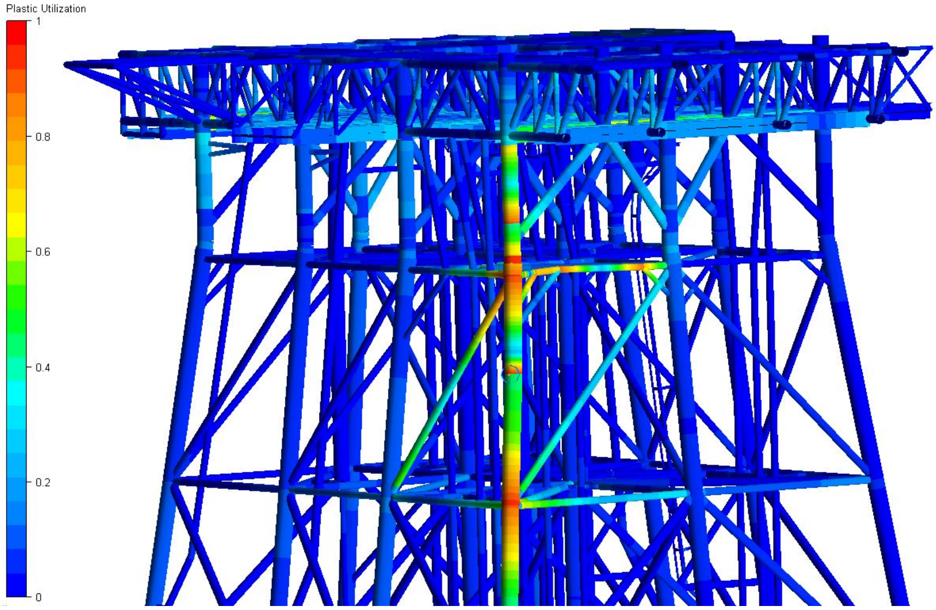
Plastic Utilization
1
0.8
0.6
0.4
0.2
0

Figure 11.13: Plastic utilization at maximum energy (Dynamic analysis)

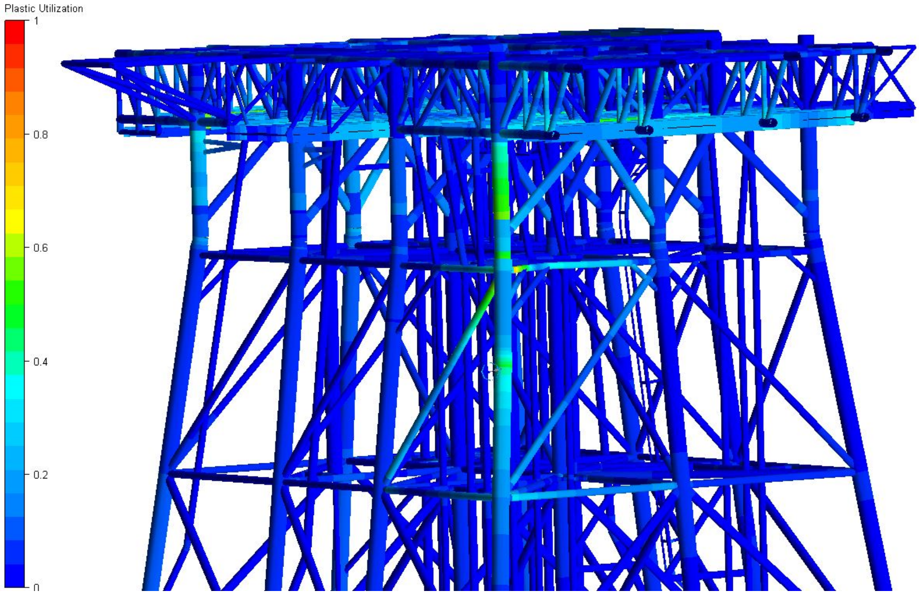
Plastic Utilization
1
0.8
0.6
0.4
0.2
0

Figure 11.14: Plastic utilization after collision (Dynamic analysis)

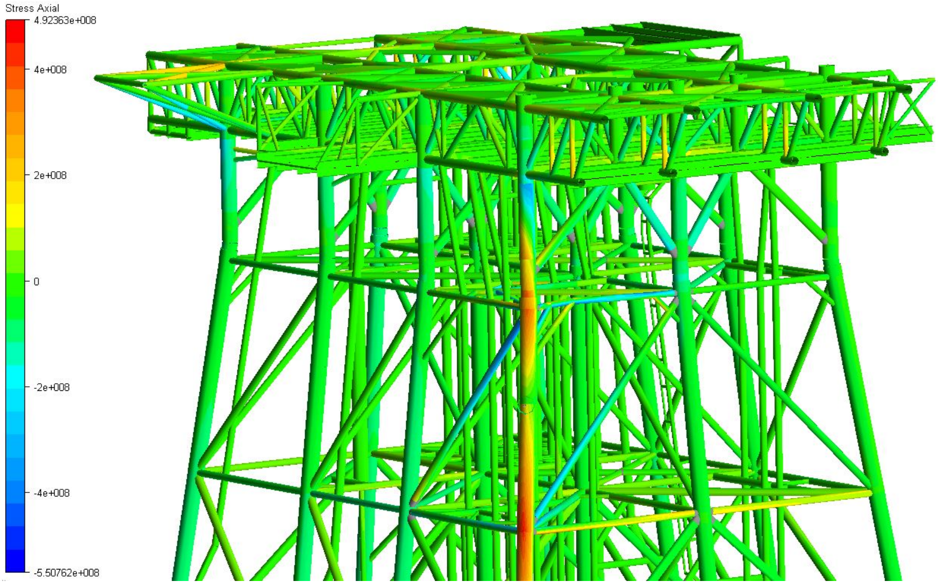
Stress Axial
4.92363e+008
4e+008
2e+008
0
-2e+008
-4e+008
-5.50762e+008

Figure 11.15: Axial stress at maximum energy

11.4 Scenario 3: Stern collision against leg A1 and A2

As seen in the LS-DYNA analysis the riser and the clamps where damaged. However, due to inaccurate modeling the result is questionable. Due to many contact points a static analysis was carried out in USFOS.

From the static ship collision analysis in USFOS the impact energy versus timestep is shown in Figure 11.16. In total 3.6MJ (22.3% of the energy) was absorbed by the diagonal while the remaining 12.9MJ was absorbed by leg A2. The diagonal fails due to frature while the leg absorbed the energy without element failure.

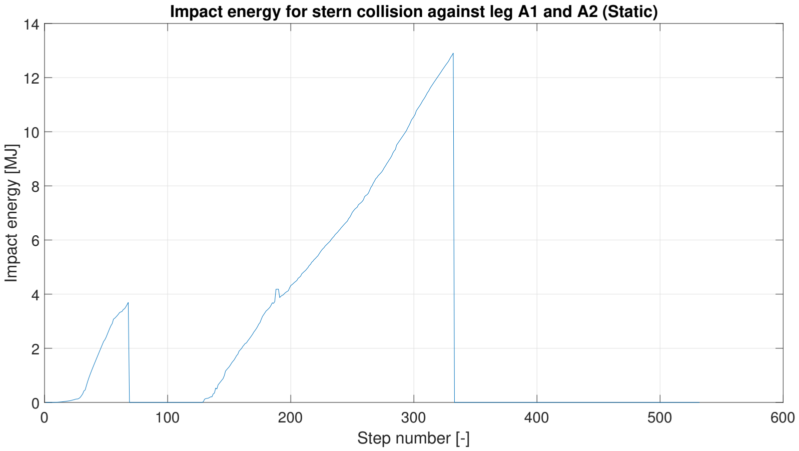

Figure 11.16: Energy absorption for static stern collision against leg A1 and A2

The jacket in damaged condition can be seen in Figure 11.17.

A joint check of the jacket-platform after the ship collision showed that neither joints exceeded the ductility limit or axial peak stress. The residual strength check was performed dynamically and based upon the plastic utilization as shown in Figure 11.17 is was suggested to run the residual strength check without both the diagonal and the damaged leg A2. There are two uncertainties related to this choice. (1) Even though leg A2 is heavily damaged it might have some residual strength or load-carrying capacity. (2) Flow history in the joint is not taken into account. Hence, it is hard to claim whether the result is conservative or not, but if possible it would have been desirable to carry out the residual strength check with the damaged model instead of decouple the ship impact and residual strength check. However, even with one leg and diagonal removed, the jacket is capable of resisting the wave without total collapse.

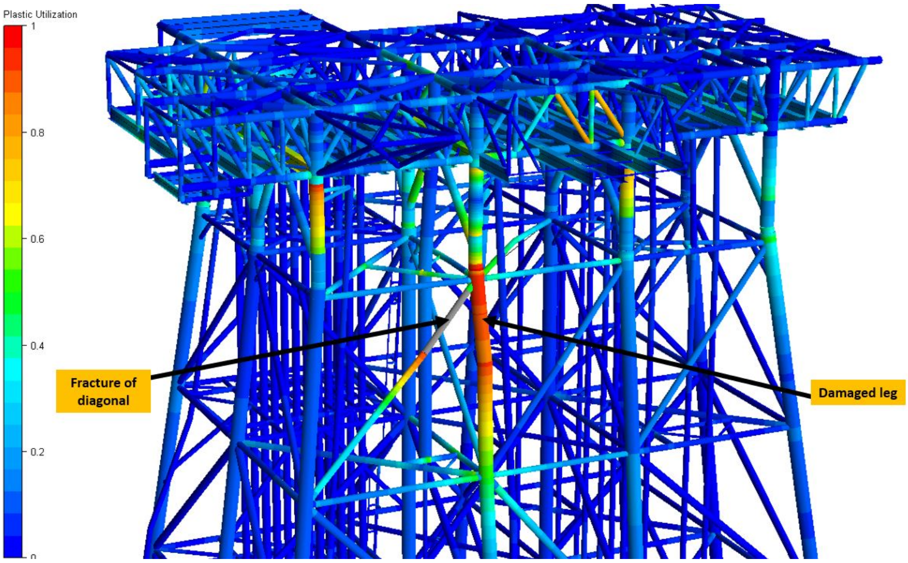
Plastic Utilization
1
0.8
0.6
0.4
0.2
0
Fracture of diagonal
Damaged leg

Figure 11.17: Jacket in damaged condition after static ship collision (plastic utilization)

11.5 Scenario 4: Bow collision against conductor area

As observed in the LS-DYNA analysis the diagonal which is in front of the conductors was damaged during the bow impact and is to be omitted for a residual strength check. It was also observed that the forecastle was damaged by the conductors. Since the conductors have no influence on the structural integrity of the jacket platform (defined as *NONSTRU* in USFOS), the bow against conductor collision was not performed in USFOS. Most of the collision energy were dissipated as strain energy in the forecastle. On this background the static analysis is a capacity analysis of the diagonal between leg C1 and C2, while the dynamic analysis is a residual strength check where the diagonal between C1 and C2 is removed.

11.5.1 Static analysis

A static analysis in USFOS shows that the diagonal dissipates 9.5 MJ of the collision energy before fracture occur.

A choice of an extent (dent width) of 0.2m was based upon a study of the dent development in LS-DYNA. A joint close to the diagonal (see Figure 11.4) fails in tension while the remaining checked joints only exceed first yield with rather low utilizations.

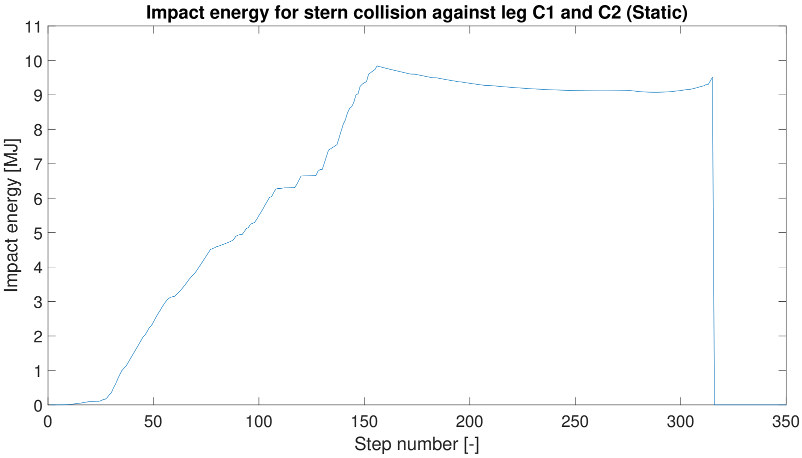

Figure 11.18: Impact energy for static collision against diagonal between leg C1 and C2

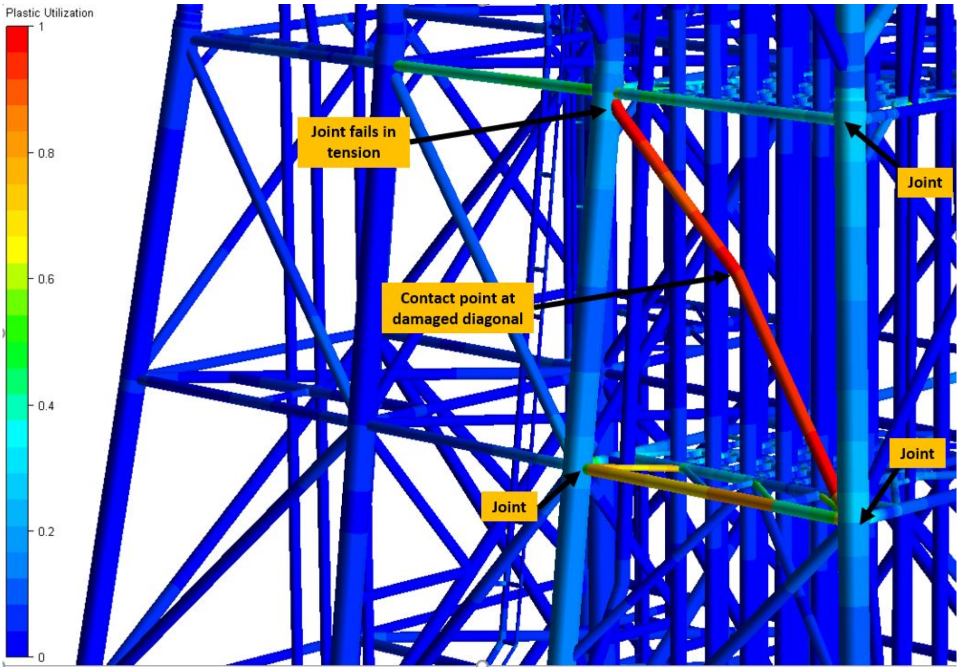
Plastic Utilization
1
0.8
0.6
0.4
0.2
0
Joint fails in tension
Contact point at damaged diagonal
Joint
Joint
Joint

Figure 11.19: Plastic utilization at fracture

In addition static pushover analyses with a Stokes $5th$ order wave was performed. Due to joint failure (see Figure 11.19) leg C2 was removed in addition to the diagonal. Some wave directions were checked and the jacket was able to resist the 100-year wave for each direction.

11.5.2 Dynamic analysis

A residual strength check shows that the structural capacity is maintained even though the diagonal is removed. The check was performed with a Stokes wave with a heading angle of $180\mathrm{deg}$. The structural integrity of the jacket is maintained without the diagonal.

Chapter 12

Comparison with hand calculations

The purpose of this chapter is to compare the reults obtained in USFOS with simple hand-calculations. Calculations are based upon elementary beam theory and the mechanism method, which is described in Appendix A. Scenario 2 (leg impact) and scenario 4 (bracing/diagonal impact) is to be verified with simple hand calculations.

Assumptions:

1. The element ends are clamped
2. The collision force is concentrated over an infinite small area

For scenario 2, the first assumption is questionable. The jacket leg goes from seabed to topside with numerous braces and bracings attached to it. However, the joints can make the jacket leg quite stiff at each elevation and even though some rotations might occur these are relatively small and clamped boundary conditions might be a good estimate. The second assumption might be reasonable. As seen in the LS-DYNA analysis for sceanrio 2 the dent width in both leg A4 and the diagonal is small (0.1m-0.3m) and a concentrated force might be a good assumption.

Based upon the geometrical - and material properties of the jacket leg between elevation $+25''$ and $-35''$ (see Figure 9.1) leg A4 has a length $l_{leg} = 18,572m$ and plastic section modulus $Z_{leg} = 126,8Mmm^3$. Hence, a yield stress $f_y = 335MPa$ implies a plastic moment capacity $M_p = 42,5MNm$ and according to Equation A.10 a critical load $P_{crit} = 18,28MN$. In the latter, it is assumed that the contact point between leg and ship is $10.6m$ away from elevation $-35''$ and $8m$ from elevation $+25'$. Normally small rotations are allowed at the elevations, which means that it would have been more benefitial to have rotational springs at the ends. Figure 12.1 shows the plastic utilization of the jacket leg during ship impacts. As the collision force reaches $19MN$ plastic hinges starts to develop at the leg. Hence, the result obtained in USFOS is credible to calculations based on plastic hinge mechanism.

The same calculations were also performed on the diagonal between leg C1 and C2. A yield stress $f_y = 345MPa$, a length $l = 25m$ and plastic section modulus $Z = 0.01472m^3$ yields a plastic moment capacity $M_p = 5,1MNm$ and a critical load $P_{cr} =$

$1,7MN$. The contact point is roughly centred at the middle of the diagonal. As seen in Figure 12.2 hinges start to develop at the diagonal ends and in the diagonal middle as soon as the load reaches $1.7MN$.

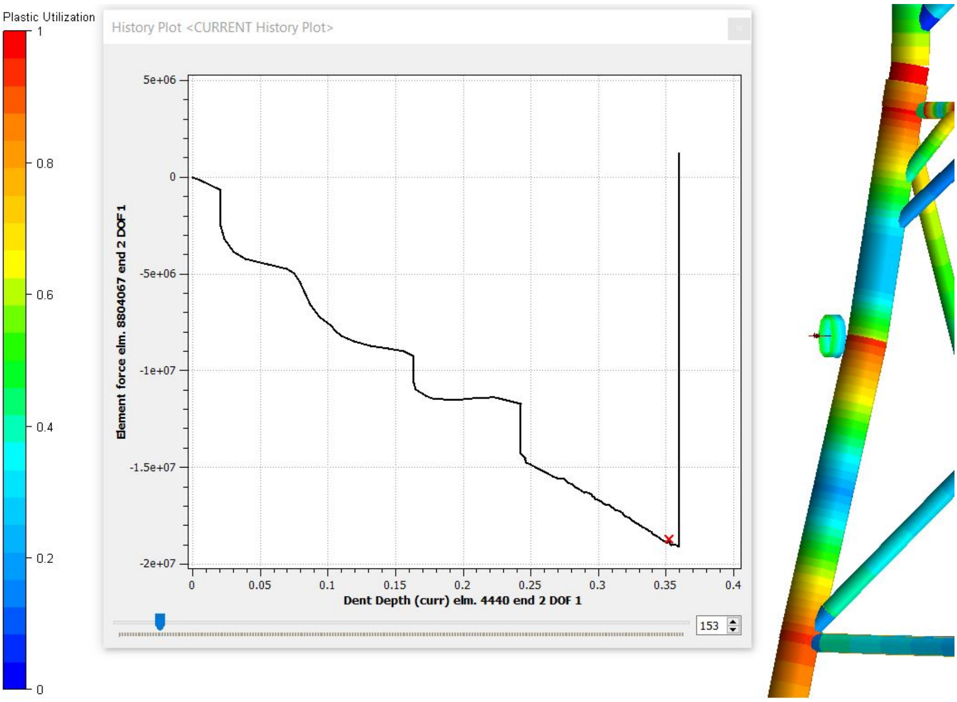

Figure 12.1: Plastic utilization of leg A4

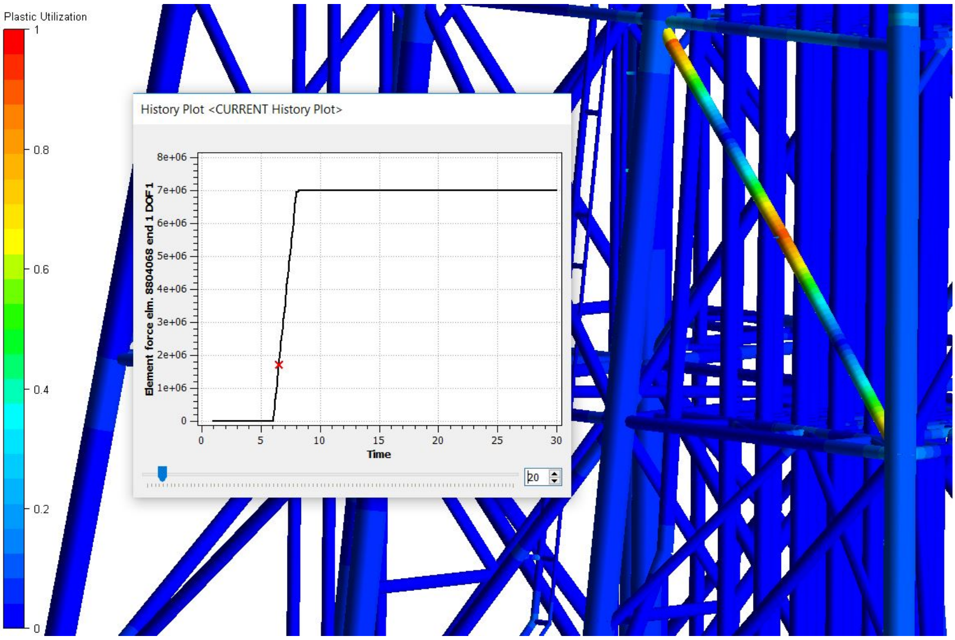
Plastic Utilization
1
0.8
0.6
0.4
0.2
0
History Plot <CURRENT History Plot>
Element force elm. 8804068 end 1 DOF 1
8e+06
7e+06
6e+06
5e+06
4e+06
3e+06
2e+06
1e+06
0
0
5
10
15
20
25
30
Time
20

Figure 12.2: Plastic utilization of diagonal between leg C1 and C2

Chapter 13

Discussion

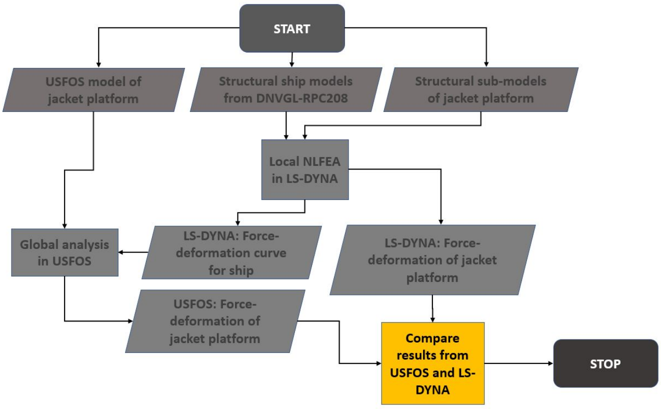
START
USFOS model of jacket platform
Structural ship models from DNVGL-RPC208
Structural sub-models of jacket platform
Local NLFEA in LS-DYNA
Global analysis in USFOS
LS-DYNA: Force-deformation curve for ship
LS-DYNA: Force-deformation of jacket platform
USFOS: Force-deformation of jacket platform
Compare results from USFOS and LS-DYNA
STOP

By performning local analyses in LS-DYNA it was possible to represent the supply ship in terms of force-deformation curves. In addition, it was also possible to receive information regarding the dent width B – and dent depth w_d. With the ship represented as a nonlinear spring, the jacket response in USFOS had some similarities with the jacket-response simulated in LS-DYNA. Despite challanges of tracking the impact energy when the SURFIMP-command was used the energy dissipation results from LS-DYNA and USFOS also coincided. Furthermore, the jacket platform satisfies both old and new requirements for ship impacts. In the following, sources of error and the uncertainties which might have affected the results shall be discussed.

13.1 Discussions regarding LS-DYNA

Some uncertainties which might have affected the results must be mentioned:

Mesh size and element type: All results obtained with FEA depend on mesh size and element type. As described in Chapter 9.3.3 the mesh size of the structural submodels of the jacket was mainly 100mm x 100mm throughout, with some exceptions. In comparison, the mesh size of the structural ship models were in the range 40 mm – 50 mm. Due to time limitations and scope of work, a mesh refinement study was not carried out. It is believed that differences in mesh sizes would affect information regarding the denting, and this effect could have been investigated in more detail. According to the critical strain dependency on mesh size (see Equation 6.6) it would have been desirable to have a finer mesh at the impact site of each element. The Belytschko-Lin-Tsay element was used in the structural ship models and recommended by Haufe et al. (2013) due to its computational efficiency. However, as mentioned in Chapter 9.3.3 the element was not recommended for coarse mesh even though it was not specified what is meant by a coarse mesh. However, it would have been desirable to compare results with different element types if time had allowed.

Joint can and brace stub: As mentioned in Chapter 9.3.1 joint cans and brace stubs were not included in the structural sub-models of the jacket platform due to complex geometry and lack of experience by the author. The consequence can be demonstrated in Chapter 10.2 and 10.4. In both cases fracture of the diagonal occur close to the jacket leg, rather than further away from the leg. Due to small structural sub-models it is believed that valuable information regarding the boundary behaviour and rigid joint behaviour were lost in the NLFEA analyses.

Inaccuracies regarding use of stern corner: The force-deformation curves for the stern collisions are believed to give a softer behaviour than initially anticipated since only a stern corner was used. With only half of the stern used the behaviour along the geometric symmetry plane (see Figure 9.7) might not be complete.

Failure criterion: As discussed in Chapter 6.3 and 9.3.6 a failure major in plane strain was set to 0.15. This was primarily chosen as a conservative value relatively to the failure strain in the ship (0.17). However, no further verification with respect to mesh size and element thickness was carried out. It is believed that the failure criterion overestimates the structural capacity of the jacket. Hence, it is recommended to study the failure criterion in more detail.

However, the structural response of collision scenario 2 (see Chapter 10.3) seems reasonable when compared to global USFOS-analyses. The finding in scenario 4 (see Chapter 10.5) is interesting, since the conductors seem to be strong enough to crush the forecastle as well as parts of the bulb (see Figure 10.20). From a structural point of view, it must be mentioned that strain rate effects were not taken into account in the analyses.

13.2 Discussion regarding USFOS

In the following, parameters which may have affected the USFOS results will be discussed.

13.2.1 Dent width B

Figure 13.1a describes a ship impact. As can be seen in Figure 13.1a the height of the contact area is equal to the dent width B. This might be a correct assumption given that the jacket leg is perpendicular to the sea surface.

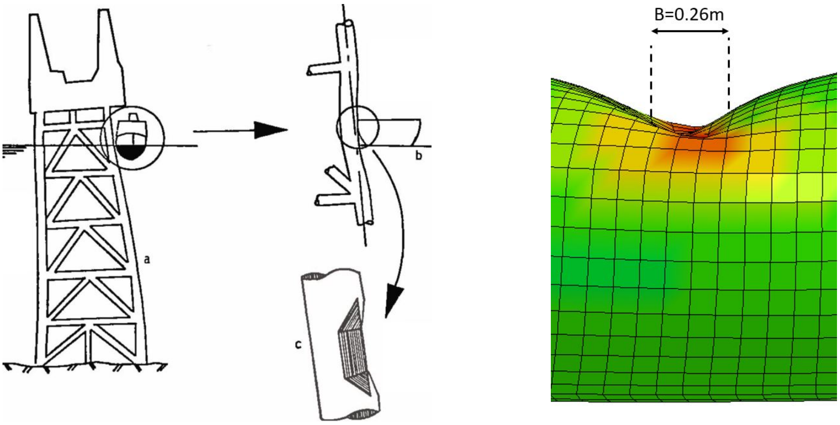

(a) Dent width (Søreide, 1981)

(b) Dent width from LS-DYNA (B=0.26m)

Figure 13.1: Comparison of dent width B

At the site of impact, however, the jacket legs have an angle of 7.12 degrees with respect to the sea surface. From the LS-DYNA analyses the width of the dents were found to be in the range of 0.1 - 0.3 meters, see Figure 13.1b. Based upon Equation 3.4 and 3.5 the resistance of tubular members increases with increasing B/D-ration, given that characteristic strength R_C, diameter D and dent depth w_d is kept constant. A smaller contact area increases the energy concentration of the collision.

Four scenarios were performed in order to investigate the influence of the dent width. All analyses were performed with BIMPACT and the entire collision energy is dissipated by the jacket platform:

1. Stern collision against leg C2 ($E_{k,0}$=16.5MJ; B=0.2)
2. Stern collision against leg C2 ($E_{k,0}$=16.5MJ; B=2.5)
3. Side collision against leg A4 ($E_{k,0}$=21MJ; B=0.2)
4. Side collision against leg A4 ($E_{k,0}$=21MJ; B=3)

For (1) - (4) the $MULT\_IMP$ option was used. The only difference between (1) and (2) is the dent width which is 0.2m and 2.5m for (1) and (2), respectively. (3) and (4) also have similar input, except for the dent width which is 0.2m and 3m for (3) and (4), respectively. In (1) and (2) the collision energy was first dissipated by element 4411 (end 1) and then by element 9037 (end 1), as can be seen in Figure 13.2a. In (3) and (4) the collision energy was first dissipated by element 4441 (end 2) and then by element (9014, end 2), as can be seen in Figure 13.2b

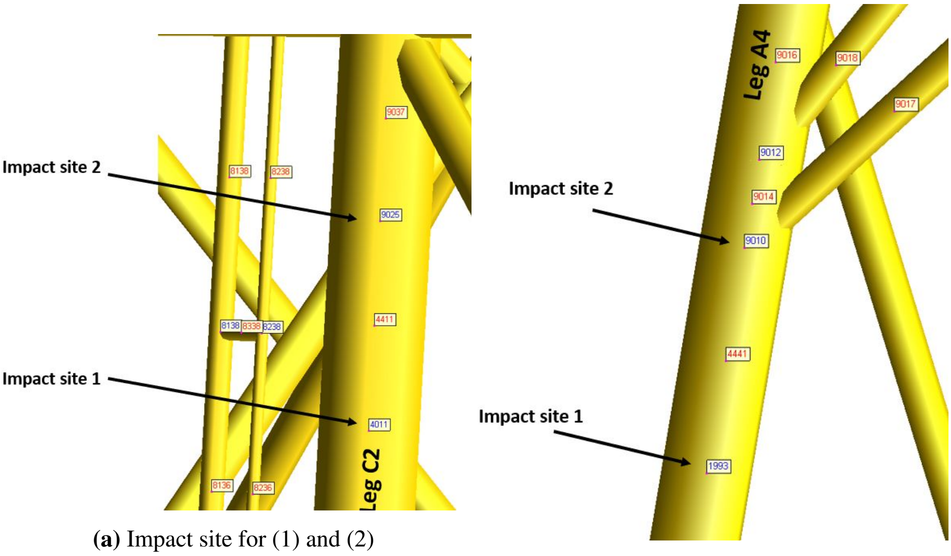
Impact site 2
Impact site 1
9037
8138
8238
9025
4411
8138
8338
8238
4011
Leg C2
8136
8236
Leg A4
9016
9018
9017
9012
Impact site 2
9014
9010
4441
Impact site 1
1993

(a) Impact site for (1) and (2)

(b) Impact site for (3) and (4)

Figure 13.2: Impact sites

The results are summarized below:

- In (1), 6.37MJ was dissipated by element 4411 while 3.5MJ was absorbed by element 9037. Hence, 6.63MJ remains.
- In (2), 8.7MJ was dissipated by element 4411 while 6.1MJ was absorbed by element 9037. Hence, 1.7MJ remains.
- In (3), the entire energy is dissipated by element 4441, but the platform collapses at unloading.
- In (4), 9MJ was dissipated by element 4441 while the remaining 12MJ was absorbed ny element 9014. No collapse during unloading.

The study shows that a higher dent width B causes a higher capacity which is in agreement with Equation 3.4 and 3.5. The significant difference in energy dissipation arises questions regarding the dent width. All extents in the USFOS-analyses were chosen based upon observations from LS-DYNA since the ship cannot be assumed as totally rigid.

A visual description of the dent width B versus height of contact area is shown in Figure 13.3, which is the same figure which was used in the Introduction. The height of the contact area is 6m and can be seen in Figure 13.3a. In comparison, the dent width which was shown in Figure 13.1b (=0.26m) is marked in red in Figure 13.3b.

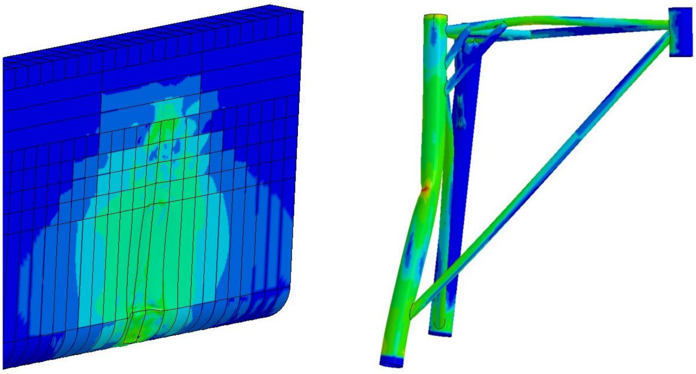

(a) Height of the contact area in the side model = 6m

(b) Dent width (marked in red) at jacket leg = 0.26m

Figure 13.3: Comparison of dent width and height of contact area

13.2.2 Fracture criteria applied to elements

As mentioned in Chapter 9.1 there were some challanges with small elements in the USFOS-model. Since strain is a relative measure (initial length dependent) an end shortening of 0.1 meter is more crucial for an element of 1 meter than for an element of 10 meter.

Difficulties with small elements in the global jacket model made the choices regarding fracture criteria difficult. Hence, some smaller elements were allowed to fail (no fracture criterion applied) since they were assumed to have little or negligible impact on the overall structural integrity. Furthermore, the global jacket model was modelled with "dummy elements". The purpose of "dummy elements" is to represent a behaviour (e.g.: linear dependencies) rather than a physical element. The conductor frame in the USFOS-model was modelled with dummy elements to represent the plates and stiffeners keeping the conductor in place. In certain cases such "dummy elements" are allowed to fail. Applying a fracture criterion on dummy elements in the conductor frame might cause the physical behaviour might be lost.

13.2.3 Incremental steps and time steps

In static analyses the external loads must be balanced by the restoring term of Equation 4.1. Hence, close to element collapse the incremental size was minimized to capture the collapse behaviour. In dynamic analyses the time step must also be tuned to capture the behaviour of buckling and element collapse. In addition tuning of incremental load steps and time steps will minimize the computer storage.

Chapter 14

Conclusion and recommendation for further work

A combination of NLFEA in LS-DYNA and global analysis in USFOS gave valuable information regarding the energy dissipation. Furthermore, information regarding the denting process in the struck member was obtained. As already discussed in Chapter 13 there are some uncertainties which must be considered for further work. The most important findings and recommendations for further work are mentioned below:

1. **Choice of dent width B in global USFOS-analyses:** Local analyses in LS-DYNA showed that setting the dent width B equal to the height of the contact area might provide a too optimistic results with respect to energy dissipation. A comparison study in Chapter 13 showed the drastic deviations between collision scenarios with different dent widths. Parts of the contact area cannot be assumed as totally rigid, e.g. the bulwark is unsupported in the upper end and will have little influence on the overall resistance of the ship. Hence, for further work it is therefore recommended that the dent width B is based upon NLFEA-observations rather than ship geometry when the leg does not stand perpendicular to the sea surface.

2. **Conductors capability of crushing the forecastle:** The bow impact against the conductor area showed that the conductors were strong enough to crush the forecastle. Hence, the ship contributed to a major part of the energy dissipation. However, a mesh convergence study was not carried out and strain rate is not taken into account. For further work, it is recommended to study this behaviour further.

3. **Structural integrity of the jacket platform:** Global USFOS analyses showed that the structural integrity of the platform was maintained throughout all collision scenarios according to the new collision requirements. However, all results obtained with USFOS must be considered in view of the USFOS-input and the uncertainties discussed in Chapter 13.2.1, 13.2.2 and 13.2.3.

4. **Damage to critical members:** The local analyses in LS-DYNA showed that the stern of the supply vessel was capable of damaging the risers before it hit the jacket leg. In addition, the braces and diagonals were not capable of dissipating the entire collision energy before local collapse, which has consequences for the riser clamps and risers. Thus, it is recommended to protect the risers further, according to NORSOK S-001 (2000)

Bibliography

Amdahl, J., 1983. Energy absorption in ship-platform impacts. Ph.D. thesis, Norwegian Institute of Technology.

Amdahl, J., Johansen, A., 2001. High-Energy Ship Collision with Jacket Legs. 11th International Offshore and Polar Engineering Conference.

Amdahl, J., Larsen, C. M., Syvertsen, K., 2010. TMR 4167 Marine konstruksjoner Del 2 - Knekking (Compendium in Norwegian). Akademika forlag.

Amdahl, J., Skallerud, B., 2002. Nonlinear analysis of offshore structures. RESEARCH STUDIES PRESS LTD.

Bell, K., 2015. Matrisestatikk. Fagbokforlaget.

Bergan, P. G., Syvertsen, T. G., 1977. Knekking av søyler og rammer. Tapir forlag.

Berge, S., 2016. Fatigue and Fracture Design of Marine structures (Compendium in TMR4200). Akademika forlag.

Cook, R. D., Malkus, D. S., Plesha, M. E., Witt, R. J., 2002. Concepts and applications for finite element analysis (4th edition). John Wiley & Sons, Inc.

DNVGL 2015-0984, 2016. FE Model Library for Collision Analysis: Description and results.

DNVGL RP-C204 (proposed version), 2017. Design against accidental loads.

DNVGL RPC208, 2016. Determination of structural capacity by non-linear finite element analysis methods.

DYNAmore, 2018a. Material selector for ls-dyna.
URL `http://www.lstc.com/dynamat/`

DYNAmore, 2018b. Time integration.
URL `http://www.dynasupport.com/tutorial/ls-dyna-users-guide/time-integration`

DYNAmore, 2018c. What are the differences between implicit and explicit? URL `http://www.dynasupport.com/faq/general/what-are-the-differences-between-implicit-and-explicit`

Faltinsen, O., 1993. Sea Loads on Ships and Offshore Structures (Cambridge Ocean Technology Series). Cambridge University Press.

Hallquist, J. O., 2006. LS-DYNA Theory manual. Livermore Software Technology Corporation.
URL `http://www.lstc.com/pdf/ls-dyna_theory_manual_2006.pdf`

Haufe, A., Schweizerhof, K., DuBois, P., 2013. Properties & limits: Review of shell element formulations.

Hysing, T., 1978. Analysis of penetration of hull. Impact and Collisions Offshore.

Johansen, A., Amdahl, J., 2000. Ship collision with Grane Platform.

Larsen, C. M., 2014. Marine dynamics (Compendium in TMR4182 Marine Dynamics). Akademia forlag.

Moan, T., 2000. Accidental Actions - Background to NORSOK N-003.

Moan, T., 2003. TMR4190 Finite Element Modelling and Analysis of Marine Structures. Akademika forlag.

Moan, T., Amdahl, J., Ersdal, G., 2017. Assessment of ship impact risk to offshore structures - New NORSOK N-003 guidelines. ELSEVIER.

Morrison, J., O'Brien, M., Johnson, J., Schaaf, S., 1950. The force exerted by surface waves on piles. Journal of Petroleum Technology 189 (2846), 149–154.

NORSOK N-001, 2004. Structural design (rev.04).

NORSOK N-003, 2017. Actions and action effects.

NORSOK N-004, 2004. Design of steel structures (rev.02).

NORSOK N-004 (rev.3), 2013. Design of steel structures (rev. 3).

NORSOK S-001, 2000. Teknisk sikkerhet (rev.03).

NORSOK Z-013, 2001. Risiko- og beredskapsanalyse (rev.02).

Paulsen, E., 2011. Analysis of the Big Orange XVIII and Ekofisk 2/4W collision in 2009. Master's thesis, Norwegian University of Science and Technology.

Qvale, K. H., 2012. Analysis and Design of Columns in Offshore Structures subjected to Supply Vessel Beam Collisions. Master's thesis, Norwegian University of Science and Technology.

Storheim, M., 2015. Structural response in ship-platform and ship-ice collisions. Ph.D. thesis, Norwegian University of Science and Technology.

Søreide, T., 1981. Ultimate load analysis of marine structures. Tapir forlag.

Søreide, T., Amdahl, J., Eberg, E., Holmås, T., Øyvind Hellan, 1988. USFOS - A Computer Program for Progressive Collapse Analysis of Steel Offshore Structures. Theory Manual. SINTEF.

Travanca, J., Hao, H., 2014. Energy dissipation in high-energy ship-offshore jacket platform collisions. ELSEVIER.

USFOS, 2014. Joint Capacity - Theory Description of use Verification. USFOS Reality Engineering.
URL `http://www.usfos.no/manuals/usfos/theory/documents/Usfos_JointCapacity.pdf`

USFOS, 2015a. Usfos manual - usfos commands, overview and description (doc.1).

USFOS, 2015b. Usfos tubular joint modelling. USFOS course with Technip in Paris.

Vredeveldt, A., Schipperen, J., Nassár, Q., Spaans, C., 2013. Safe jacket configurations to resist boat impacts. Collision and Grounding of Ships and Offshore Structures, 261–266.

Watan, R., 2011. Analysis and Design of Columns in Offshore Structures subjected to supply vessel Collisions. Master's thesis, Norwegian University of Science and Technology.

Yu, Z., 2017. Hydrodynamic and structural aspects of ship collisions. Ph.D. thesis, Norwegian University of Science and Technology.

Appendix

Appendix A

Structural mechanics

A.1 Tubular cross section analysis

A tubular cross section with diameter D and thickness t is shown in Figure A.1

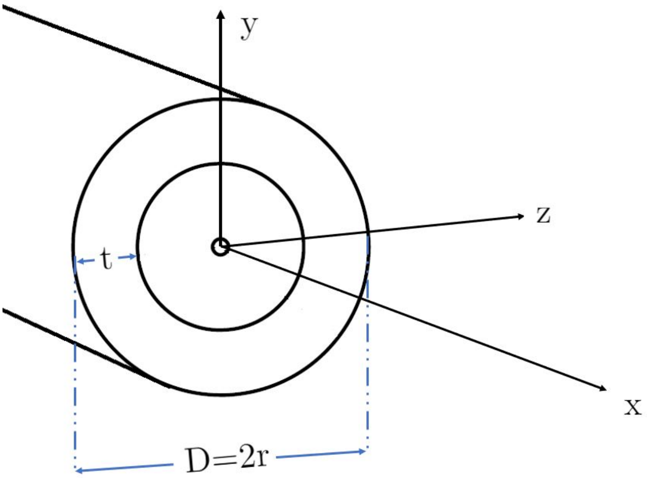

Figure A.1: Tubular thin-walled cross section

The second moment of inertia about the z-axis I_Z is expressed as

$$I = \frac{\pi}{8} (D - t)^3 t \tag{A.1}$$

Furthermore, the elastic section modulus W and the plastic section modulus are expressed in Equation A.2 and A.3, respectively

$$W = \frac{\pi}{32}\left(\frac{D^4 - (D-2t)^4}{D}\right) \tag{A.2}$$

$$Z = \frac{1}{6}\left(D^3 - (D-2t)^3\right) \tag{A.3}$$

Stress components in tubular members due to hydrostatic pressure

$$\sigma_X = \frac{p}{2}\left(\frac{r}{t}\right) \tag{A.4}$$

$$\sigma_\theta = p\left(\frac{r}{t}\right) \tag{A.5}$$

Hydrodtatic pressure alone will not cause buckling of tubular members. As soon as the axial stress component cause a deflection of the tubular member the attack surface will be increased along the bottom and decreased along the top which will cause a net horizontal force positive in the vertical direction.

Tubular members with internal pressure, such as pipelines and risers will have some contributions due to circumferential stresses. The equivalent stress σ_{eq}

$$\sigma_{eq} = \sqrt{{\sigma_X}^2 + {\sigma_\theta}^2 - \sigma_X\sigma_\theta} \tag{A.6}$$

A.2 Temperature dependency

The ultimate strength of steel depends on the temperature, which can be visualized in Figure A.2. Figure A.2 shows that the ultimate strength of steel increases with decreasing temperature but experiences a drop in ultimate strength at a given temperature (Berge, 2016). The figure also shows that the behaviour is valid both for notched and smooth specimens. T_D is defined as the *design temperature* and is defines the transition from ductile to brittle behavior.

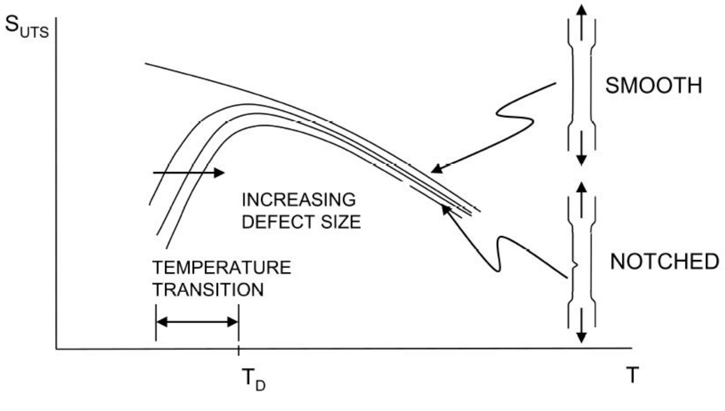

Figure A.2: Ultimate strength of steel versus temperature (Berge, 2016)

A.3 Non-linear structural analysis

Figure A.3 shows the different stiffness definitions. K_O is the initial stiffness or the slope at initial configuration. The change in incremental stiffness due to change in geometry is expressed by the geometrical stiffness *geometrical stiffness* K_G (Bergan and Syvertsen, 1977). In general,

$$R = K(r)r = (K_O + K_G)\,r \tag{A.7}$$

where $K(r)$ is denoted *secant stiffness*. Furthermore, the *incremental stiffness* K_I is expressed as in Equation A.8

$$dR = \frac{d}{dr}\left(K(r)\right)dr = K_I dr \tag{A.8}$$

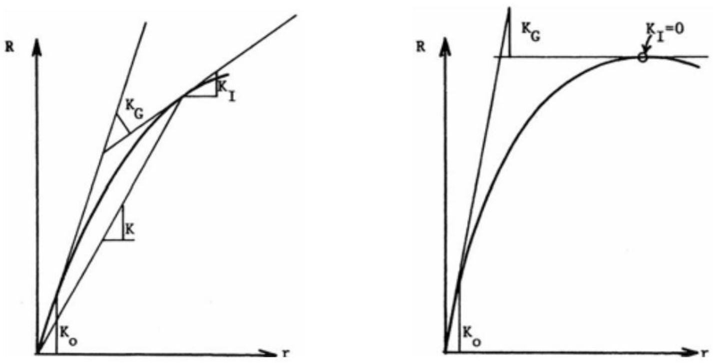

Figure A.3: Definitions of stiffness contributions (Bergan & Syvertsen, 1977)

A.4 Collapse load and hinge mechanism

An elastic-perfectly plastic material is considered. Figure A.4 shows how the bending moment distribution develops from the elastic range (a) towards the plastic range (c) via the elasto-plastic range (b) at a spesific part of a beam element.

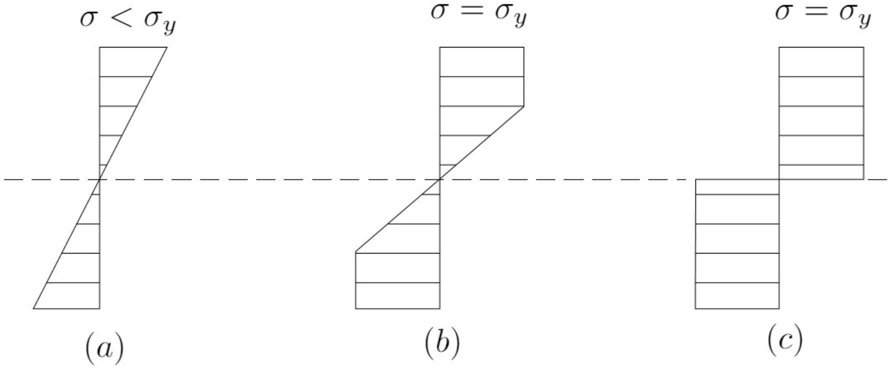

Figure A.4: Development of plastic hinge

The material fiber can not carry any more load beyond yield. As seen in (b) the stress is constant over the plastic zone while it is still varies linear within the elastic sone. At (c) the cross section is fully plastic utilized and a *plastic hinge* is therefore established at this point.

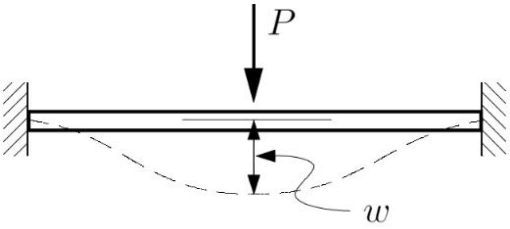

Figure A.5: Clamped beam subjected to concentrated force

Figure A.5 shows a clamped beam subjected to a concentrated force P at the middle. From the unit load method the displacement w is expressed as in Equation A.9

$$w = \frac{1}{192}\frac{Pl^3}{EI} \tag{A.9}$$

where l and EI are the beam length and beam stiffness, respectively.

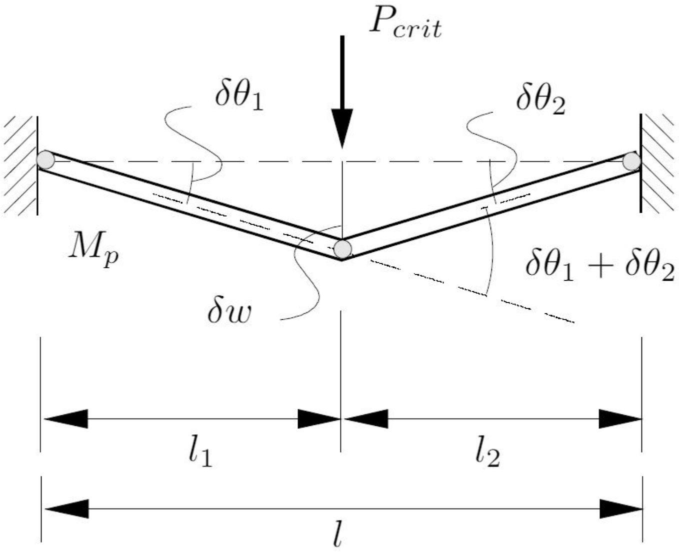
P_{crit}
$\delta\theta_1$
$\delta\theta_2$
M_p
$\delta\theta_1 + \delta\theta_2$
δw
l_1
l_2
l

Figure A.6: Collapse mode

The collapse mode for a beam with a concentrated load is shown in Figure A.6. Based upon the principle of virtual work, the internal work δW_i will be

$$\delta W_i = 2M_p\left(\delta\theta_1 + \delta\theta_2\right)$$

The external work δW_e will be

$$\delta W_e = P_{crit}\delta w = P_{crit} l_1 \delta\theta_1$$

From geometrical assumptions

$$\delta\theta_1 = \frac{l_2}{l_1}\delta\theta_2$$

By equating the internal - and external virtual work the collapse load is given as

$$P_{crit} = 2M_p\left(\frac{1}{l_1} + \frac{1}{l_2}\right) \tag{A.10}$$

When the load is concentrated at the beam middle $l_1 = l_2 = l/2$ the critical collapse load $P = 8M_p/l$.

Appendix B

LS-DYNA: Dimensions of structural ship models

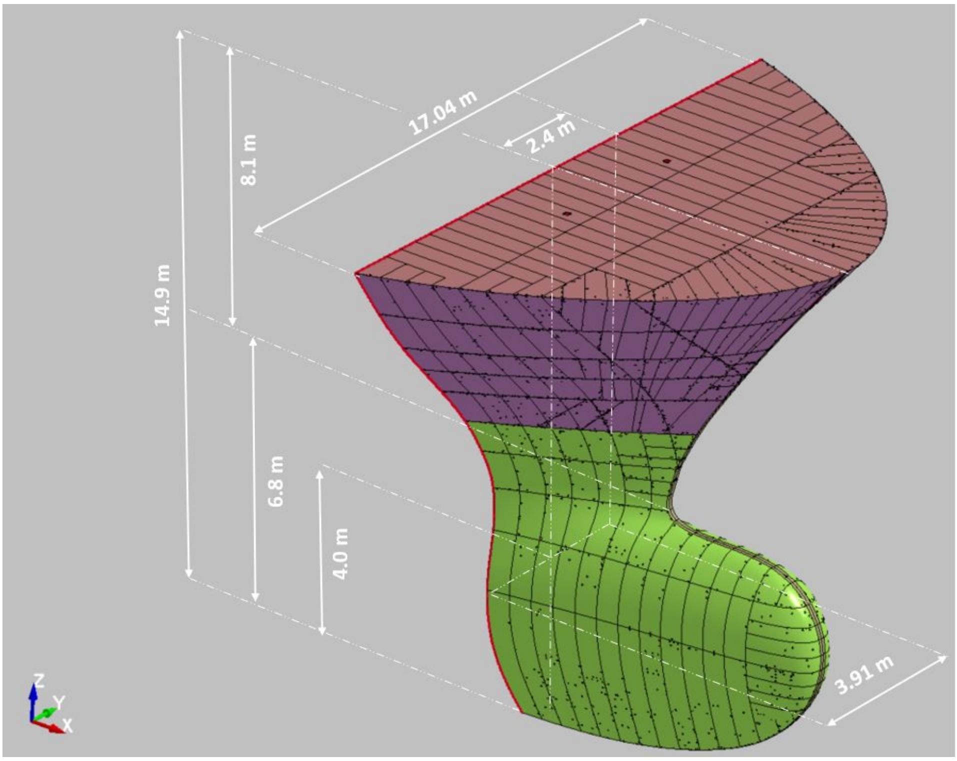
17.04 m
2.4 m
8.1 m
14.9 m
6.8 m
4.0 m
3.91 m
Z
Y
X

Figure B.1: Dimensions of structural bulbous bow model

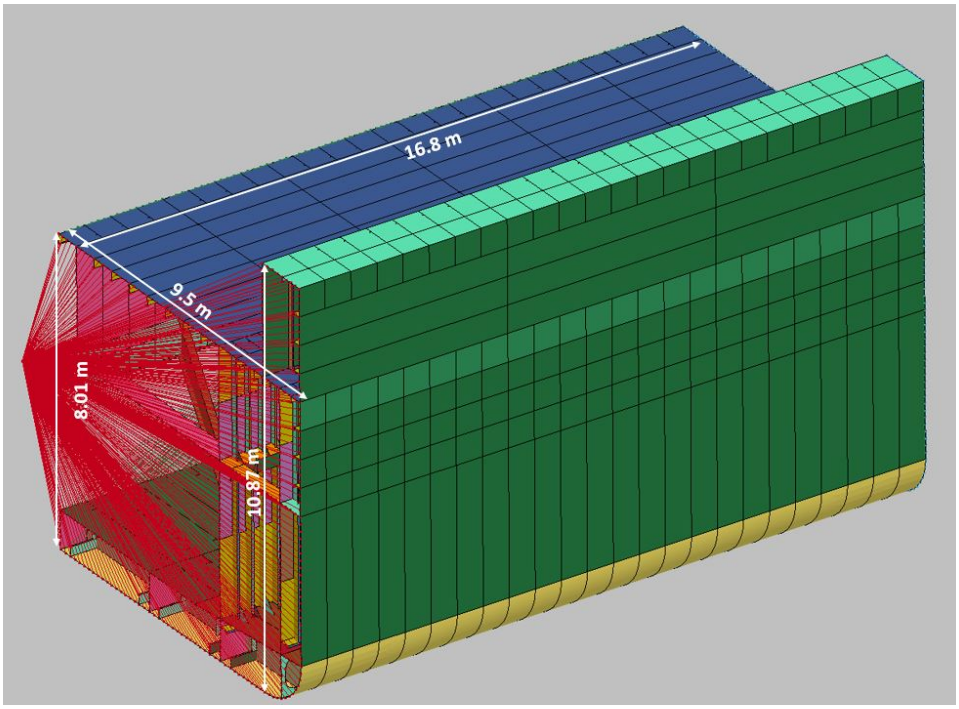
16.8 m
9.5 m
8.01 m
10.87 m

Figure B.2: Dimensions of structural side model

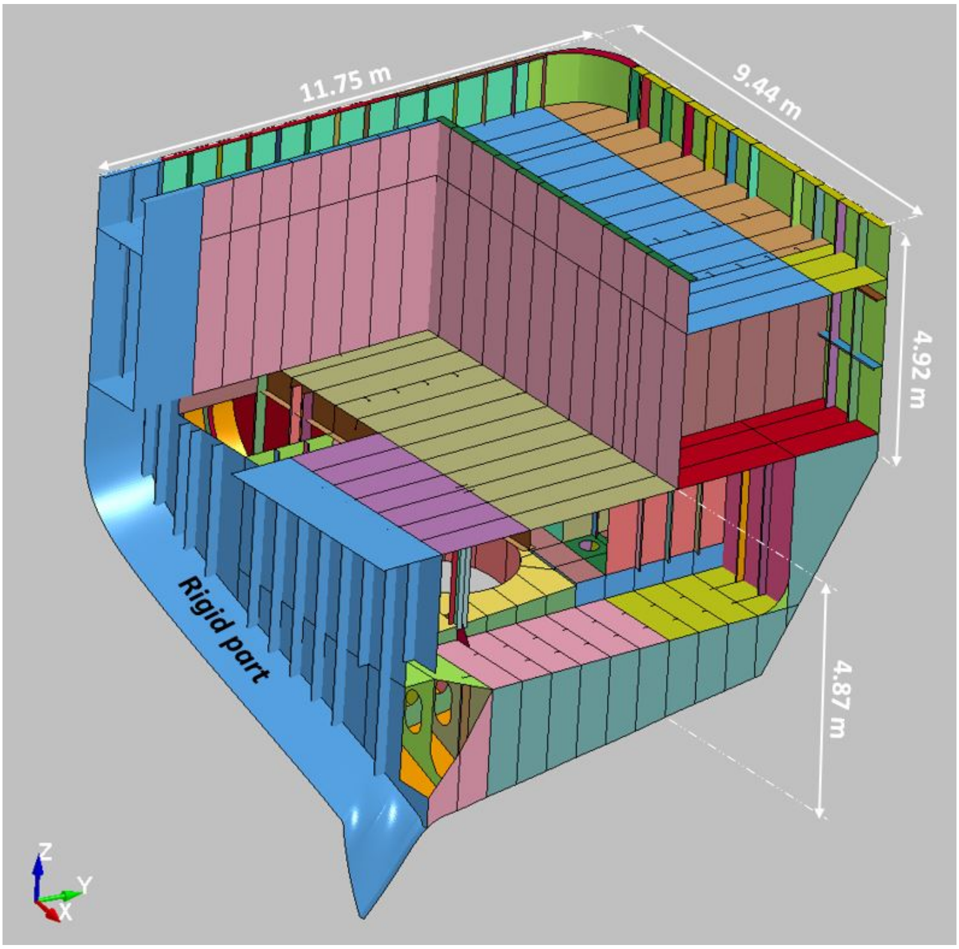
11.75 m
9.44 m
4.92 m
4.87 m
Rigid part
Z
Y
X

Figure B.3: Dimensions of structural stern corner model

Appendix C

LS-DYNA: Keywords

The purpose of this chapter is to give a brief description of the keywords used in LS-DYNA.

C.1 LS-DYNA: Control

The choice of control input is partly based upon recommendations by Storheim (2015) and partly on values used in the modelling and analysis of the structural ship models included in DNVGL-RPC208 ((DNVGL RPC208, 2016), (DNVGL 2015-0984, 2016)).

```
*CONTROL_ACCURACY
$#       osu       inn    pidosu      iacc
           0         2         0         0
*CONTROL_BULK_VISCOSITY
$#        q1        q2      type     btype
         1.0      0.06         1         0
*CONTROL_CONTACT
$#  slsfac    rwpnal    islchk    shlthk    penopt    thkchg
orien    enmass
         0.1       1.0         2         2         1         0
1        0
$#  usrstr    usrfrc     nsbcs    interm     xpene     ssthk
ecdt    tiedprj
           0         0         0         0       4.0         0
0        0
$#   sfric     dfric       edc       vfc        th     th_sf
pen_sf
         0.0       0.0       0.0       0.0       0.0       0.0
0.0
```

```
$#   ignore    frceng   skiprwg    outseg   spotstp   spotdel
spothin
          1         1         1         1         0         0
0.0
$#     isym    nserod    rwgaps    rwgdth     rwksf      icov
swradf    ithoff
          0         0         1       0.0       1.0         0
0.0        0
$#   shledg    pstiff    ithcnt    tdcnof     ftall    unused
shltrw
          0         0         0         0         0
0.0
*CONTROL_DYNAMIC_RELAXATION
$#   nrcyck     drtol    drfctr    drterm    tssfdr    irelal
edttl    idrflg
        250     0.001     0.995       0.0       0.0         1
0.04           0
*CONTROL_ENERGY
$#     hgen      rwen    slnten     rylen
          2         2         2         1
*CONTROL_HOURGLASS
$#      ihq        qh
          1       0.1
*CONTROL_SOLID
$#    esort   fmatrix   niptets    swlocl    psfail   t10jtol
icohed    tet13k
          0         0         0         2         0       0.0
0         0
$#    pm1       pm2       pm3       pm4       pm5       pm6       pm7
pm8       pm9      pm10
        0         0         0         0         0         0         0
0         0         0
*CONTROL_SOLUTION
$#     soln       nlq     isnan     lcint
          0         0         1      1001
*CONTROL_TERMINATION
$#   endtim    endcyc     dtmin    endeng    endmas
        2.0         0       0.0       0.0       0.0
*CONTROL_TIMESTEP
$#   dtinit    tssfac      isdo    tslimt     dt2ms      lctm
erode     ms1st
        0.0       0.9         0       0.0-3.0000E-6         0
0         0
$#   dt2msf   dt2mslc     imscl    unused    unused     rmscl
        0.0         0         0                           0.0
```

Time scaling is defined in the control input *dt2ms* in *CONTROL_TIMESTEP*. Selective mass scaling was used throughout the critical time step was set to 3e-06 seconds. The same value was also implemented in the structural ship models included in DNVGL RPC208 DNVGL RPC208 (2016) DNVGL 2015-0984 (2016). However, mass scaling was not recommended by

C.2 LS-DYNA: Material

The input card for *MAT_MODIFIED_PIECEWISE_LINEAR_PLASTICITY* is shown below.

1. mid = material ID
2. ro = material density $[kg/mm^3]$
3. e = Young's modulus $[N/mm^2]$
4. pr = Poisson's ratio $[-]$
5. sigy = yield stress $[N/mm^2]$
6. epsmaj = major in plane strain $[-]$
7. lcss = stress-strain curve
8. numint = number of through-thickness integration points

Until the stress reaches $sigy$ the stress-strain relationship is linear. When $sigy$ is exceeded the stress-strain relationship will follow a user-defined stress-strain curve (in this case curve-ID 70). Thus, the strain components are given in terms of plastic strains

$$\epsilon^p = \epsilon - \epsilon^e = \epsilon - \frac{sigy}{e}$$

```
*MAT_MODIFIED_PIECEWISE_LINEAR_PLASTICITY_TITLE
St523N_over63mm
$#      mid        ro         e        pr      sigy      etan
fail      tdel
        707.85000E-9  210000.0       0.3     284.0       0.0
0.0       0.0
$#        c         p      lcss      lcsr        vp   epsthin
epsmaj    numint
        0.0       0.0        70         0       0.0       0.0
0.15       5.0
$#     eps1      eps2      eps3      eps4      eps5      eps6
eps7      eps8
        0.0       0.0       0.0       0.0       0.0       0.0
0.0       0.0
```

```
$#       es1        es2        es3        es4        es5        es6
es7        es8
         0.0        0.0        0.0        0.0        0.0        0.0
0.0        0.0
```

According to recommendations by Storheim, smooth stress-strain curves should be used for NLFEA analyses in LS-DYNA. Strain rate is not taken into account in these analyses (lcsr=0). However, in the case of strain rate the visco-plastic formulation was recommended to be set to 1 (vp=1) Storheim (2015).

Appendix D

USFOS: Commands

The purpose of this chapter is to describe the most frequent used commands used in the USFOS-analyses. For further reading and information, it is referred to the USFOS manual USFOS (2015a).

D.1 BIMPACT

```
BIMPACT ldcs elnox elpos energy extent. xdir ydir zdir ship
```

BIMPACT is a static command in USFOS where the impact energy is defined in Nm. As seen in the input, the command is applied at an element *elnox* and the element position (either local end 1 or local end 2) with directions in global x-,y- and z-direction. Furthermore, an extent is also given (see Figure D.1 and Chapter 3.1).

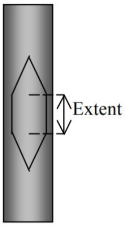

Figure D.1: Extent defined in USFOS (USFOS-manual)

If the BIMPACT-command *ship* is set to zero then all the energy is absorbed by the structure. If the value is more than zero indentation of ship will be accounted for, according to the command *MSHIP*.

The command might also be used in combination with *MULT _IMP* where the energy dissipation is continued into another element if the original element fails.

D.2 SURFIMP

SURFIMP is a relatively new command in USFOS. It is similar to BIMPACT, and takes the denting of tubular members into account. Another advantage is that the command can be used for both statical - and dynamical analyses. Two options are possible: *SURFIMP (Loadcase)* and *SURFIMP (Attach)* (see input below):

```
SURFIMP    LoadCase    LCase Type ID Extent Fx Fy Fz

SURFIMP   Attach   Elem ID End Extent
```

SURFIMP (Loadcase) is similar to BIMPACT and suitable for static analyses. A force-deformation or force-time curve from LS-DYNA is valuable information for Fx, Fy and Fz. The extent has the same definition as *BIMPACT*.

For dynamic ship impact analyses the *SURFIMP (Attach)* is suitable. The command is applied to an element and corresponding element end with an extent as given in *BIMPACT*. A sketch of the command setup is shown in Figure D.2.

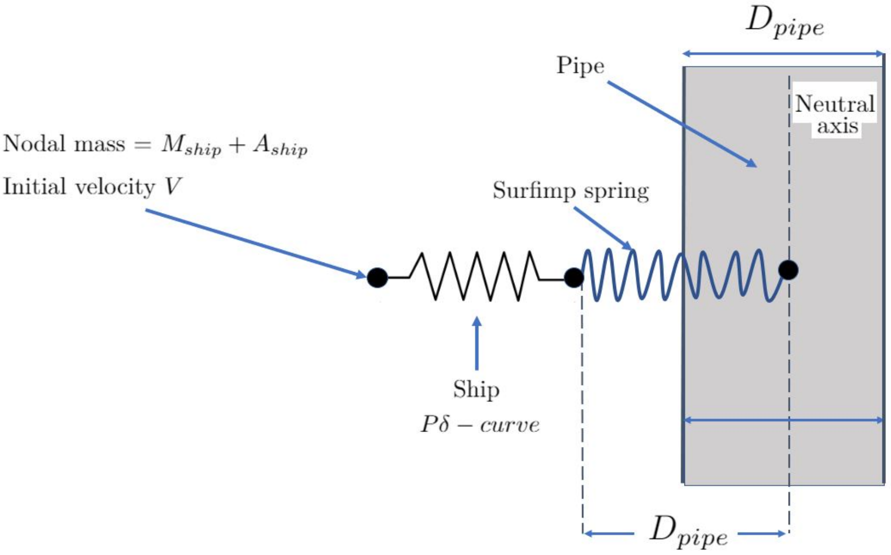

Figure D.2: SURFIMP explained

The ship is modelled as a non-linear spring with the force-deformation characteristics obtained from local analyses in LS-DYNA. In addition a second spring defines the dent depth in the pipe element. USFOS automatically defines this spring with the same length as the pipe diameter. The dynamic properties of the ship are modeled as nodal mass (including both the ship displacement and added mass) and an initial velocity. During the analyses in USFOS there were some difficulties with this command. A list of recommendations are given in the end of the chapter.

D.3 WAVEDATA

```
WAVEDATA LC type Heigth Period Direct Phase Surflev Depth
```

For residual strength check a Stokes 5th order wave was applied to the jacket. It was desirable to use a wave of 25m and 14.39 seconds. As seen in the input *WAVEDATA* is defined with a wave height, wave period and direction (0 degrees according to global x-direction). For Stoke's 5th order wave the *WAVEDATA*-input type is set to 2. The wave theory for the Stoke's wave is based upon Skjelbreia and Hendrickson from 1961. *WAVEDATA* can be used in both statical and dynamical analyses.

D.4 CHJOINT

```
CHJOINT node Chord1 Chord2 geono CapRule CapLevel Qf_SafetyCoeff
```

For joint checks the command *CHJOINT* is used. The nodal position of the joint is defined together with the chord element. Is the joint is modelled with a joint can, the can element shall be defined as *Chord1*. If not the chord member is defined with *geono*, with can diameter and can thickness. The *CapRule* defines the capacity formulas, e.g. NOR_R3 is used for NORSOK formulas (revision 3). In addition, failure mode is defined (see Chapter 3.2.3).

Unless otherwise mentioned *mean* is chosen as the capacity level. Furthermore a safety factor can be chosen. Since it is the ALS-criteria which is used, the safety factor is set to unity, according to Chapter 2.2

D.5 JntOption

```
JNTOPTION Keyword Joint ID
```

Grouted joints are defined with *CHJOINT* and *JntOption*. As mentioned in Chapter 3.2.3 grouted joints will not fail in compression.

Appendix E

Recommendations for SURFIMP

During the master's thesis the *SURFIMP*-command was used. Through *trial-and-error* and discussions with supervisor it turned out that there were some bugs with the code. The purpose of this chapter is to describe the challanges with the *SURFIMP (Attach)*-command and proposed solutions.

1. **Joint sections:** Close to joint sections there were some problems with the command. It is believed to have something to do with more than two elements sharing the same end node. Hence, sub-elements were made in order to ensure that only one tubular member where hit (see Figure 9.2).
2. **Force-deformation curve:** The steepest slope of the force-deformation curve must be in the start. This has to do with unloading as the initial slope is equal to the unloading slope.
3. **Static - and dynamic analysis:** The command can be used for both static - and dynamic analyses. However, for the jacket model the combination of statically loading of *GRAVITY* and dynamically loading of *SURFIMP (Attach)* lead to a negative determinant of the tangential stiffness matrix which lead to negative unloading of gravity and failure for the jacket platform in tension. Even though it is not computational efficient this was solved by applying the gravity dynamically.
4. **Degrees of freedom:** The *SURFIMP (Attach)*-command is defined with a force-deformation curve with a specified degree of freedom. Furthermore, a user-defined force-deformation value (k-value) for the remaining degrees of freedom is given. According to the user-manual the k-value must be larger than any slope of the user-defined force-deformation curve. However, for coupled motions (e.g. 45 degrees in x- and y-direction) the k-value must be tuned in such a way that the force-deformation curve can be compressed in both x- and y-direction.